1-9-2018

Plexin-B1 Signaling in Contact Inhibition of Locomotion Between Osteoclasts and Osteoblasts

Abhijit Deb Roy
University of Connecticut, abhijit.debroy@gmail.com

Plexin-B1 Signaling in Contact Inhibition of Locomotion Between Osteoclasts and Osteoblasts

Abhijit Deb Roy, PhD

University of Connecticut, 2018

Bone remodeling is critical for maintenance of bone health and requires a balance of bone resorption by osteoclasts followed with formation by osteoblasts. These opposing activities are spatially and temporally segregated and coordinated on the bone surface. Chemoattraction between osteoclasts and osteoblasts has been extensively investigated and has been proposed to direct osteoblasts to the site of bone resorption. However, the mechanism by which osteoclasts and osteoblasts are spatially segregated on the bone surface remains unknown. In this thesis, I demonstrate that osteoclasts induce contact inhibition of locomotion in migrating osteoblasts, which may enable spatial segregation of these cells. I identify Semaphorin 4D, expressed on the surface of osteoclasts, and its receptor Plexin-B1, expressed by osteoblasts, to be critical for the induction of contact inhibition of locomotion. I developed an optogenetic tool to initiate Plexin-B1 signaling using blue light, named optoPlexin. Localized stimulation of optoPlexin in subcellular regions elucidated spatial and temporal dynamics of signaling pathways involved in mediating contact inhibition of locomotion. In addition, I used optoPlexin to develop a novel protein-protein interaction assay in live cells, which revealed a previously unknown role of the RGS-like domain of PDZ-RhoGEF in mediating recruitment by Plexin-B1.

Plexin-B1 Signaling in Contact Inhibition of Locomotion

Between Osteoclasts and Osteoblasts

Abhijit Deb Roy, PhD

University of Connecticut, 2018

This thesis provides new understanding of the interactions between osteoclasts and osteoblasts during bone remodeling, illustrates the impact of localized Semaphorin 4D-Plexin-B1 stimulation in migrating osteoblasts, and provides new information on the molecular mechanism of Plexin-B1 signaling. The observations on spatial regulation of signaling pathways in cells undergoing contact inhibition of locomotion are pertinent to understanding the molecular pathways mediating cell repolarization. Furthermore, the novel optogenetic approach utilized to locally stimulate Plexin-B1 may be extended to other plexins, and potentially to other repulsive-guidance molecules. Thus, this work presents a significant advance not only in the field of bone biology and semaphorin-plexin signaling, but cell biology in general.

Plexin-B1 Signaling in Contact Inhibition of Locomotion Between Osteoclasts and Osteoblasts

Abhijit Deb Roy

M.S., University of Connecticut

B.Tech., National Institute of Technology Warangal

A Dissertation

Submitted in Partial Fulfillment of the

Requirements for the Degree of

Doctor of Philosophy

at the

University of Connecticut

2018

APPROVAL PAGE

Doctor of Philosophy Dissertation

Plexin-B1 Signaling in Contact Inhibition of Locomotion

Between Osteoclasts and Osteoblasts

Presented by
Abhijit Deb Roy, B.Tech., M.S.

Major Advisor

_____

Yi Wu

Associate Advisor

_____

Carol Pilbeam

Associate Advisor

_____

Ann Cowan

Associate Advisor

_____

Kimberly Dodge-Kafka

Associate Advisor

_____

Leslie Loew

Associate Advisor

_____

John Carson

University of Connecticut
2018

Acknowledgements

I am fortunate and grateful for all that I have and all that I do not. I dedicate this work to my parents, who have been supportive, or at least tolerant, of my choices; baffled though they were as to why I would give up a perfectly fine job to go back to school half way around the globe.

First, I thank my advisor, Dr. Yi Wu for being an incredibly good teacher, mentor and critic. I am grateful for the amount of time and effort you spent on training me. And I want to thank you for being supportive through the bad times, science related or otherwise. I thank my committee members for being invested in my training and me. Dr. Ann Cowan and Dr. John Carson: thank you for always taking the time out to answer the many naïve questions I have had, for your support and guidance through many failed experiments, and for helping me with my presentation skills. Dr. Kimberly Dodge-Kafka: thank you for accommodating the many unscheduled visits to your office with random questions and ideas. Dr. Leslie Loew: thank you for helping me refine my logic in experimental design. Dr. Carol Pilbeam: thank you for always being there to support and guide me, for forcing me to look at data objectively and from different perspectives, and for keeping me grounded. I thank the faculty at CAM for being always available and willing to answer questions and entertain crazy ideas. You make CAM a truly wonderful experience for every graduate student that I have known.

I thank Dr. Shilpa Choudhary, Dr. Sofya Borinskaya, Dr. Marc Rigatti, Dr. Clifford Locke, Dr. Rene Norman, Dr. Ahmed Elmokadem, Dr. Prem Shrestha, Adam Lafontaine, Judy Bloom, Carissa Sirois, Yuezhe Li and Yamalia Roberts for your friendship, and help with numerous things through my graduate training and providing support when I have needed. I thank my M.S. thesis advisor, Dr. Ruth Washington for her guidance and support, and for still keeping tabs on my progress. I want to thank my school principal Jaya Deb for always having faith and encouraging me to pursue everything that I wanted to.

Finally, I thank my partner and husband, Dr. Spencer Nyholm for putting up with my insanities, for being incredibly smart and kind and supportive, and for just being. I cannot fathom if this would have been without you.

Table of Contents

List of Figures

List of Tables

List of Movies

Abbreviations:

RANKL	Receptor activator of nuclear factor kappa-B ligand
RANK	Receptor activator of nuclear factor kappa-B
OPG	Osteoprotegerin
PDGF	Platelet-derived growth factor
TGF-β	Transforming growth factor beta
BMP-2	Bone morphogenetic protein 2
IGF	Insulin like growth factor
S1P	Sphingosine-1-phosphate
BMP-6	Bone morphogenetic protein 6
CTHRC1	Collagen triple helix containing-1
SDF-1	Stromal cell-derived factor 1
IL-8	Interleukin 8
CIL	Contact inhibition of locomotion
Rac1	Ras-related C3 botulinum toxin substrate 1
Cdc42	Cell division control protein 42 homolog
Eph receptor	Erythropoietin-producing human hepatocellular receptor
RhoA	Ras homolog gene family, member A
Ras	Rat sarcoma
GTP	Guanosine triphosphate
PAR-3	Partitioning defective 3 homolog
PTEN	Phosphatase and tensin homolog
EMT	Epithelial-mesenchymal transition

Met	Hepatocyte growth factor receptor
Ron	Macrophage stimulating protein receptor
PDZ	PSD95, Dlg1, zo-1
PSD95	Post synaptic density protein 95
Dlg1	Drosophila disc large tumor suppressor 1
Zo-1	Zona occludens-1
GAP	GTPase activating protein
GEF	Guanine nucleotide exchange factor
LARG	Leukemia associated RhoGEF
PRG	PDZ-RhoGEF
GIPC	GAIP interacting protein, C-terminus 1
GAIP	G alpha interacting protein
VEGFR	Vascular endothelial growth factor receptor
Rap1	Ras-proximate 1
CD45	Cluster of differentiation 45
SH3	Src homology 3
ABL	Abelson murine leukemia viral oncogene homolog
TIM2	T-cell/transmembrane, immunoglobulin, and mucin 2
CD75	Cluster of differentiation 75
FAK	Focal adhesion kinase
SYK	Spleen tyrosine kinase
TREM2	Triggering receptor expressed on myeloid cells 2
DAP12	TYRO protein tyrosine kinase-binding protein

Fes	Feline sarcoma oncogene
OTK	Offtrack kinase
ErbB2	Human epidermal growth factor receptor 2
Pyk2	Protein tyrosine kinase 2
ROCK	Rho associated coiled-coil kinase
CD72	Cluster of differentiation 72
HIV-1	Human immunodeficiency virus 1
PAS	Period-ARRNT-singleminded
PIP_3	Phosphatidylinositol (3,4,5)-triphosphate
BMM	Bone marrow macrophages
POB	Primary calvarial osteoblasts
siRNA	short interfering RNA
shRNA	short hairpin RNA
RNA	Ribonucleic acid
CRISPR	Clustered regularly interspersed short palindromic repeats
Cas9	CRISPR associated protein 9
IgG1	Immunoglobulin 1
PH	Plekstrin homology domain
Akt	Protein kinase B
NA	numerical aperture
WT	wild type
DH	Dbl homology domain

CHAPTER I

Introduction

Bone and its remodeling

Bone is a rigid mineralized connective tissue found in vertebrates. It provides structure, shape and support to the animal body, protects internal organs and enables fast and complex movements of animal limbs. In addition, bones act as a reservoir for minerals and growth factors, provides a site for maintenance of stem cells and produces different types of cells including red and white blood cells. In humans, the load bearing long bones are composed of two morphologically distinct types: cortical and trabecular bones. Cortical bones are the dense matrix on the cortex of most bones and provide strength by being resistant to bending and torsion. Trabecular or cancellous bone form a honeycomb-like network inside bones. Trabecular bones are weaker and more flexible than cortical bones, and may act as shock absorbers. During movement and other load-bearing activities, trabecular bone may undergo localized damage. Unless remedied, such damage may accumulate and compromise skeletal integrity over time. Bone remodeling, a process by which older bone is replaced by new bone plays a critical role in the restoration of bone strength and maintenance of skeletal integrity[1–3]. Bone remodeling primarily involves three types of cells: osteoclasts, osteoblasts and osteocytes.

Remodeling is initiated by resorption of bone by osteoclasts, followed by deposition of bone matrix by osteoblasts. Osteocytes may play a role in directing osteoclasts to sites of bone resorption[4]. Resorption and formation of bone matrix are quantitatively coupled so that the amount of bone resorbed is replaced by deposition[3]. Imbalances in this coupling can lead to pathological states, the most

prominent being osteoporosis marked by a loss of bone mineral density and weaker bones making patients prone to fractures. During remodeling, bone resorption in damaged trabeculae are spatially and temporally discrete events, for proper remodeling it is important that the consequent bone deposition occurs at the site of resorption after the resorption is completed and the active osteoclasts are no longer present. Such intricate spatiotemporal orchestration of osteoclast and osteoblast activities involves many ‘coupling factors’ that regulate their migration and differentiation.

Fracture healing is distinct from bone remodeling. After fracture, there is a rapid inflammatory response, followed by proliferation of fibroblasts that form a loose connective tissue called granulation tissue. Osteoclasts migrate to the site and resorb bone fragments and prepare the broken bone ends for healing. The cells in the periosteum, which is the outer layer of bones, proliferate and differentiate into chondroblasts and forms collagen rich ‘hyaline cartilage’; and osteoblasts, which lay down ‘woven bone’: a form of bone matrix with disorganized collagen fibers. As these new collagen matrices close the gap produced by the fracture, over time they are replaced by more organized lamellar bone matrix and formation of trabecular bone. Finally, over a significantly longer time scale, these trabecular bones undergo remodeling to form compact bones and the bone is healed to a state close to the pre-fracture form[5].

This section will provide a brief overview of the cells involved in bone remodeling, the aforementioned coupling factors and regulation of osteoblastic migration to the site of resorption.

Bone cells

Osteoclasts: Osteoclasts are large multinucleated cells of hematopoetic origin that degrade bone. Osteoclasts are formed by fusion of mononuclear macrophage lineage cells. Receptor activator of nuclear factor kappa ligand (RANKL), which is expressed by osteoblastic lineage cells, is critical for osteoclastogenesis[2,6]. Macrophages express RANK, which is activated by RANKL from osteoblast-lineage cells. RANKL is generally thought to be plasma membrane bound, indicating that cell-cell contact between macrophages and osteoblast-lineage cells are critical for osteoclastogenesis (Figure 1a). Furthermore, osteoblast-lineage cells also express osteoprotegerin (OPG), which acts as a decoy receptor for RANKL, thus inhibiting osteoclastogenesis[6]. Osteoclasts migrate to specific sites on the bone surface and initiate resorption by forming an actin-rich sealing zone and secreting protons to efficiently dissolve the mineralized hydroxyapatite component of bone, followed by degradation of the collagen matrix by metalloproteases and cathepsins[1]. Uncontrolled increase in osteoclast numbers or activity is associated with osteoporosis and rheumatoid arthritis, whereas defects in osteoclast resorption can cause osteopetrosis. One common strategy to combat osteoporosis is bisphosphonate treatment, which acts by decreasing osteoclast survival and action[7]. Long term decreases in osteoclast viability, and thus severe decreases in bone resorption effectively halts remodeling. Such lack of remodeling leads to a ‘frozen bone’ syndrome, where damages accumulate in the skeleton, impairing bone integrity and increasing the probability of failure.

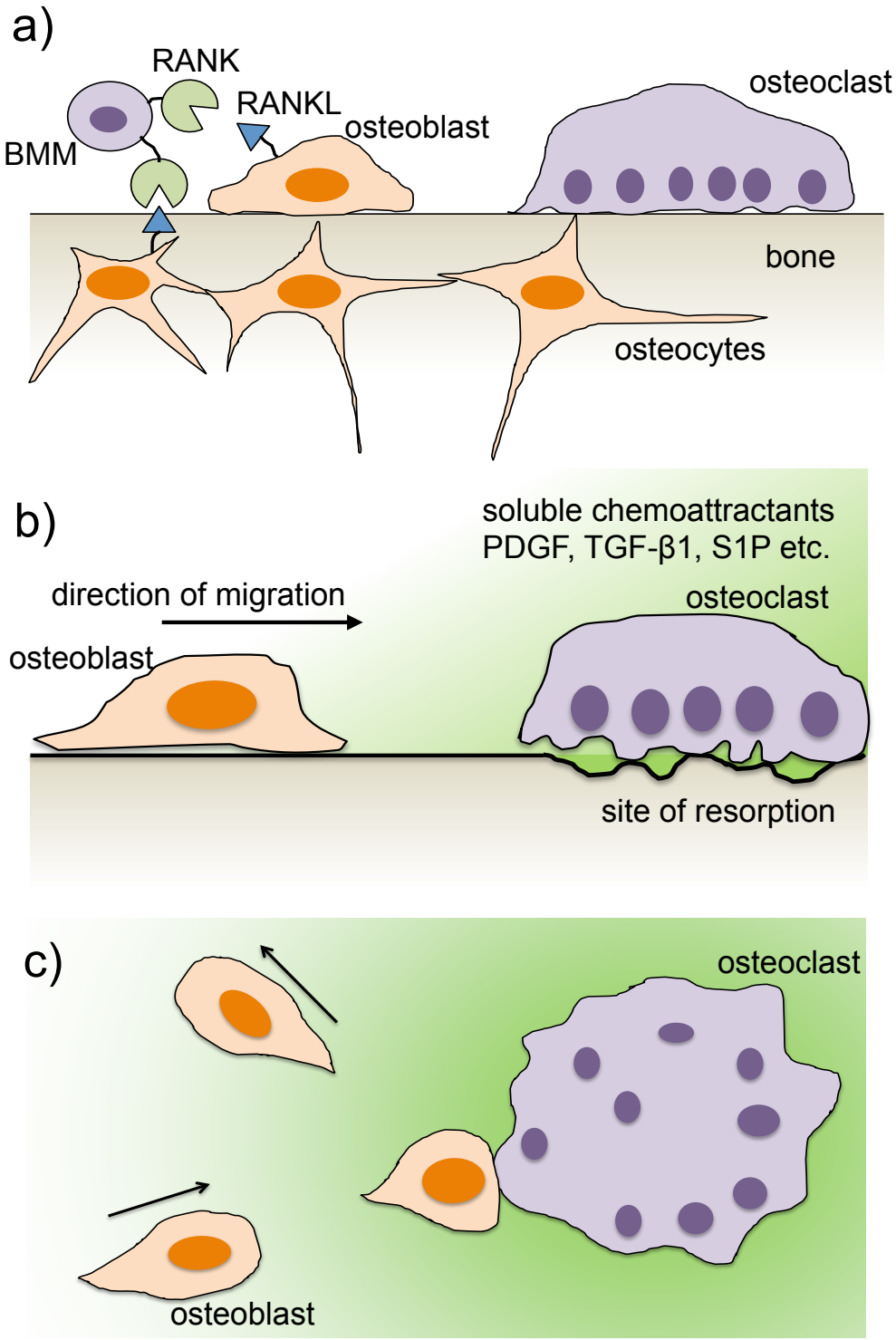

Figu

between pre-osteoclasts and osteoblastic lineage cells during RANKL mediated osteoclastogenesis. b) Chemotaxis of osteoblasts towards the site of resorption. c) Repulsion of osteoblasts upon contact with osteoclasts

Osteoblasts and osteocytes: Osteoblasts are mesenchymal lineage cells that synthesize bone. They are generally spindle shaped or polygonal. During bone remodeling, osteoblasts restore the bone removed by osteoclasts by the same amount in the same region of resorption, and thus regulate bone integrity. Pre-osteoblasts are thought to migrate to site of resorption after the osteoclasts have prepared the substrate and moved away, differentiate and deposit bone matrix. Over time this matrix gets mineralized bringing the bone back to its previous strength, marking the end of the remodeling cycle[1]. In the course of matrix deposition, some of the osteoblasts get entrapped in the matrix and terminally differentiate into osteocytes. Osteocytes have a stellate shape and are non-motile. They form intricate connected network spanning the bone matrix through long extended cytoplasmic processes in the bone canaliculi. Osteocytes have been proposed to respond to mechanical loading to coordinate bone remodeling, although the molecular mechanisms involved in such signaling remains elusive. *In*-vitro assays with cultivating osteocytic cell lines in matrigel have demonstrated their capability of exchanging cytoplasmic material, and may be one way by which they secrete cytokines. In addition, recently, osteocytes have been demonstrated to express RANKL and proposed to support, if not predominantly mediate, osteoclastogenesis[4]. However, the mechanism by which macrophages may access membrane-bound RANKL in osteocytes embedded in bone matrix is not well understood.

Coupling factors in bone remodeling

The osteoblastic cells interact with osteoclast precursors and osteoclasts at multiple stages during the bone remodeling process. Bone remodeling is initiated by osteoclastic resorption. Osteoclastogenesis is regulated by the ratio of RANKL and OPG expressed by osteoblast lineage cells. Accounting for the highly localized nature of osteoclastic resorption, spatial and temporal regulation of osteoblastic migration to the site of resorption is critical for proper bone remodeling. The coupling of osteoblasts to osteoclasts may be realized through multiple ways. During bone matrix formation, osteoblasts deposit growth factors such as PDGF, TGF-β, BMP-2 and IGFs, which are released during osteoclastic resorption and may promote osteoblast migration[3,8–10]. Additionally, osteoclasts also secrete factors such as S1P, BMP-6, CTHRC1, and cardiotropin-1 that may promote osteoblast migration to the site of resorption[3,11,12] (Figure 1b). While the focus has been on coupling factors expressed or regulated by either osteoclasts or osteoblasts, the bone microenvironment contains many different types of cells, which may also secrete some of these factors, thus making the coordination of bone resorption and formation much more nuanced and thus, more complex. Finally, changes in the topography of bone surface after osteoclastic action may also play a role in mediating osteoblast migration and function[13,14].

Osteoblasts respond to chemoattractants released to locate the site of active resorption. Migration of osteoblastic cells to the site of resorption presumably happens in different phases: recruitment of osteoblastic progenitors

to the bone surface and migration of pre-osteoblasts to the specific site of resorption. Resorption is initiated around 4-8 weeks prior to bone deposition phase. Since migratory factors released from the bone matrix during the early stages of resorption would presumably diffuse away during this period, it is likely that these factors recruit of osteoblast progenitors to the bone surface. Once on the bone surface, factors released from the matrix as well as those secreted by osteoclasts may guide them to the appropriate site. Since osteoclasts and osteoblasts are not usually observed the same space on bone surface, we may reason that osteoblasts occupy the site of resorption only after the osteoclasts have migrated away or undergone apoptosis. In the absence of active osteoclasts, there is no obvious source for chemoattractants, and how the pre-osteoblasts identify the exact location of resorption is not well understood. Haptotaxis or durotaxis, or a combination of both may play an important role in directing pre-osteoblasts to the resorption pits, but that requires the pre-osteoblasts to be present on the bone surface prior to completion of resorption. Additionally, osteoclasts and osteoblasts have completely opposing functions, and express factors that inhibit one another's differentiation and activity. Thus, ideally, the osteoblast progenitors should be recruited to the bone surface, and migrate towards but not occupy the site of resorption until the osteoclasts have completed resorption. Indeed *in vivo*, osteoblasts and osteoclasts are observed spatially segregated on the bone surface and rarely in contact with one another[15,16]. In the presence of only a chemotactic gradient, osteoclasts and osteoblasts should be clustered together. Thus, the current model of bone

remodeling does not explain segregation of osteoclasts and osteoblasts on the bone surface and fails to give a complete picture of spatial regulation of bone remodeling. A combination of chemotaxis and repulsion upon contact between the two cell types may be explain how pre-osteoblasts may be recruited to the general region of resorption and yet be kept away from sites with active osteoclasts (Figure 1c). Although repulsion-like behavior occurring between osteoblasts and osteoclastic cells has been reported intermittently[17,18], such behavior and the pertinent signaling mechanisms have not been examined.

Repulsion between cells

Directional cell migration is critical for proper embryonic development as well tissue homeostasis in adult animals, defects in which may cause disease states. Directionality in migration may be achieved by attractive or repulsive cues, respectively guiding cells towards or away from a source. Chemoattractive factors and chemotaxis in cells have been extensively studied across many systems. Chemotaxis is achieved by polarizing a migrating cell to promote and stabilize protrusions towards and inhibiting protrusions away from the target. Conversely, repulsion may be elicited by destabilizing protrusions towards the target and inducing repolarization of the direction of migration. In addition, repulsion between cells may occur in response to soluble factors or require contact between cells. There were also some early reports of long distance repulsion between cells through electrostatic forces[19,20]; although such responses may not be of particular physiological import.

Repulsion in response to soluble factors was first reported in a response of bacterial cells by antimicrobial agents or factors released by neutrophils. Soluble repulsive factors may act by countering effects of chemoattractants; however, repulsion is not mere inhibition of chemotaxis. Repulsive response in eukaryotic cells in response to soluble factors was first reported and has been extensively studied in neuronal guidance[21]. Repulsive factors in neuronal development were experimentally studied in the context of axon growth cone collapse[22–24], which were extended to neurite retractions and collapse of protrusions in other cells. In particular Netrins, ephrins, semaphorins and Slit

have been have been proposed to play key roles in axonal repulsion based upon collapse assays utilizing solubilized ligands[22–28]. It is noteworthy that Netrin, ephrin and semaphorin families have both secreted and plasma membrane bound members. Additionally, some of these plasma membrane bound ligands may undergo proteolytic cleavage and act as soluble repulsive guidance cues. More recently, immune cells have been reported to undergo migration down a gradient of growth factors. This phenomenon has been variously called fugetaxis, reverse chemotaxis and chemorepulsion. In particular SDF-1, S1P and IL-8 have been implicated in repulsion of immune cells[29–32]. Additionally, Slit has also been reported to inhibit response to chemoattractants[33]. Chemorepulsion of immune cells has been proposed to mediate emigration of T-cells from the thymus[34], and may be utilized by viruses and cancer cells to avoid detection by the immune system[31,35]. Conversely, chemorepulsion may be utilized to reduce rejection in organ transplants by utilizing cells expressing repulsive factors in allografts.

Repulsion between cells was first reported to occur between fibroblasts after contact, wherein cells ceased to persist in their direction of motion after contact with another cell[36]. Unlike chemorepulsion mediated by soluble factors released into the extracellular environment, repulsion after contact is arguably mediated by membrane bound factors and thus may only be effective when two cells, expressing the appropriate ligand-receptor pair come in contact. This work is mainly focused on contact repulsion or contact inhibition of locomotion (CIL), which is discussed in greater details in the following section.

Contact inhibition of locomotion

Contact inhibition of locomotion (CIL) is the phenomenon where cells migrate away from one another following cell-cell contact. Abercrombie and Heaysman first reported such behavior in 1953 from their observation of migratory behavior of chick fibroblasts *in vitro.* Abercrombie coined the term 'contact inhibition' to describe their observation of 'directional prohibition' of cell migration upon contact with other cells[36]. While significant in its own regard, investigation into CIL enabled probing into the fundamental questions of cell migration such as persistence, maintenance and changes in front and back polarity etc. Shortly after two decades of investigation into its various facets, the term 'contact inhibition' in context of cell motility as well as investigation into repulsion between cells fell out of favour. This was partly due to an increased interest in 'contact inhibition of proliferation', coined in mid 1960s, which had been gaining traction in the scientific community trying to identify differences between 'normal' and cancer cells grown in culture. Additionally, the physiological relevance of CIL was not obvious, and the events that CIL was composed of, such as directional cell migration, cell-cell contact, front and back polarity of migrating cells were being studied independently[37]. Furthermore, some groups that were studying repulsion between cells were using the term 'contact repulsion' to avoid confusion with contact inhibition of proliferation. Recently, the term CIL has come back in vogue in part due to the efforts of Roberto Mayor, whose work focuses on the impact of CIL on directional migration of neural crest cells[38–40]. There is considerable variation in the phenomena that are defined or

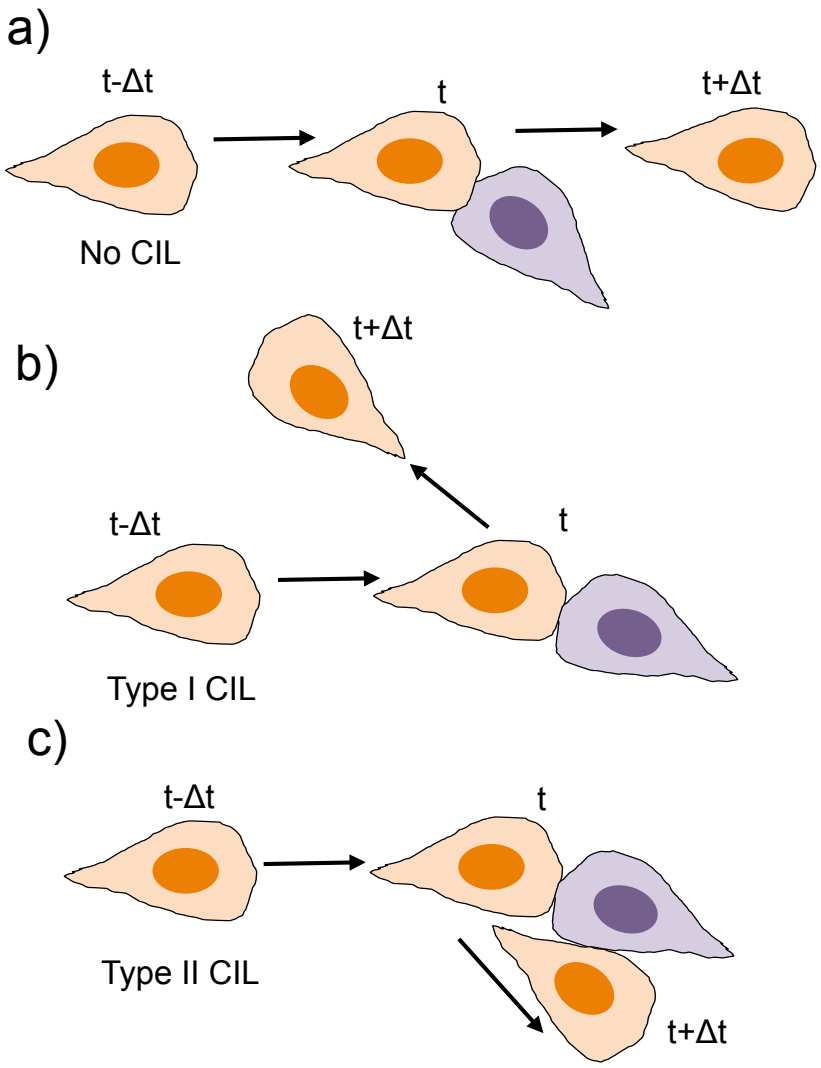

Figure 2. Contact inhibition of locomotion (CIL). (a) absence of CIL, (b) type I and (c) type II CIL.

described as CIL, perhaps due to the originally broad and relatively vague definition of CIL as ‘cessation of a cell continuing to migrate in the same direction after contact with another cell’ covered, and still covers a wide range of cellular behavior. Indeed, it may be easier to describe what CIL is not than what it is. When contact with another cell does not alter the direction or magnitude of motility of a migrating cell, it has not experienced CIL (Figure 2a).

Types of contact inhibition of locomotion

In an effort to define the different responses cells undergo that may be ascribed to CIL, it has been proposed to be classified into as many as six types. Abercrombie had classified CIL into two types: type I (Figure 2a) involved contraction of the leading edge at the site of contact, repolarization and migration away from the site of contact; and type II (Figure 2b), which involved inability of a cell to move over or across another cell and may involve cessation of movement or gliding past the cell in contact[37,41]. From a molecular signaling perspective, type I CIL may be described to involve repolarization induced by signaling pathways initiated upon contact, whereas type II may be described as a cell migrating away from or around a physical barrier to motility. Although superficially distinct, type I and type II may not be entirely independent of one another since physical contact between two cells may initiate signaling depending on changes in mechanical forces or membrane tension experienced by the cells or the nature of the substrate available, and the extracellular environment may modulate the response of repolarization signaling initiated upon contact. It is perhaps easier to define type I CIL as change in migratory behavior mediated by signaling across

two cells upon contact through plasma membrane localized ligand-receptor complexes. CIL may be further categorized as homotypic: between similar cells, or heterotypic: between different types of cells. Contact between cells of similar of different types can yield completely different responses in the same cells. This work primarily pertains to type I heterotypic CIL between osteoblasts and osteoclasts, and is discussed in details in chapter II.

Assays to study and quantify contact inhibition of locomotion

Regardless of the categories and classifications, it is worth remembering that CIL is neither discrete nor uniform behavior. It ranges the gamut of cessation of motility, moving around another cell or a complete reversal of direction of migration. Such wide range of responses makes it particularly tricky to decide whether a cellular response is CIL or not. To account for the diverse responses that may be CIL, researchers have utilized different experimental assays and analytical approaches to qualitatively and quantitatively study CIL[37,42–44]. Some of them are briefly discussed below.

Mixing assay: Two different groups of cells or tissue explants are placed next to one another, and the degree of overlap between the two groups of cells after a certain period of time is measured. Presence of CIL will decrease the degree of overlap or mixing of the two groups. The difference in distance traversed by cells when placed next to the other group versus alone, or the degree of mixing indicates the impact of CIL on their spreading (Figure 3a).

Radial outgrowth: A group of cells that undergo homotypic CIL will spread radially outwards away from their neighbors. This behavior may be

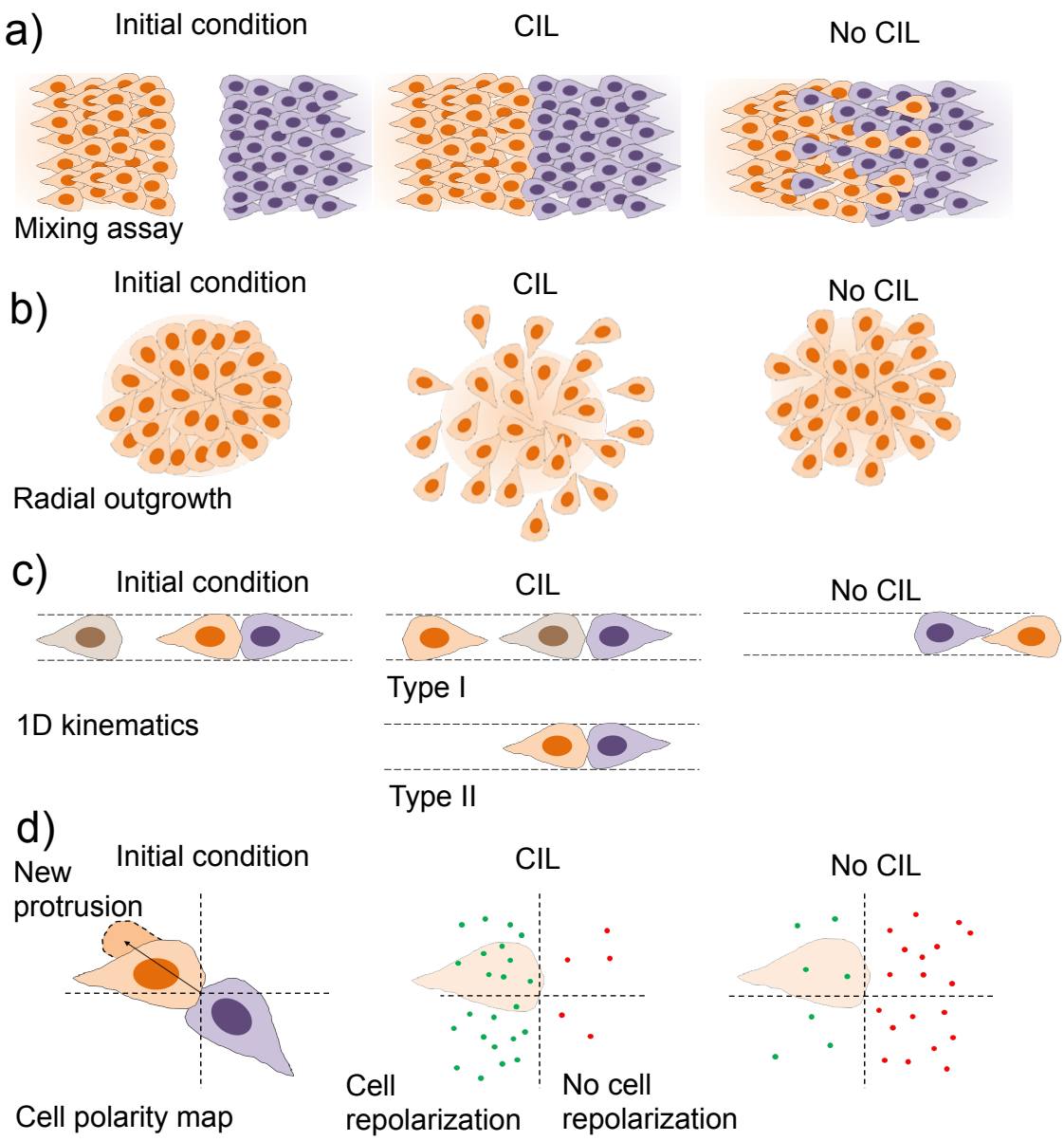

Figure 3. Assays to evaluate CIL. (a) Mixing assay, (b) radial outgrowth assay, (c) one dimensional kinematics post collision and (d) cell polarization map after collision.

utilized to assess CIL in cells by measuring the spread of cells from a relatively confluent culture or tissue explant (Figure 3b). This assay is, of course, not useful for heterotypic CIL, or if the cells predominantly move collectively.

Cell-cell contact kinematics: Observing changes in the trajectory of cells coming in contact with another can be utilized to assess CIL. In the absence of CIL, contact with another cell will have minimal impact of the migrating cells, where if CIL occurs, the direction of migration of the cells should be altered significantly. Measurements of such changes in direction upon contact should be compared against free moving cells to account for random switches in direction in freely moving cells. As an extension, some groups have utilized patterned substrates to restrict cell movement in a line[42,45], which simplifies quantification of CIL (Figure 3c). However, restricting movement in a single line may significantly alter cell behavior by changing the threshold required for change in direction.

Changes in cell morphology and polarity: The basic definition of CIL pertains to a change in the state of motion of a cell upon contact with another. Observing contacts between migrating cells can enable identification of changes in cell morphology and polarity. In particular, a polarity map to identify the location of new protrusions formed with respect to the site of contact has been used to qualitatively identify CIL (Figure 3d). This may be particularly useful when investigating CIL *in vivo*.

Each of these assays has their pros and cons. In particular, whether these assays are relevant in assessing cell behavior in a three-dimensional *in-vivo* environment remains to be determined. In addition to subjective observation, it is

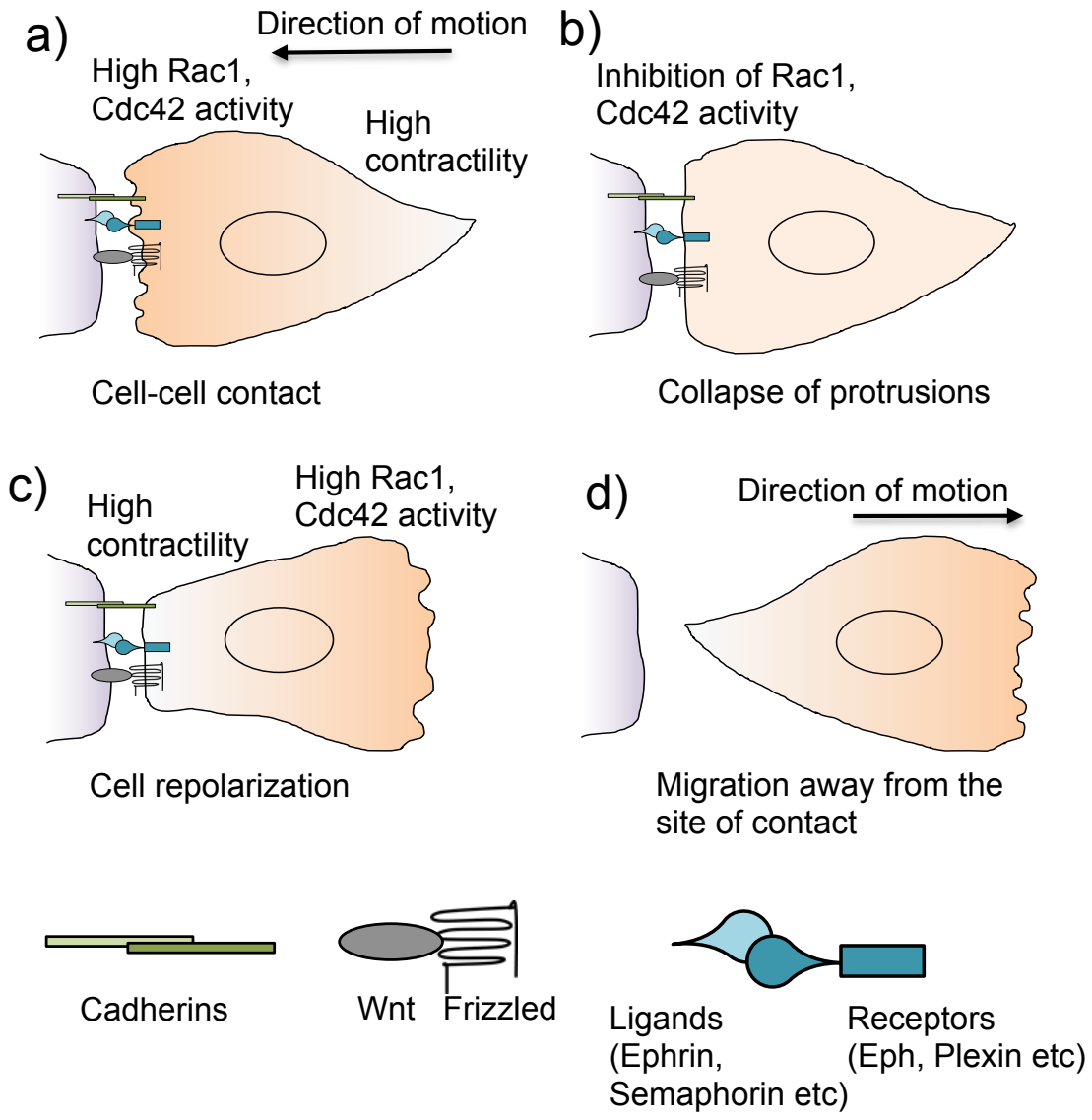

Figure 4. Stages of type II CIL. (a) Cell-cell contact, (b) inhibition of protrusion, (c) cell repolarization and (d) migration away from the site of contact.

useful to quantify cell behavior to distinguish between CIL and lack of it. Different groups have measured the frequency of protrusion collapse upon contact, separation between cells and deviation in direction of migration post contact to quantify CIL. We have quantified CIL between osteoblasts and osteoclasts using all three approaches, which are described in chapter II.

Molecular mechanisms of contact inhibition of locomotion

Type I CIL response in cells may be divided into four events that occur one after another to orchestrate one seamless response (Figure 4). Obviously, these events are neither independent of nor separated from one another and there may be different degrees of overlap depending on context. Nevertheless, it may be useful to utilize these subjectively defined stages of CIL to delve into the molecular pathways that regulate CIL.

Cell-cell contact: Type I CIL presumably involves activation of signaling pathways in the cell through membrane bound molecules on the other cell (Figure 4a). This would require a relatively stable cell-cell contact. Recent studies have pointed at the role of cadherins in formation of cell-cell junctions[46,47]. Furthermore, other proteins that mediate formation of adherens junctions such as vinculin, p120, α-catenin and β-catenins have also been reported to play different roles in CIL[37,39,48]. However, these proteins are also involved in making stable cell-cell contacts, and the reason behind the transience of the junctions in CIL is not well understood. One possibility is the role of different cadherins in organizing stable versus transient junctions. In particular, E and N-cadherin have been respectively proposed to mediate stable contacts and repulsion between cells.

Wnt-Frizzled signaling may be engaged upon cell contact. Furthermore, engagement of other membrane-bound molecules may modify or over-ride the nature of cell-cell contacts. In particular repulsive guidance molecules such as Ephrins and Eph receptors and SLIT-ROBO signaling have been implicated in mediating CIL between cells[37,49,50]. In a similar vein, here I have attempted to demonstrate the role of Semaphorins and Plexins, more specifically Semaphorin 4D and Plexin-B1 in mediating CIL. Aside from cadherins, how much this ligand-receptor coupling may stabilize cell-cell contact is not known. Since the very nature of CIL implies a relatively short contact between cells, how such ligand-receptor pairs identify these sites of contact is an interesting question. It is possible that diffusion on the plasma membrane enables accumulation at the site of contact, which in turn is stable until a critical threshold of repulsive signal is achieved.

Collapse of protrusions: Cell-cell contact and cessation of protrusions at the site of contact, in order, are hallmarks of CIL. Members of the Rho family of small GTPases are well known regulators of front and back polarity in cells. More specifically, Rac1 and Cdc42 are known to promote actin polymerization and protrusions, whereas RhoA is generally thought to promote myosin driven contractility to inhibit protrusions and mediate retractions. In addition, phosphatidylinositols, which are lipid components of the plasma membrane are also involved in regulation of protrusions and retractions through cross-talk with small GTPases. Cessation or collapse of protrusions involves inhibition of Rac1 and/or Cdc42 activities at the leading edge (Figure 4a, 4b). The precise

mechanism of such inhibition is not well understood, although it is possible that different pathways may engage different molecules to inhibit Rac1 and Cdc42. N-Cadherin, PAR3 and Dishevelled have been reported to mediate Rac1 inhibition in Neural Crest cells[39,51–54]. Ephrin and Eph receptor mediated CIL may involve activation of RhoA, which has an inhibitory relationship with Rac1. Although cross-talk between small GTPases[55], in particular that between RhoA and Rac1 (and Cdc42) seem to be consistent across many instances of CIL, the exact molecular signaling pathways that mediate such crosstalk need further elaboration.

Repolarization: Inhibition of protrusions at the site of cell-cell contact is usually followed by increased contraction, converting the former protrusion into a retraction. Around the same time, a new protrusion is formed away from the site of contact that causes the cell to repolarize (Figure 4c). It may be speculated that such repolarization primarily involves spatial reorganization of the factors that maintain front and back polarity in a migrating cell. RhoA activation appears to play a critical role in the induction of contractility at the site of contact. Such contractility may result in increased mechanical tension around the region of contact, which has been observed in CIL between Drosophila macrophages[56]. In addition, RhoA may activate PTEN[57], which is a known inhibitor of phosphoinositide-mediated protrusions. Additionally, increased tension in the actin cytoskeleton may also induce repolarization of cells through mechanosensitive signaling pathways, although the precise mechanism of such repolarization remains to be elucidated. Repolarization of the cell also involves

reorientation of microtubules away from the site of contact towards the new protrusions. In Drosophila marcophages, microtubule catastrophe around the site of cell-cell contact has been observed, but the signaling mechanism involved in this reorientation is not currently known[56]. Although simple in concept, repolarization of a cell involves reorganization of all the essential cytoskeletal components: actin, microtubules and plasma membrane, and thus potentially involves a large degree of crosstalk across the pathways that mediate these different cytoskeletal elements, the precise nature of which is currently not well understood.

Migration away from the site of contact: Once repolarized, the cells may continue to migrate away from the site of contact (Figure 4d). While positive feedback may be involved in maintaining the front and back after repolarization, the physical separation of the cells involves disruption of the cell-cell junction, active retraction and stabilization of new protrusions away from the site of contact. Since protrusions are stabilized by integrin mediated adhesions, focal adhesions may be spatially regulated to enable persistent migration. Migration of cells away from the site of contact may involve a simple disruption of adhesions or maturation of adhesions followed by dissolution. The nature of adhesions depends on cell-type and substrate; more work is needed to understand the role played by adhesions in CIL.

Physiological relevance of contact inhibition of locomotion

Recently CIL, especially homotypic, has been extensively studied in different systems *in vitro* as well as *in vivo.* CIL has been implicated in many

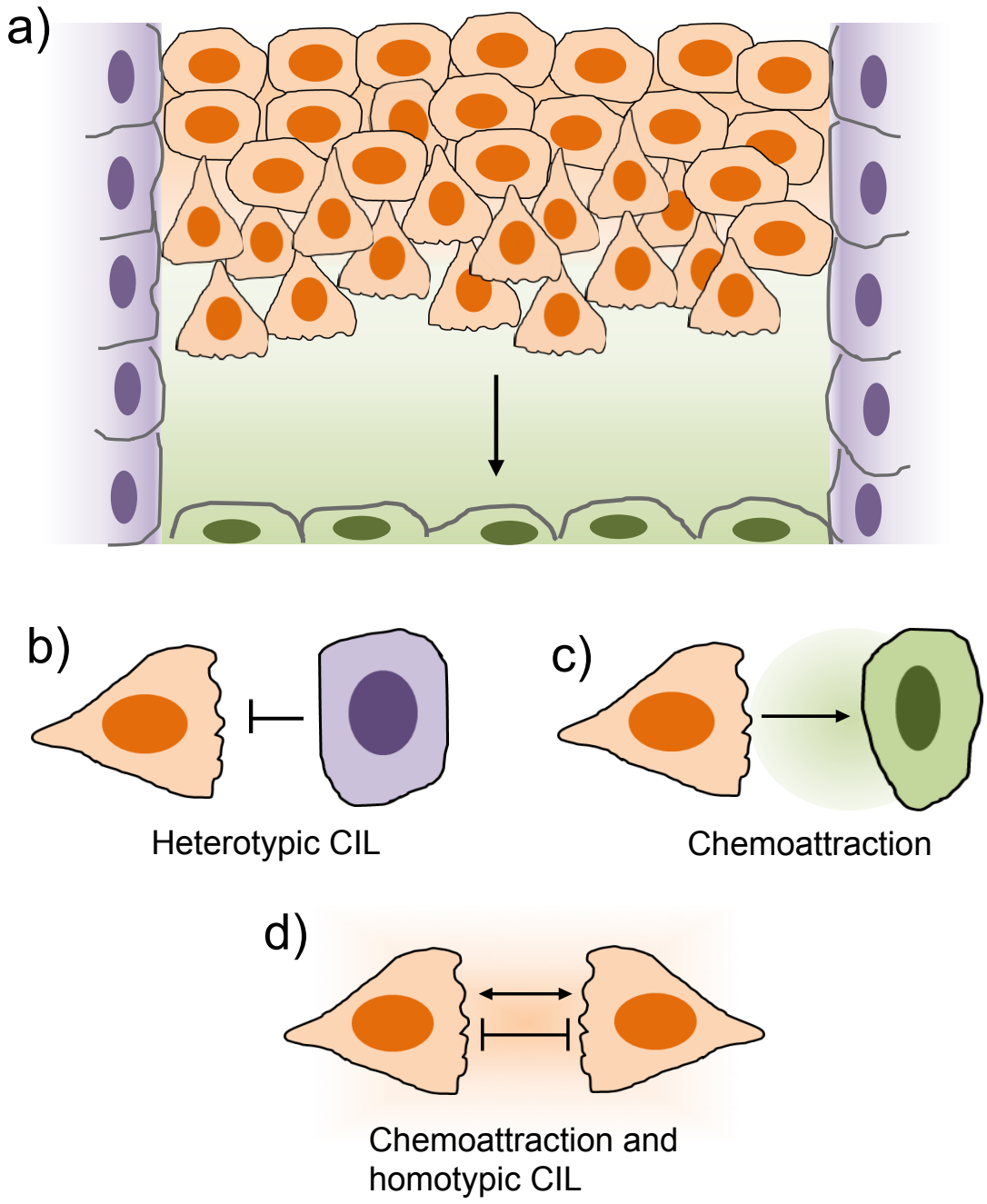

Figure 5. Co-ordination of directed collective migration through chemoattraction and CIL. (a) Directed collective cell migration, (b) heterotypic CIL, (c) chemoattraction and (d) homotypic CIL and chemoattraction.

physiological phenomena: collective migration, tissue patterning, cell dispersion and maintenance of tissue boundaries[40,51]. CIL may regulate dispersion of Cajal-Retzius cells and macrophages during embryogenesis[58]. However, the exact positioning of these cells is not random, and perhaps involves an intricate balance of homo and heterotypic CIL, as well as other cues present *in*-vivo. Heterotypic CIL may be involved in maintenance of tissue borders. This is particularly relevant in cancer metastasis, since loss of CIL may enable malignant cells to effectively migrate into tissues. Although loss of CIL has been proposed to promote invasiveness of cancer cells *in* vitro, whether the same happens *in* vivo remains to be further examined. A shift from E-Cadherin to N-Cadherin mediated cell-cell contacts correlates with both induction of CIL and EMT[51], although any direct connections between the two phenomena remain to be examined. Macrophages show an interesting behavior, wherein they appear to undergo homotypic[56], but not heterotypic CIL[51]. This might be explained by their role in looking for sites of infection or wounds where homotypic CIL enables greater spread, and lack of heterotypic CIL enables tissue penetration to effectively migrate to the site of injury. However, how the macrophages may overcome homotypic CIL to aggregate at sites of injury is not known. Unlike cell dispersion, the role of CIL in collective migration, although perhaps counter-intuitive, is particularly fascinating (Figure 5). Heterotypic CIL may enable greater directional persistence of a collectively migrating group of cells by restricting spread. In addition, homotypic CIL in the presence of co-attraction between migrating cells may enable efficient protrusion formation and maintenance only in

cell-free regions (Figure 5). A combination of homotypic and heterotypic CIL between placode cells and neural crest cells has been demonstrated to be critical for a ‘chase and run’ behavior that may be critical during embryogenesis. Such behavior might explain how cells can efficiently respond to relatively low concentrations of chemoattractants to migrate to their destination. The molecular mechanisms that lead to collective migration versus cell dispersal stemming from a seemingly similar phenomenon are not well understood.

Semaphorin and Plexin signaling

Membrane bound repulsive ligand receptor pairs are of particular interest in CIL. Ephrins and Eph receptors, and semaphorins and plexins are arguably the most well studied families of repulsive guidance factors. My work is primarily focused on Semaphorin 4D and its receptor Plexin-B1, and this section will provide a brief introduction to semaphorin and plexin signaling.

Functional domains of semaphorins and plexins

Semaphorins are a group of membrane associated or secreted glycoproteins, which have been categorized into eight groups. Semaphorins expressed by invertebrates are categorized in groups 1 and 2, and the last group is reserved for semaphorins expressed in viruses. In vertebrates, semaphorins have been classified into groups 3 to 7, of which group 3 are secreted and the rest are membrane associated. Group 4 semaphorins may have an intracellular PDZ domain, which may be involved in reverse signaling through plexins (Figure 6). All semaphorins have a conserved extracellular 'Sema' domain, which shows structural similarities to β-propeller repeats in α-integrins. Sema domains are found in the extracellular regions of semaphorins, plexins, and receptor tyrosine kinases Met and Ron. Plexins are a group of transmembrane proteins and are the major receptors for semaphorins. Based on sequence homology plexins have been classified into four groups: A-D. All plexins share a largely homologous structure (Figure 6): an extracellular sema domain with which they form heterodimers with semaphorins, a single transmembrane helix, a juxtamembrane region followed by a RasGAP homology region and a RhoGTPase binding

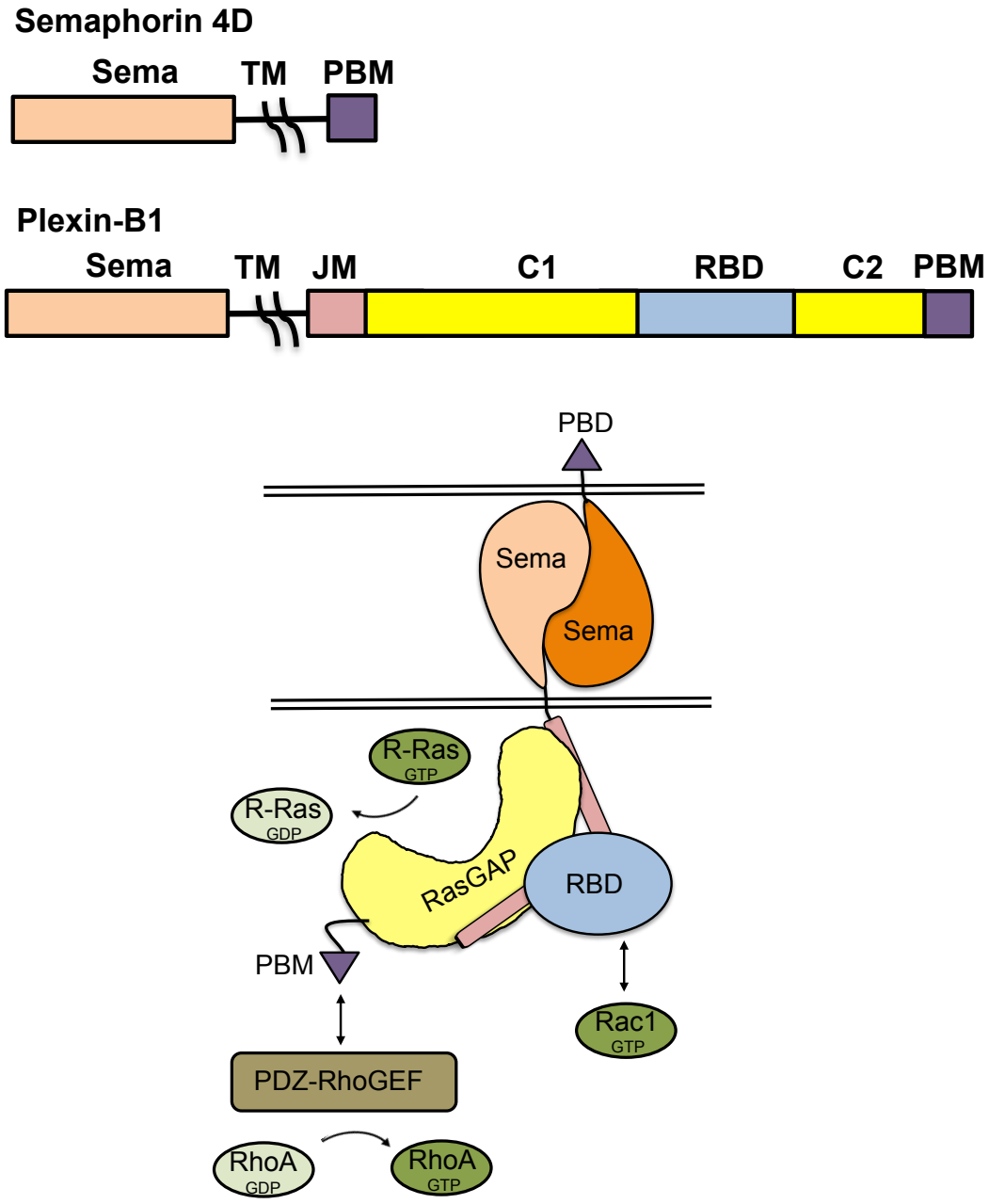

Figure 6. Semaphorin 4D and Plexin-B1 domains and signaling. Sema, sema domain. TM, transmembrane domain. PBM, PBZ binding domain (same as PBD or PDZ binding domain). JM, juxtamembrane domain. C1, C2, halves of RasGAP domain of Plexin-B1. RBD, Rho GTPase binding domain.

domain (RBD). The RasGAP domain is unique in that the domain is divided into two segments, referred to as C1 and C2, with each segment containing one of the catalytic arginine residues critical for RasGAP action. C1 and C2 are connected by an unrelated RBD that associates with GTP-loaded Rho GTPases. Although the linear sequence C1 and C2 are separated by about 200 amino acids, structural studies do not reflect any such separation, with C1 and C2 segments cohesively forming a RasGAP domain and the RBD shifted away. The juxtamembrane region folds into a helix-loop-helix conformation and aligns between the RasGAP domain and the RBD. Additionally, B family plexins have a C-terminal PDZ binding domain (PBD) with which they can recruit and activate PDZ-domain containing RhoGEFs: PDZ-RhoGEF and Leukemia associated RhoGEF (LARG). Plexin-D1 also has a C-terminal PBD, and has been recently reported to recruit and activate GIPC1 (GAIP interacting protein, C-terminus 1) through interaction with its PDZ domain. GTPase binding to plexin-RBD is critical for the RasGAP activity of plexins. For this reason, plexins are thought to function as AND gates, integrating extracellular as well as intracellular signals. All semaphorins, except group 3, directly associate with plexins through their sema domains. Group 3 semaphorins require neuropilins as a co-receptor for association with plexins. Neuropilins are single pass transmembrane proteins with a size of ~900 amino acids. They have very short intracellular regions, and are generally thought to function primarily as a co-receptor for plexins and receptors for vascular endothelial growth factors (VEGFR). Whether they directly

mediate any signaling pathways independent of semaphorins, plexins or VEGFRs is not well known[60–62].

All plexins have a RasGAP domain through which they may inhibit Ras GTPases. In particular, A and B family plexins have been reported to inhibit R-Ras, M-Ras and Rap1 GTPases through its RasGAP domain. Although R-Ras was the first Ras GTPase reported to be regulated by plexin RasGAP domain, there is some controversy about whether it is indeed directly inhibited by plexins[63–65]. Rho GTPase binding to plexin-RBD regulates its RasGAP activity. As mentioned earlier, B-family plexins recruit PRG and LARG through their C-terminal PBD leading to activation of RhoA[66–68]. Although the interaction between Plexin PBD with the PDZ domain of the RhoGEFs is thought to be constitutive[68], GTPase binding to plexin-RBD has been reported to promote RhoA activation[69]. The molecular mechanism of GTPase regulation of plexin signaling is not well understood. This is particularly interesting since structural studies have reported minimal conformational changes upon Rac1 binding to Plexin-A1 or Plexin-B1 RBD[70]. Recently, Rac1 and Rnd1 have been reported to bind to a second region of Plexin-B1 that is proximal to the site of Ras binding. This additional interaction between Rac1 or Rnd1 with plexins has been proposed to promote a trimeric conformation of Plexin-Ras complex[71].

Group 4 semaphorins have a short intracellular region (~ 20 amino acids) and have a putative PBD in their C-terminus, which raises the possibility of a reverse signaling pathway with Plexins acting as the ligand. In immune cells, Sema4D was reported to associate with a tyrosine phosphatase CD45[72].

Sema4C and Sema4F interact with PSD-95 in neurons[73,74]. Whether these associations are dependent on plexin remains to be investigated. Recently, Plexin-B1 has been reported to act as a ligand for Sema4A, promoting interaction between Sema4A intracellular domain and Scrib through a PBD-PDZ interaction[75]. This association was proposed to competitively inhibit the formation of β-Pix-Scrib complex, leading to inhibition of Rac1 activity. This in turn has been proposed to be critical for promotion of cell migration by Plexin-B1, although how inhibition of Rac1 could lead to migration was not explained.

Family 6 semaphorins have the largest intracellular domain of all semaphorins, and some of these have proline rich sequences, which may act as docking sites for SH3 domains. Sema6D intracellular domain forms a molecular complex with ABL tyrosine kinase through its SH3 domain, and this interaction is promoted by Plexin-A1[76]. Src kinase may similarly bind with Sema6B[77]. In addition to plexins, semaphorins may also have other lower affinity receptors. For example, Sema4A and Sema4D bind with receptors TIM2 and CD75 in immune cells[78]. Whether these receptors may induce reverse signaling through semaphorins remain to be investigated. Also, the sema domains of semaphorins and plexins share certain structural homology with extracellular domains of α-integrins, and might associate with β-integrins to activate FAK or other associated kinases[60]. However, the exact nature of such association and downstream signaling needs further investigation.

Tyrosine kinase activation by plexin signaling

Semaphorins can activate tyrosine kinases through plexins, and may act as a non-canonical activator for these kinases[79]. Specific plexins may associate with different kinases, resulting in differential regulation of downstream signaling, and cellular response. These associations are dependent on the types of cells, with the same plexin associating with different kinases in different cells. In dendritic cells and pre-osteoclasts, Plexin-A1 has been reported to activate intracellular tyrosine kinase SYK through a complex formation with TREM2 and DAP12[80]. In neurons and COS-7 fibroblast-like cells, A-family plexins associate with Fes and Fyn kinases leading to growth cone or cell collapse[81]. In the cardiac system, depending on the cell type, Plexin-A1 may associate with either VEGFR2 or with OTK to promote or inhibit migratory behavior[82]. As mentioned earlier, neuropilins associate with VEGFR, and may regulate complex formation with Plexin-As[83,84]. In addition, neuropilins have been implicated in semaphorin dependent recruitment of FES and FAK kinases[85]. Sema4D has been reported to activate ErbB2 or Met through co-clustering with Plexin-B1 through their extracellular domains in different cells. Activation of either Met or ErbB2 can phosphorylate unique tyrosine residues on Plexin-B1 intracellular domain, and also have opposite effects on RhoA activation. This differential signaling leads to opposite outcomes in cell behavior, with ErbB2 activation associated with increased motility and Met activation leading to decreased motility[86–88]. Conversely, Sema5A induced association of Plexin-B3 with Met has been reported to promote both cell collapse as well as increased motility[89]. Sema4D-

Plexin-B1 signaling has also been reported to activate Src and Pyk2 kinases, although the molecular pathways connecting these molecules are not currently well understood[90].

Plexin signaling in physiology and pathology

Although semaphorins and plexins were first identified as a family of repulsive guidance molecules, they are now recognized to play different roles in different physiological systems; and dysregulation of their signaling is associated with many pathological states[91]. Indeed, semaphorins have been reported to act as both attractive and repulsive cues. For example, Sema3A may induce collapse of growth cones as well as promote neurite outgrowth[92,93]. Inhibition of Sema3A appears to support neural regeneration in instances of corneal transplant and spinal injuries[94,95]. Plexins were initially studied in the context of neuronal guidance. Consistent with their role as repulsive guidance cues, semaphorins often define regions of exclusion for corresponding plexin expressing neurons in the brain. Sema4D, Sema7A, Plexin-A1 or Plexin-B1 knock-out mice show reduced susceptibility to development of experimental autoimmune encephalitis, an experimental model for multiple sclerosis[91]. In cultured neurons, Sema4D-Plexin-B1 signaling has been proposed to regulate dendritic spine density and maturation through RhoA-ROCK signaling[96]. Sema3E-Plexin-D1 signaling has been demonstrated to negatively regulate synapse formation *in vivo*[97].

Plexins play diverse roles in angiogenesis. A-family plexins have been reported to promote angiogenesis by promoting motility of endothelial cells.

Surprisingly, this enables both fusions of smaller vessels to form large ones, as well as division of vessels to form smaller ones that are more spread out to cover a larger surface area[60]. Plexin association with VEGFR has been proposed to promote angiogenesis. Conversely, Plexin-D1 acts as a negative regulator for angiogenesis, with Sema3E marking regions of exclusion for vasculature[98,99]. Sema4A and Sema4D were the first semaphorins identified in immune cells. In addition to plexins, these semaphorins may utilize Tim2 and CD72 to modulate immune cell behavior. The major impact of plexin signaling on immune cells may be mediated by the RasGAP activity on Ras molecules and subsequent modulation of integrin engagement[60,91]. Sema4D has been reported to inhibit migration of monocytes and dendritic cells through Plexin-B1[100]. Viral semaphorins show the greatest homology with Sema7A, which is expressed by immune cells[60]. Sema7A knock-out mice show resistence to West Nile virus infection[101,102]. Vaccinia virus semaphorin (A39R) activates Plexin-C1 signaling, and has been demonstrated to inhibit migration of monocytes and dendritic cells towards virus-infected cells, and also inhibit phagocytosis[103,104]. HIV-1 infection increases Sema4D expression in dendritic cells, which may promote further infection[105].

In particular due to association with tyrosine kinases and Ras signaling, plexins have been studied in the context of cancer biology. Plexin-A1 has been implicated in promoting malignancy in lung cancers[106]. Plexin-A1 and Plexin-A4 have also been implicated in promotion of tumor growth through its promotion of angiogenesis[91,107–109]. Sema4D produced by tumor cells has been reported to

attract Plexin-B1 expressing endothelial cells into the tumor microenvironment and promote angiogenesis, leading to increased tumor growth[110,111]. However, the exact mechanism by which Sema4D may act as an attractant is remains unexplained. Knock-out of Plexin-B1 reduces instances of metastases in ErbB2-positive breast cancer in a mice model[112]. Antibody mediated inhibition of Plexin-B2 also reduced tumor growth in a mouse model[113]. Similarly, knockdown of Sema3E, or its receptor Plexin-D1 in cancer cells has been reported to reduce metastasis in a mouse xenograft model[114–116]. Semaphorins and plexins are now increasingly being investigated for their roles in skeletal biology[117]. Sema3A knock-out mice show an osteopenic phenotype[118], whereas Plexin-A1 knock-out mice have increased bone mass[80]. Sema4D, Plexin-B1 or Plexin-B1 null mice have an osteopetrotic phenotype[15,119]. Soluble Sem4D treatment has been shown to inhibit osteoblast differentiation *in vitro,* and may also regulate osteoclast function. Anti-Plexin-B1 antibodies are being investigated for therapeutic use in osteoporosis[120]. As discussed earlier, spatial regulation of cell migration is particularly relevant in the context of bone remodeling. Although there is a good deal of information available about semaphorin and plexin signaling pathways through biochemical assays, little is known about the spatial regulation of plexin signaling, which is particularly significant in its role as a repulsive guidance molecule. My work focuses on spatial regulation of Plexin-B1 signaling in osteoblasts, and its impact on directional migration. It is discussed in details in Chapter II.

Spatial control of signaling pathways

Conventional approaches of studying the impact of a ligand on cell motility usually involve ligand perfusion in culture and observing changes in cell morphology or motility. Boyden chamber assays have been utilized to characterize the response of cells to chemo-attractants and repellents. However, such assays often involve concentration gradients far beyond physiologically relevant levels, and do provide little information regarding the spatial and temporal coordination of cell polarizing events that enable directional response to these stimuli. Repulsive interactions between cells have in particular been predominantly studied by utilizing bath application of soluble ligands with an expectation of a cell or protrusion collapse as the end point. More recently, microfluidic devices have been utilized to get greater control of concentration gradients[45]; but such control often comes with the caveat of movement restricted in a single dimension. CIL has been investigated by investigating collisions between randomly migrating cells, and utilizing ligand immobilized on solid beads. Since contact between cells may engage many signaling pathways, it is difficult to establish causality utilizing cell-cell interaction, especially in the absence of stark phenotypes. Although ligand-coated beads may alleviate such concerns, collisions in a culture sparse enough to observe single cell behavior is a low probability event, which makes investigating spatial regulation of signaling events particularly difficult. Recently, optogenetic approaches have been successfully used to achieve spatial and temporal resolution in initiating signaling

pathways *in vitro* and *in vivo*. Some of these approaches are discussed in this section.

Optogenetic toolkits for cell biology

Optogenetics is generally defined as genetically encoded tools expressed in living cells (or animals) that enable the use of light to drive signaling pathways. In other words, optogenetic tools are light dependent actuators of molecular pathways. The prototypical optogenetic tool was based on plant channelrhodopsin2 that was utilized in cultured mammalian neurons to generate light mediated membrane currents[121,122]. Since then, many more optogenetic tools have been developed for use in the context of neuroscience. Genetic encoding enables expression of the light sensitive proteins in specific neurons. Since only these particular neurons are now sensitive to illumination, light can now be used as a trigger to map out the neural network and effects of specific neuronal circuits in cellular response and animal behavior. Huge strides have indeed been made in our understanding of relationship between animal behavior and specific neural circuits. In addition to the basic research and understanding, optogenetic approaches are being investigated to design light based therapies. Light dependent stimulation enables better temporal control than conventional approaches, and also allows spatial restriction of signaling pathways to subcellular regions. Furthermore, many optogenetic tools are reversible in nature, enabling investigation of cyclic activation of pathways. These particular properties make optogenetic approaches highly desirable in understanding spatiotemporal regulation of signaling pathways in cells. Optogenetic tools to activate specific

signaling cascades are usually developed using chimera proteins with light sensitive modules that undergo a desirable change upon illumination and the proteins of interest whose signaling should be activated upon illumination. In this section, I will briefly discuss some of the optogenetic modules that have been developed and utilized in the recent years to understand spatial and temporal regulation of signaling pathways in the field of cell biology.

LOV domain: The Light-Oxygen-Voltage domains are blue-light sensitive (~440-470 nm) protein domains that are found in plant, bacterial, algal and fungal species. LOV domains contain a Period-ARRNT-singleminded (PAS) domain core with a flavin cofactor. Light activation of the flavin cofactor leads to unfolding of the C-terminal J-α helix and undocking from the PAS core[123,124]. This conformational change in the LOV domain was exploited to successfully design many optogenetic modules. Photoactivatable Rac1 (PA-Rac1) based on the LOV2 domain of *Avena sativa* phototropin1 (AsLOV2) was the first genetically encoded tool for activating a small GTPase using light[125]. PA-Rac1 adopts an autoinhibited conformation in dark, wherein the LOV-domain would sterically block the effector-binding domain of a constitutively active mutant of Rac1 (Figure 7a). Upon blue light activation, the J-α helix unwinds to expose the effector-binding domain, which is now available to initiate downstream signaling cascades. Localized activation of PA-Rac1 induced membrane ruffling and directional migration in cells, *in vitro* and *in vivo*[125,126]. The AsLOV2 domain has been utilized to develop an optogenetic module (iLID) that undergoes hetero-

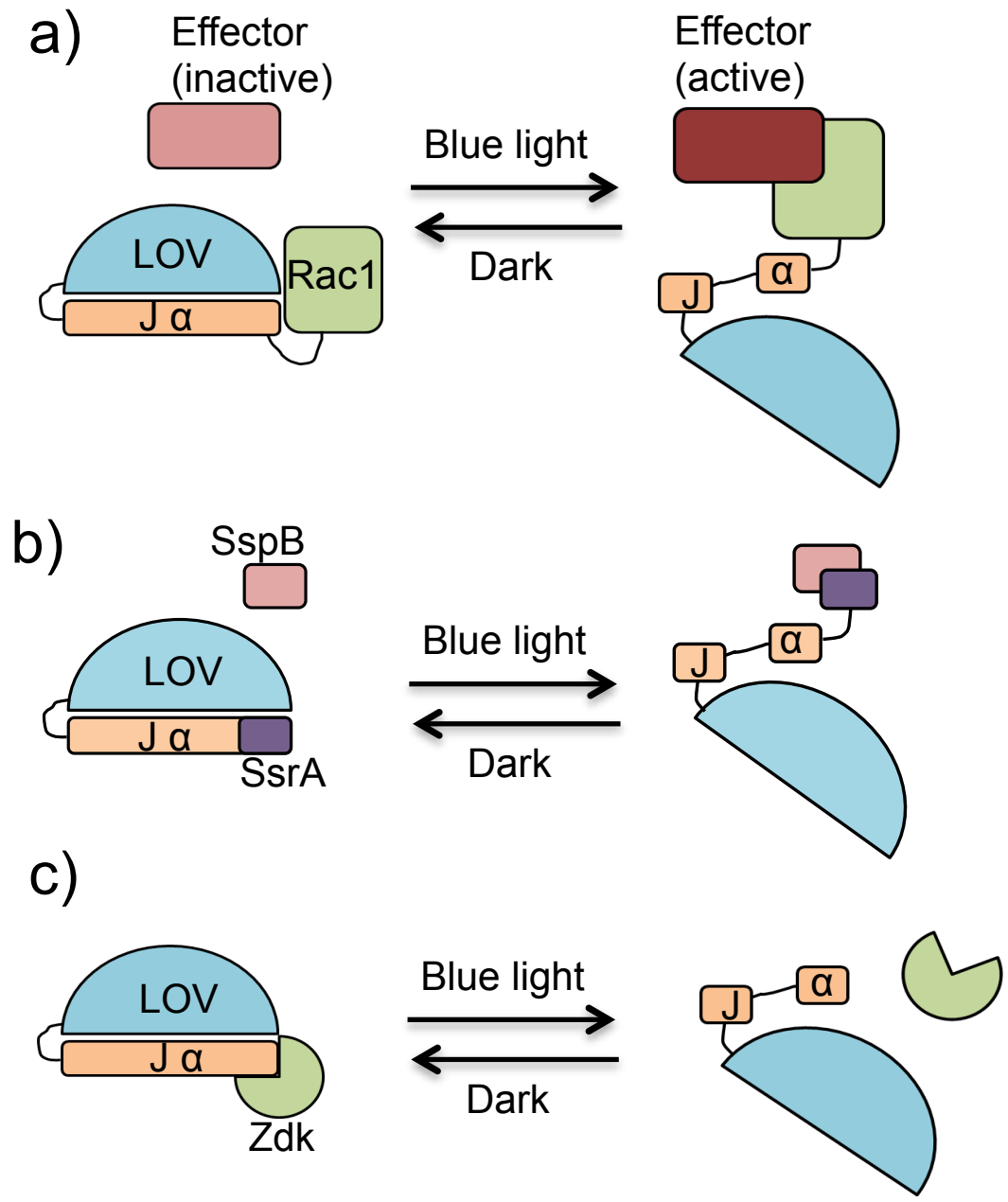

Figure 7. LOV domain based optogenetic modules. (a) Photoactivatable Rac1, and other small GTPases, (b) iLID dimerization tool and (c) LOVTRAP

dimerization upon illumination[127]. iLID dimerization module utilizes high affinity protein hetero-dimerization pairs: seven amino acid residues from bacterial SsrA protein that shows structural homology with the J-α helix was fused at the C-terminus of the helix (Figure 7b). In the dark, the J-α helix occludes the SsrA residues from binding with another bacterial protein SspB, and this inhibition was relieved upon light dependent unwinding of the J-α helix. In addition, point mutations were introduced in the AsLOV2 and SspB domains to modulate the dark and light affinity of the iLID components. The iLID dimerization module has been utilized to efficiently translocate proteins from one cellular compartment to another. Conversely, another AsLOV2 domain based optogenetic hetero-dimerization module (LOVTRAP) was recently developed that exists as a dimer in dark, and undergoes dissociation in light[128] (Figure 7c). LOVTRAP module may be utilized to sequester exogenously expressed proteins to specific cellular compartments in dark, and release them into the cytosol using light dependent dissociation.

Vivid and Magnets: Vivid (VVD) is a fungal LOV domain from the filamentous fungi *Neurospora crassa*. VVD utilizes a flavin cofactor for photoactivation, and undergoes homodimerization upon blue light activation (Figure 8a). Of the many optogenetic dimerization (or oligomerization) modules currently available, VVD is the smallest in size. However, because it forms a weak homodimer, it is difficult to use VVD for efficient and specific translocation. Furthermore, VVD has very slow dark recovery rates[129]. Recently, targeted mutations were applied to the dimerization interface of VVD to increase the

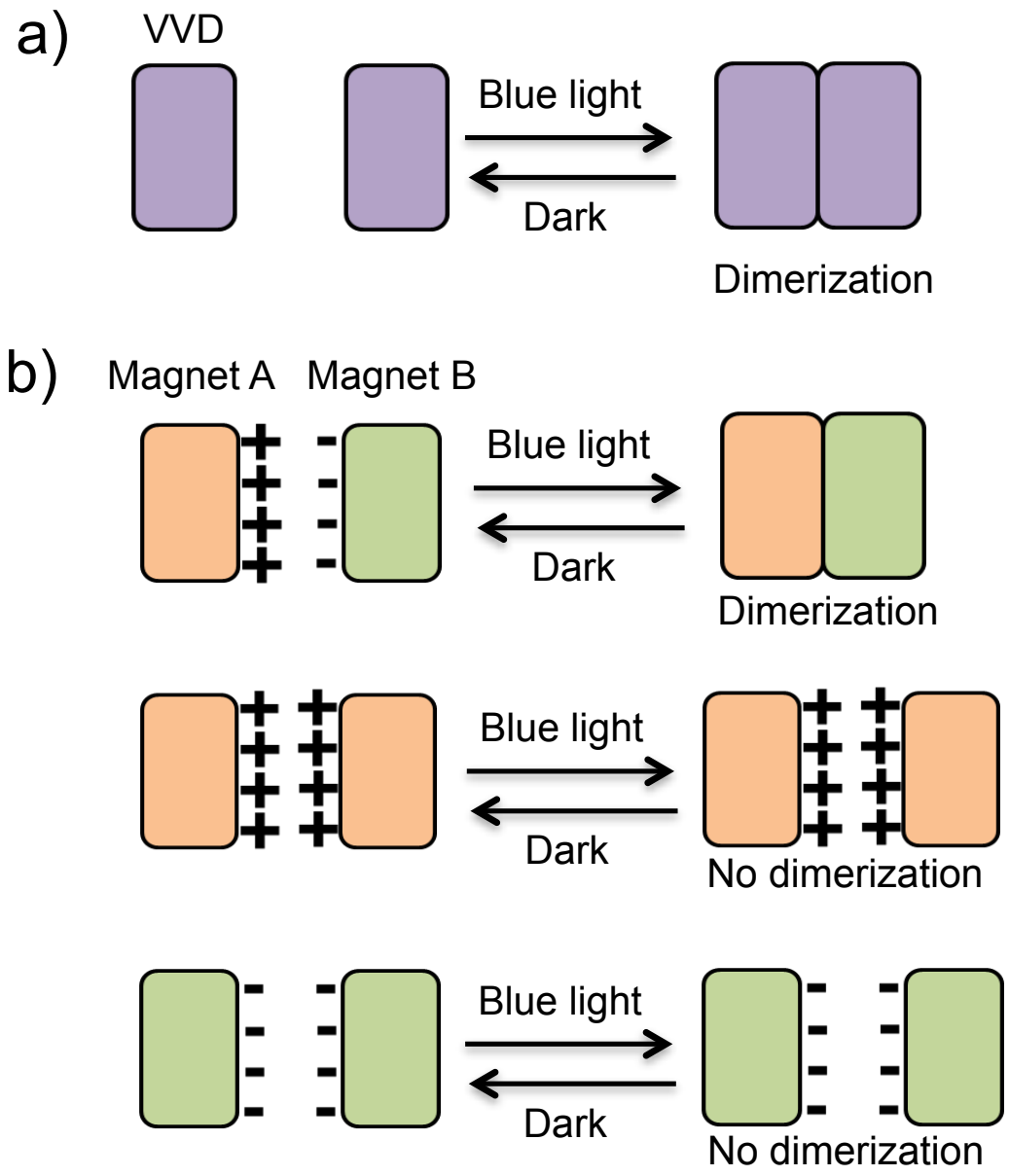

Figure 8. Vivid (VVD) based optogenetic dimerization modules. (a) VVD homo-dimerization and (b) Magnets undergoing hetero-dimerization and not homo-dimerization.

number of either positively or negatively charged residues[130]. This produced two distinct VVD variants that would preferably heterodimerize through electrostatic interactions. In addition, other mutations were applied to the VVD molecule to significantly improve its dark recovery kinetics. This new VVD based heterodimerization module is called Magnets (Figure 8b). AsLOV2, PhyB and Cry2 based dimerization modules (discussed next) have a disadvantage in that only one of the molecules is photoresponsive, and so it may be difficult to maintain a very tight spatial control due to diffusion of photoactivated dimers. Magnets have the unique property that both the molecules undergoing dimerization are photosensitive, which may enable better spatial control compared to other optogenetic modules. Unlike other dimerization modules, Magnets interact through electrostatic interactions, and that might limit their usage in case of target proteins with highly charged surfaces.

PhyB-Pif: Phytochrome B (PhyB) is another plant photoreceptor that is activated by red light (650 nm) and inactivated by far red light (~750 nm). For activation, PhyB requires a phycocyanoblin (PCB) cofactor, which is synthesized by photosynthetic organisms[131]. When exogenously expressed in mammalian cells, PCB must be externally supplied such that PhyB may auto-catalytically ligate with PCB and become photosensitive. Upon red light activation, PCB bound PhyB can bind to a transcription factor called Phytochrome interacting factor 6 (PIF6) (Figure 9). This heterodimer is stable for hours in dark, and can be induced to rapidly dissociate by illumination with far red light (~750 nm). Although the inducible reversibility of the PhyB-PIF6 toolkit is

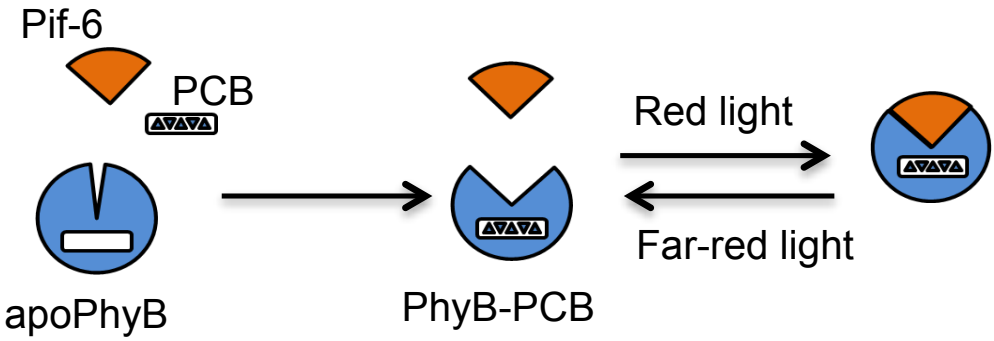

Figure 9. Phytochrome-B based optogenetic dimerization module. PhyB, Phytochrome-B. PCB, Phycocyanobilin. Pif-6, Phytochrome interacting factor 6

particularly attractive, the need to add an exogenous co-factor to 'complete' the system makes it cumbersome, especially since the purity of the PCB can have a big impact on the efficiency of light response. On the other hand, this may be used to one's advantage, since unlike other optogenetic modules, there is no need to exclude light from experimental samples until PCB is made available. Recently, biosynthetic enzymes have been designed that may be exogenously expressed in mammalian cells to produce PCB.

Cyrptochrome-2: Cryptochrome 2 (Cry2) from *Arabidopsis thaliana* is another plant photoreceptor that is activated by blue light (~400-490 nm). Cry2 utilizes endogenously expressed flavin molecule for activation. Cry2 responds to blue light by undergoing homo-oligomerization to form protein clusters (Figure 9a) and hetero-dimerization with a transcription factor Cryptochrome interacting basic helix-loop-helix protein (CIB1) (Figure 9b). These unique responses make Cry2 particularly attractive in developing light dependent hetero-dimerization and/or clustering modules[132–134]. Similar to iLID and the PhyB-PIF system, the hetero-dimerization property of Cry2-CIB1 enables recruitment of a protein of interest to a specific compartment. Cry2 has a relatively slow off-rate in dark (minutes) compared to iLID (seconds). Although this restricts the usage of Cry2 module for rapid switching between on and off states, it also allows for maintenance of localized photoactivation with lesser degree of illumination, and enables investigating changes in other signaling molecules. A point mutation that significantly enhances the oligomerization property of Cry-2 (Cry2-olig) has been utilized to activate robust clustering upon photoactivation[135].

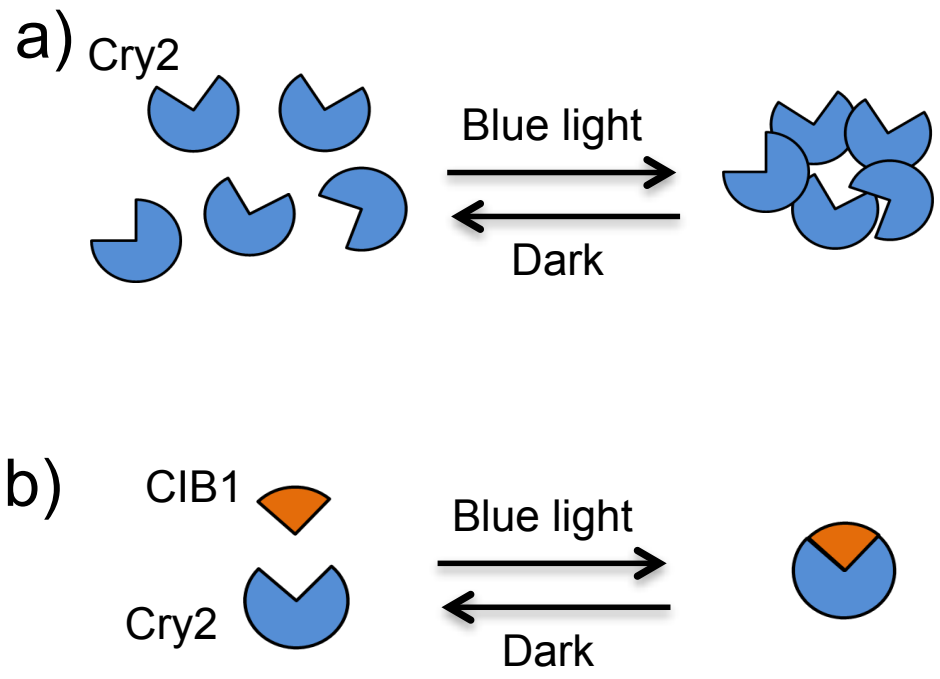

Figure 10. Cryptochrome 2 based optogenetic modules. (a) Homo-oligomerization of Cry2 and (b) heterodimerization of Cry2 with CIB1. Cry2, cryptochrome 2. CIB1, cryptochrome interacting basic helix-loop-helix protein.

All of these optogenetic modules have been utilized to develop tools to photoactivate different signaling cascades in living cells and animals, ranging from transcriptional regulation to directional migratory response. I have used the Cry2-CIB1 module for optogenetic activation of Plexin-B1 signaling in cells, and discussed the details of the tool design in Chapter II.

CHAPTER II

Optogenetic activation of Plexin-B1 reveals contact-repulsion between osteoclasts and osteoblasts

Abhijit Deb Roy, Taofei Yin, Shilpa Choudhary, Vladimir Rodionov, Carol Pilbeam, Yi I. Wu

This chapter was published in Nature Communications in its current form, with minor changes in the figure order.

Author contributions: A.D.R. initiated the project, and designed and performed most of the experiments and data analyses. T.Y. developed the DORA biosensors. S.C. characterized Sema4D and Plexin-B1 mRNA expressions, isolated BMMs and POBs, and differentiated osteoclasts for the coculture assays. Y.I.W. guided the project and wrote the final version of the manuscript based on contributions from all the authors.

Abstract

During bone remodeling, osteoclasts induce chemotaxis of osteoblasts and yet maintain spatial segregation. We show that osteoclasts express the repulsive guidance factor Semaphorin 4D and induce contact inhibition of locomotion (CIL) in osteoblasts through its receptor Plexin-B1. To examine causality and elucidate how localized Plexin-B1 stimulation may spatiotemporally coordinate its downstream targets in guiding cell migration, we develop an optogenetic tool for Plexin-B1 designated optoPlexin. Precise optoPlexin activation at the leading edge of migrating osteoblasts readily induces local retraction and, unexpectedly, distal protrusions to steer cells away. These morphological changes are accompanied by reorganization of Myosin II, PIP_3, adhesion and active Cdc42. We attribute the resultant repolarization to RhoA/ROCK-mediated redistribution of β-Pix, which activates Cdc42 and promotes protrusion. Thus, our data demonstrate a causal role of Plexin-B1 for CIL in osteoblasts and reveals a previously unknown effect of Semaphorin signaling on spatial distribution of an activator of cell migration.

Introduction

In multicellular organisms, migrating cells respond to attractive or repulsive cues to precisely control speed and directionality and reach their destination with spatial and temporal accuracy. Contact inhibition of locomotion (CIL) describes the repulsive effect on a migrating cell upon contact with another cell. CIL has been implicated in many physiological and pathological phenomena such as embryonic development, tissue patterning, collective migration and cancer metastasis. While CIL has long been observed *in vitro*[17,36,136] and recently *in vivo*[47,56,58,59,137], the precise spatial and temporal dynamics of the underlying signaling remain obscure.

Guidance molecules such as semaphorins have been proposed to mediate repulsion *in vivo*[44,66,138,139]. In vertebrates there are 5 classes of semaphorins, numbered from 3 to 7, each comprising of several members[60]. Excluding Semaphorin 3s, which are secreted, most semaphorins are either transmembrane or membrane-tethered proteins, suggesting a prerequisite role of cell-cell contact in their signaling. Semaphorins signal primarily through the Plexin family of single-pass transmembrane receptors[60]. Semaphorins interact with plexins through their respective extracellular sema domains[61,140]. The binding is thought to relieve autoinhbition of the receptor and mediate clustering of plexin intracellular domains[71,141,142]. The intracellular region of plexins contains a RasGAP domain that inactivates R-Ras[63]. B family plexins contain a PBZ binding domain (PBD) at their C-terminus through which they associate with two PDZ-domain containing RhoGEFs, PDZ-RhoGEF (PRG) and Leukemia-associated RhoGEF (LARG), and activate RhoA[67,68,143].

During bone remodeling osteoclasts release different factors to mediate chemotaxis of osteoblasts to the site of resorption[144,145,8,9]. Semaphorin 4D (Sema4D) expressed by osteoclasts, has been shown recently to regulate osteoblast-mediated bone formation[15,119]. Ablation of Sema4D or Plexin-B1 reduced the spacing between osteoclasts and osteoblasts *in vivo*[15], suggesting that osteoclasts may also repel osteoblasts, which is contrary to the paradigm of chemoattraction between the cells. Whether osteoclasts induce repulsion in osteoblasts has not been directly demonstrated and the molecular pathways that may mediate such response have not been explored.

In the current study, we demonstrate that osteoclasts repel osteoblasts upon contact and determine that CIL between these cells is dependent on Sema4D-Plexin-B1 signaling. To elucidate the spatiotemporal dynamics of Plexin-B1 downstream effectors that mediate repulsion, we develop an optogenetic tool (optoPlexin) to initiate Plexin-B1 signaling at precise times and subcellular locations. In contrast to a collapse phenotype upon whole cell activation, localized optoPlexin stimulation induces a coordinated retraction at the site of illumination and protrusions at distal regions. Similar to CIL with osteoclasts, the repulsion phenotype induced by precise optoPlexin stimulation does not alter the inherent motility of the cells. Employing biosensors for Myosin II, PIP_3 and Rho GTPases including RhoA, Cdc42 and Rac1, we define the spatial and temporal regulation of signaling downstream of Plexin-B1. Finally, we identify a novel mechanism by which Plexin-B1 coordinates cell repolarization through RhoA-ROCK mediated redistribution of β-Pix.

Results

Osteoclasts induce contact inhibition of locomotion in osteoblast.

To examine whether osteoclasts affect osteoblast migration, we isolated primary bone marrow macrophages (BMMs) and primary calvarial osteoblasts (POBs) from mice. Upon differentiation in culture, the BMMs formed multinucleated osteoclasts and were then overlaid with POBs. Similar to earlier reports, we observed that the osteoclasts pushed the obsteoblasts away upon contact[17,18]. There were physical gaps between these two cell types and the osteoblasts lacked lamellipodial protrusions toward the osteoclasts (Figure 11a, Movie 1). To investigate how osteoblast migration was altered, we performed a "wound healing" assay (Figure 12a, b) in which POBs or MC3T3-E1 cells were seeded next to osteoclasts. On removing the insert, both POBs (Movie 2) and MC3T3-E1 cells (Movie 3) formed lamellipodial protrusions and migrated towards the osteoclasts. Upon contact with osteoclasts, these protrusions rapidly collapsed, followed by formation of new protrusions away from the site of contact and a change in migration direction (Figure 11b, 12d, Movies 2, 3). In MC3T3-E1 cells, the protrusions collapsed on average 6 minutes after initiation of contact with osteoclasts and new distal protrusions formed about a minute after (Figure 13a). While the migration speed before and after contact remained unaltered (Figure 13b), the contact acceleration index (Cx, see methods for details) showed a clear reversal of migration direction with respect to the trajectory before contact (negative values). The Cx approached zero prior to contact indicating directional

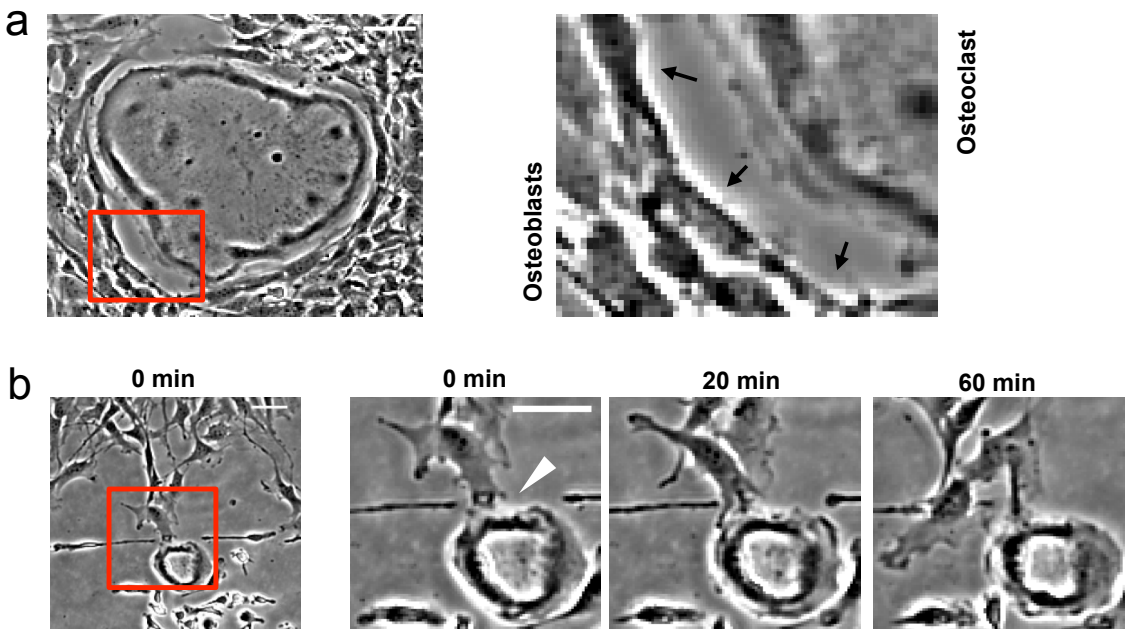

Figure 11. Osteoclasts repel osteoblasts on contact. (a) Phase contrast images showing separation between osteoclasts and osteoblasts in a co-culture. The inset (106 µm X 92 µm) is magnified on the right panel to show the gap between the osteoclast and the osteoblasts and the lack of protrusions in osteoblasts. The arrows point towards the osteoblasts. (b) Phase contrast images showing contact between an osteoblast and an osteoclast. The inset is magnified to show changes in cell morphology and migration between time of contact and 20 and 40 minutes after contact. White triangle points to the site of cell-cell contact. Scale bar, 50 µm.

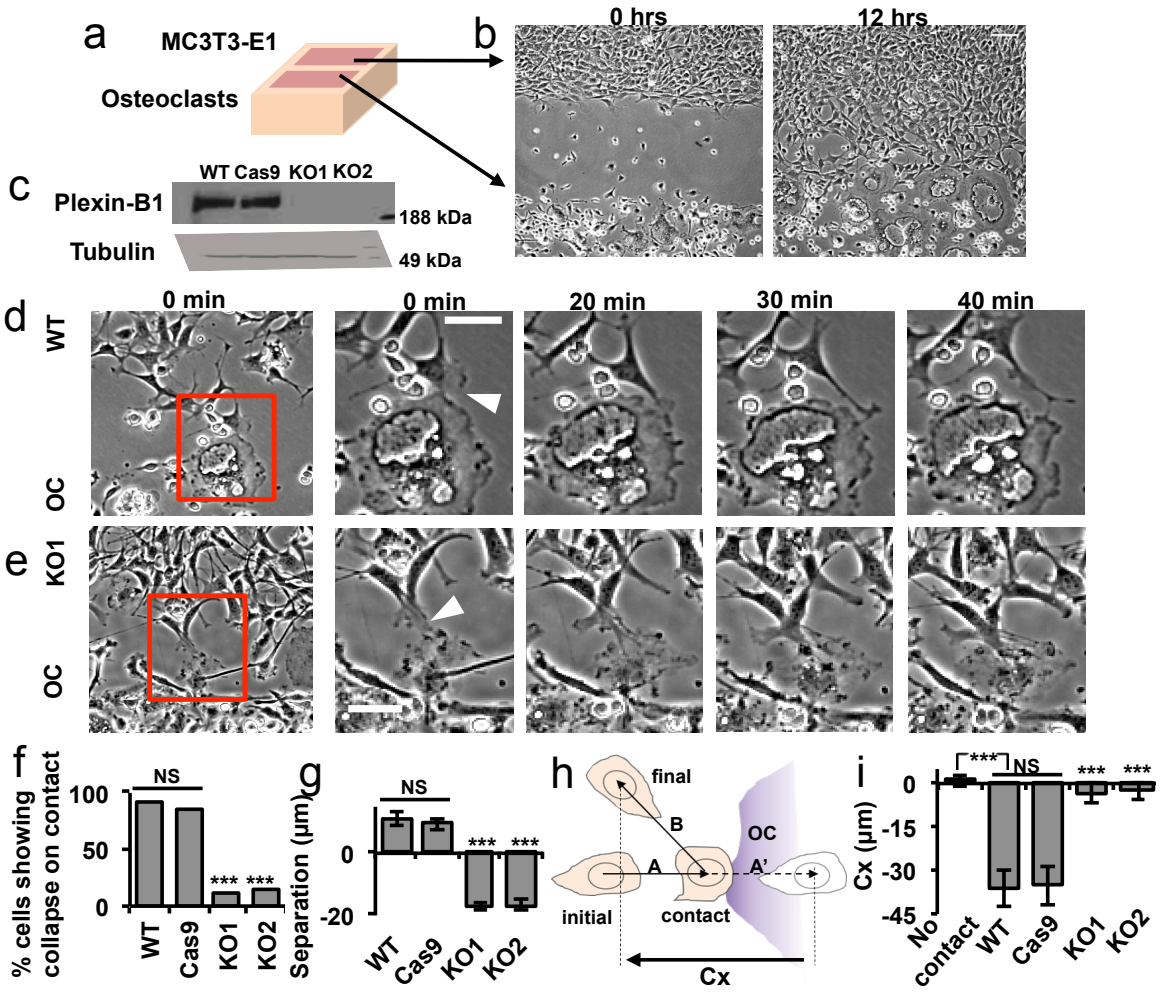

Figure 12. Plexin-B1 mediates CIL between osteoclasts and osteoblastic cells. (a) Cartoon representation of culture inserts used for co-culture of osteoclasts with primary osteoblasts or MC3T3-E1 cells. (b) Phase contrast images acquired immediately and 12 hours after lifting the culture insert showing migration of MC3T3-E1 cells towards osteoclasts. Scale bar, 50 µm. (c) Comparison of Plexin-B1 expression in wild type (WT), Cas9, KO1 and KO2 MC3T3-E1 cells. Tubulin was used as a loading control. (d), (e) Phase contrast images showing a MC3T3-E1 WT (d) or MC3T3-E1 KO1 (e) cell in contact with an osteoclast (OC). Insets are magnified to show changes in cell morphology and migration between time of contact and 20, 30 and 40 minutes after contact. Scale bar, 50 µm. White triangles point to the site of cell-cell contact. (f) Percentage of WT, Cas9, KO1 and KO2 MC3T3-E1 cells that show collapse of protrusions within 30 minutes after contact with an osteoclast. n = 209-301. (g) Separation between MC3T3-E1 cells and osteoclasts 40 minutes after contact. n = 41-45. (h) Cartoon describing contact acceleration index (Cx). (i) Cx values for WT cells, Cas9, KO1 and KO2 MC3T3-E1 cells without (WT only) and after contact with osteoclasts. n = 20. For g and I means ± s.e.m. are shown. *** $p<0.001$, * $p<0.05$, NS, not significant, Student's t-test.

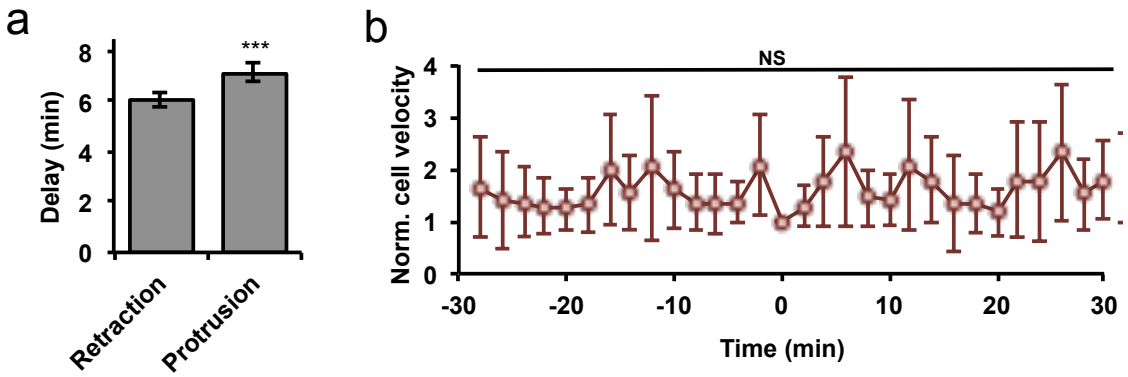

Figure 13. Characterization of CIL between osteoclasts and osteoblasts (a) Delay in initiation of retraction at the site of contact and initiation of new distal protrusions in WT MC3T3-E1 cells upon contact with osteoclasts. n=85 cells, mean ± s.e.m. are shown. (b) Velocities of MC3T3-E1 cells coming in contact with osteoclasts, normalized to the velocity right before contact at time 0 . n=29 cells, mean ± s.e.m. are shown. *** $p<0.001$, * $p<0.05$, NS, not significant.

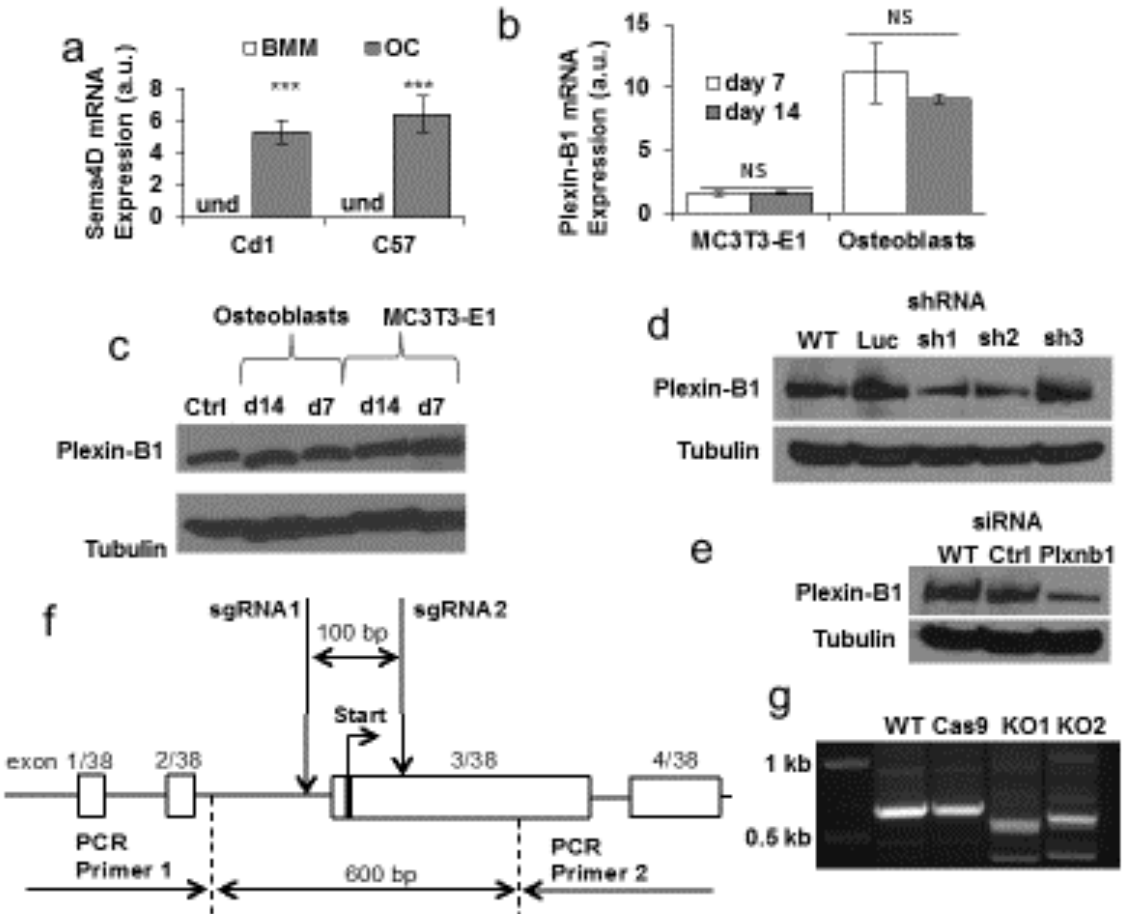

Figure 14. Sema4D/Plexin-B1 expression and knock-out strategy (a) Comparison of Sema4D mRNA expression in pre-osteoclasts (BMMs treated with M-CSF) and osteoclasts (BMMs treated with M-CSF and RANKL) from Cd1 and C57BL/6 mice. Osteoclastogenesis was confirmed by visual inspection of formation of multinucleated cells on fourth day of RANKL treatment. und, undetectable. (b) Comparison of Plexin-B1 mRNA expression in MC3T3-E1 cells and primary calvarial osteoblasts from C57BL/6 mice. mRNA were extracted after 7 and 14 days of phosphoascorbate mediated differentiation. (c) Comparison of Plexin-B1 expression in MC3T3-E1 and pimary calvarial osteoblasts from C57BL/6 mice after 7 and 14 days of maintenance in differentiating media. COS-7 cells overexpressing Plexin-B1 were used for positive control. (d) Comparison of Plexin-B1 expression in WT MC3T3-E1 cells and MC3T3-E1 cells stably expressing shRNA against Luciferase (Luc) or Plexin-B1 (sh1, sh2 and sh3). (e) Comparison of Plexin-B1 expression in WT MC3T3-E1 cells and cells transiently transfected with a non-targeting siRNA pool (Ctrl) or Plexin-B1 siRNA pool (PlxnB1). (f) Cartoon representation of the sgRNA design strategy for CRISPR-Cas9 mediated Plexin-N1 knock out (see main text). (g) Comparison of PCR product using primer 1 and 2 on genomic DNA in WT, Cas9, KO1 and KO2 MC3T3-E1 cells to probe for deletion targeted by sgRNA1 and sgRNA2. For a & b means ± s.e.m. are shown, n=3 wells of cells. *** $p<0.001$, * $p<0.05$, NS, not significant. For c, d and e tubulin was used as a loading control.

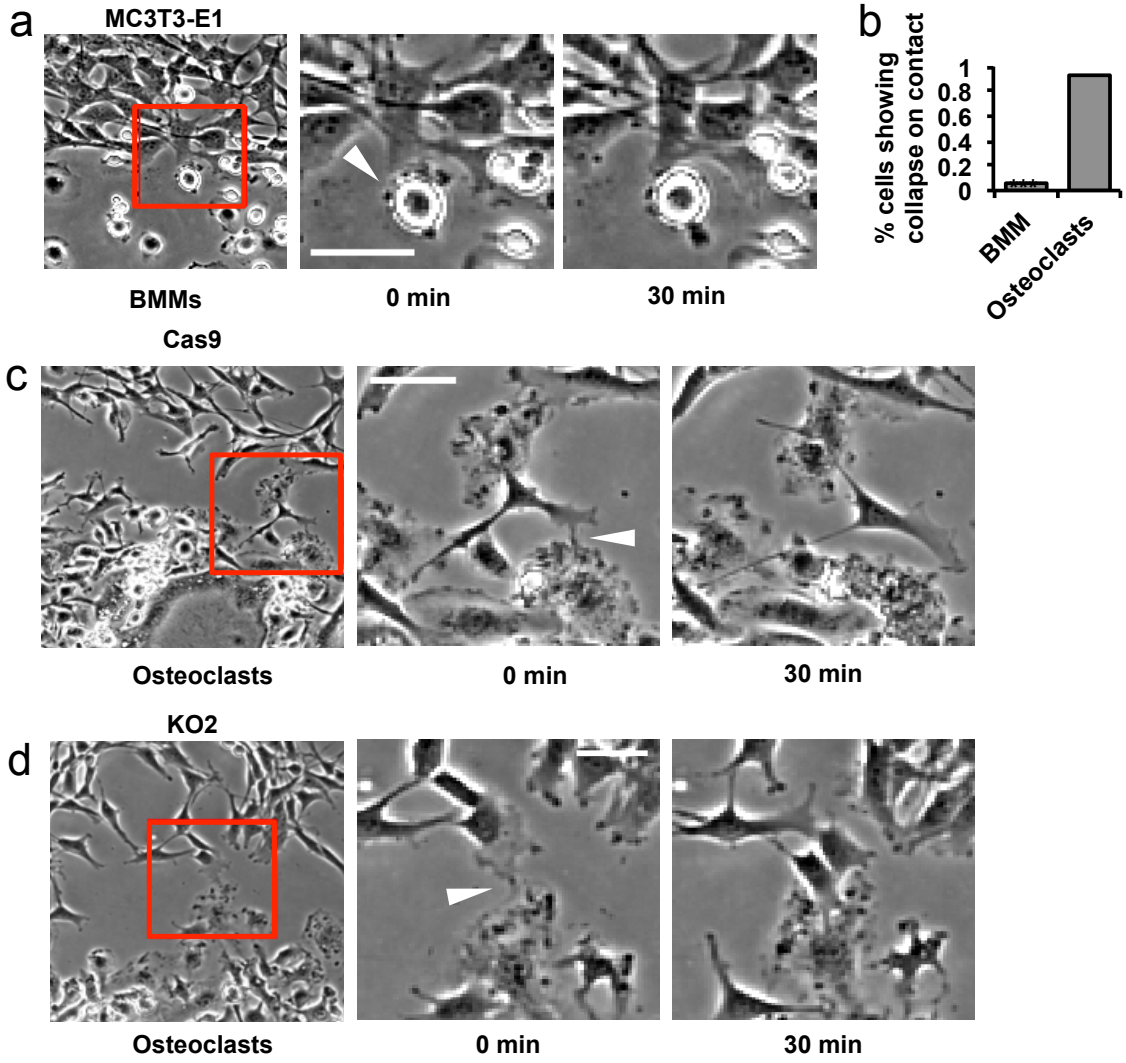

Figure 15. Pre-osteoclasts do not induce CIL in osteoblasts (a) Phase contrast images showing contact between a MC3T3-E1 cells and a BMM. (b) Percentage of MC3T3-E1 cells that show collapse of protrusions within 30 minutes after contact with a BMM or an osteoclast. n ≥ 40. ***, p<0.001. (c), (d) Phase contrast images showing contact between MC3T3-E1 Cas9 (c) or MC3T3-E1 KO2 (d) cell and an osteoclast. The inset is magnified to show changes in cell morphology and migration between time of contact and 30 minutes after contact. Scale bar, 50 µm. White triangles point to the site of cell-cell contact.

Name	Sequence	Description
sgRNA1 - Fw	CACCGACAGTCCTGTCCCGTAGCAT	sgRNA1 forward primer
sgRNA1 - Re	AAACATGCTACGGGACAGGACTGTC	sgRNA1 reverse primer
sgRNA2 - Fw	CACCGCCGCAGGGTGACGACACACC	sgRNA2 forward primer
sgRNA2 - Re	AAACGGTGTGTCGTCACCCTGCGGC	sgRNA2 reverse primer
PCR Primer 1 - Fw	AAGGAACAAGATTGAGTGTGG	Forward primer upstream of sgRNA1
PCR Primer 2 - Re	CCTGATCTGTCCCAGGCTCCG	Reverse primer downstream of sgRNA2
Sequencing primer	GCCTCTGGGCTCACCAGGAGC	primer (reverse) for sequencing PCR product

Table 1. List of primers used for CRISPR-Cas9 mediated Plexin-B1 knock-out

persistence (Figure 12h, i). Thus our data indicates that osteoclasts induce CIL in obsteoblasts without compromising their intrinsic motility.

Plexin-B1 mediates osteoclast-induced CIL in osteoblasts

Sema4D is expressed by BMMs upon differentiation to osteoclastic lineage using Receptor activator of nuclear factor κ-B ligand (RANKL). Consistent with previous reports[15,119], Sema4D expression was undetectable in BMMs, but was markedly increased during RANKL-mediated osteoclastogenesis (Figure 14a). In support of a role of Sema4D in CIL, BMMs failed to induce collapse of protrusions or change in direction of migration in MC3T3-E1 cells (Figure 15a, b, Movie 4). Both POBs and MC3T3-E1 cells expressed Plexin-B1 and no significant changes were observed in mRNA or protein levels upon differentiation (Figure 12c, 14b, c). To examine whether CIL between MC3T3-E1 and osteoclasts was mediated by Plexin-B1, we conducted knock-down experiments with several independent shRNA lentivirus, siRNA pools as well as CRISPR/Cas9-mediated knock-out experiments. Despite our best efforts, only modest silencing of protein expression (Figure 14d, e) was achieved with siRNA and shRNA without compromising cell motility. In contrast, the CRISPR/Cas9 mediated knockout approach (see Methods for details) completely eliminated Plexin-B1 expression (Figure 12c). Two Plexin-B1 null MC3T3-E1 clones, KO1 and KO2, were used in cell migration assays. Cas9 expression alone did not affect Plexin-B1 expression (Figure 12c), nor did it alter osteoclast-mediated contact repulsion of MC3T3-E1 cells (Figure 12f, 15c, Movie 5). KO1 and KO2 cells failed to show collapse of protrusions upon contact with osteoclasts and maintained contact with osteoclasts for prolonged periods of

time (Figure 12e, f, 15d, Movies 6, 7). Furthermore, KO1 and KO2 cells did not migrate away from the osteoclasts (Figure 12g). Finally, comparison of Cx values (Figure 12i) indicated that in contrast to WT and Cas9 cells, KO1 and KO2 cells failed to undergo repulsion after contact. Thus our data demonstrated that Plexin-B1 is required for CIL in osteoblastic MC3T3-E1 cells.

Development of an optogenetic tool for the Plexin receptor

To activate Plexin-B1 in osteoblasts, we initially attempted several Sema4D ligand based approaches. Perfusion of soluble Sema4D-Fc ligand induced RhoA activation in MC3T3-E1 cells and cell collapse as indicated by loss of protrusions and decrease in total cell area (Figure 16). Contact between osteoclasts and osteoblasts may initiate Sema4D-Plexin-B1 signaling specifically at the site of contact. To understand the role of Plexin-B1 in CIL, we locally pumped Sema4D-Fc near protrusions of POBs using a microinjection pipette (Figure 17). The cells responded with a blunted protrusion or retraction locally and 4 out of 5 times produced a new protrusion(s) in distal regions, which is consistent with CIL. In contrast, no significant morphological changes were observed with control IgG1 (Figure 17). Because it is difficult to confine soluble ligand in the medium, we used immobilized Sema4D-Fc on silica beads as localized sources of Sema4D stimulation. Despite rapidly clustering Plexin-B1 on the plasma membrane (Figure 18, Supplementary Movie 8), the Sema4D-Fc beads failed to induce RhoA activation, morphological changes or even recruit RhoGEFs (Figure 19, 20, see Methods for details).

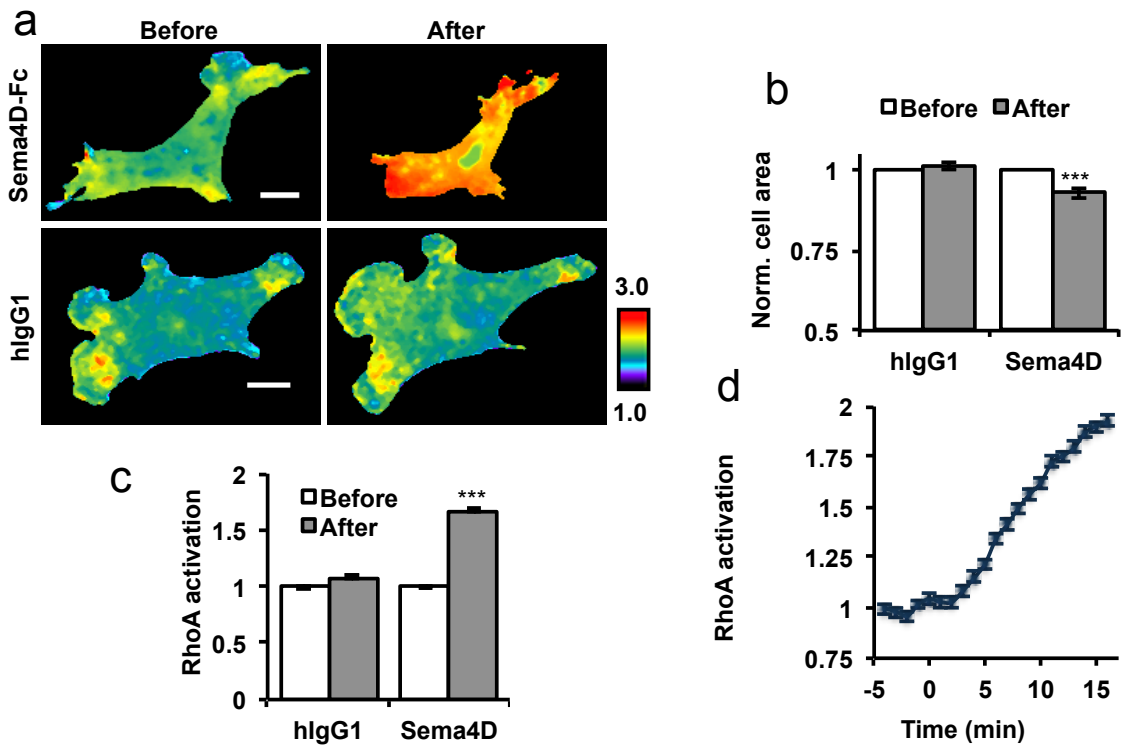

Figure 16. Sema4D induces RhoA activation and cell collapse in osteoblastic cells. (a) Ratiometric images showing changes in morphology and RhoA activation in MC3T3-E1 cells expressing DORA-RhoA on treatment with 200 nM Sema4D-Fc or hIgG1. Scale bar, 10 µm. (b) Changes in cell area of MC3T3-E1 cells treated with 200 nM Sema4D-Fc or 200 nM hIgG1, normalized to cell area before treatment. n ≥ 11 cells. (c) Changes in RhoA activity of MC3T3-E1 cells treated with 200 nM Sema4D-Fc or 200 nM hIgG1, normalized to activities before treatment. n ≥ 11 cells. (d) Temporal changes in RhoA activity in MC3T3-E1 cells treated with 200 nM Sema4D-Fc. n=17 cells. For b,c and d means ± s.e.m. are shown. *** $p<0.001$, * $p<0.05$, NS, not significant.

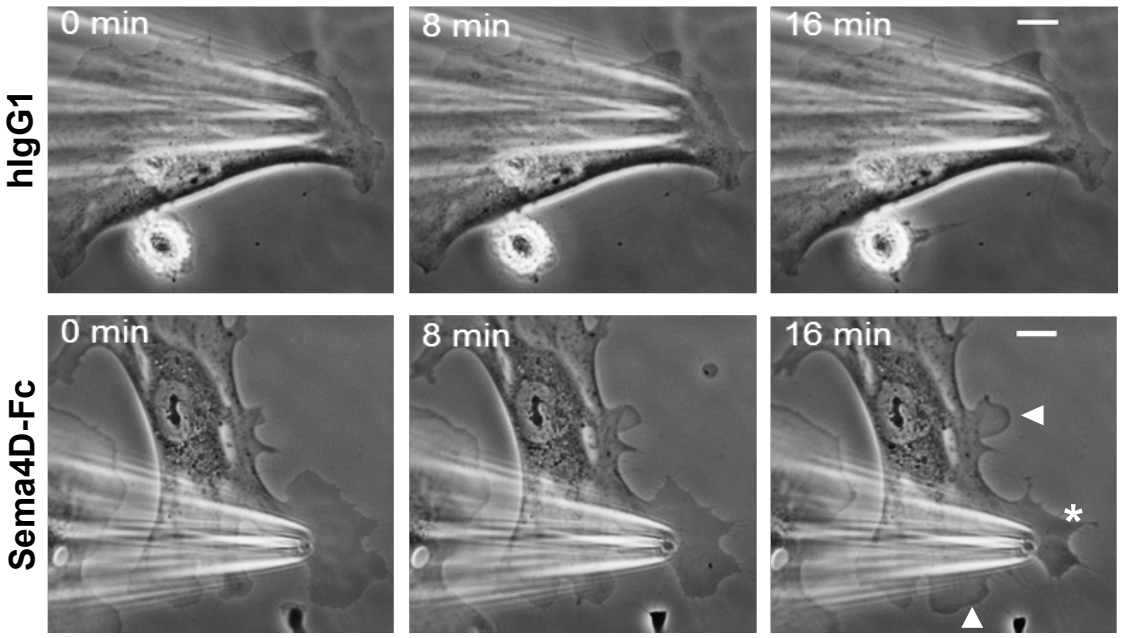

Figure 17. Localized perfusion of Sema4D induces CIL-like repolarization in primary osteoblasts. Representative DIC images showing changes in morphology in murine calvarial osteoblasts from C57BL/6 mice upon localized Sema4D-Fc or hIgG1(control) perfusion. Calvarial osteoblasts were differentiated for 7 days before imaging. 1 µM Sema4D-Fc or hIgG1 was perfused at protrusions using positive pressure through a micropipette. Local perfusion of Sema4D-Fc induced local retractions and distal protrusions in osteoblasts (4 out of 5). No morphological changes observed in response to local perfusion of hIgG1 (3 out of 3). Scale bar, 10 µm. Asterisk, induced retraction. Arrowhead, induced protrusion.

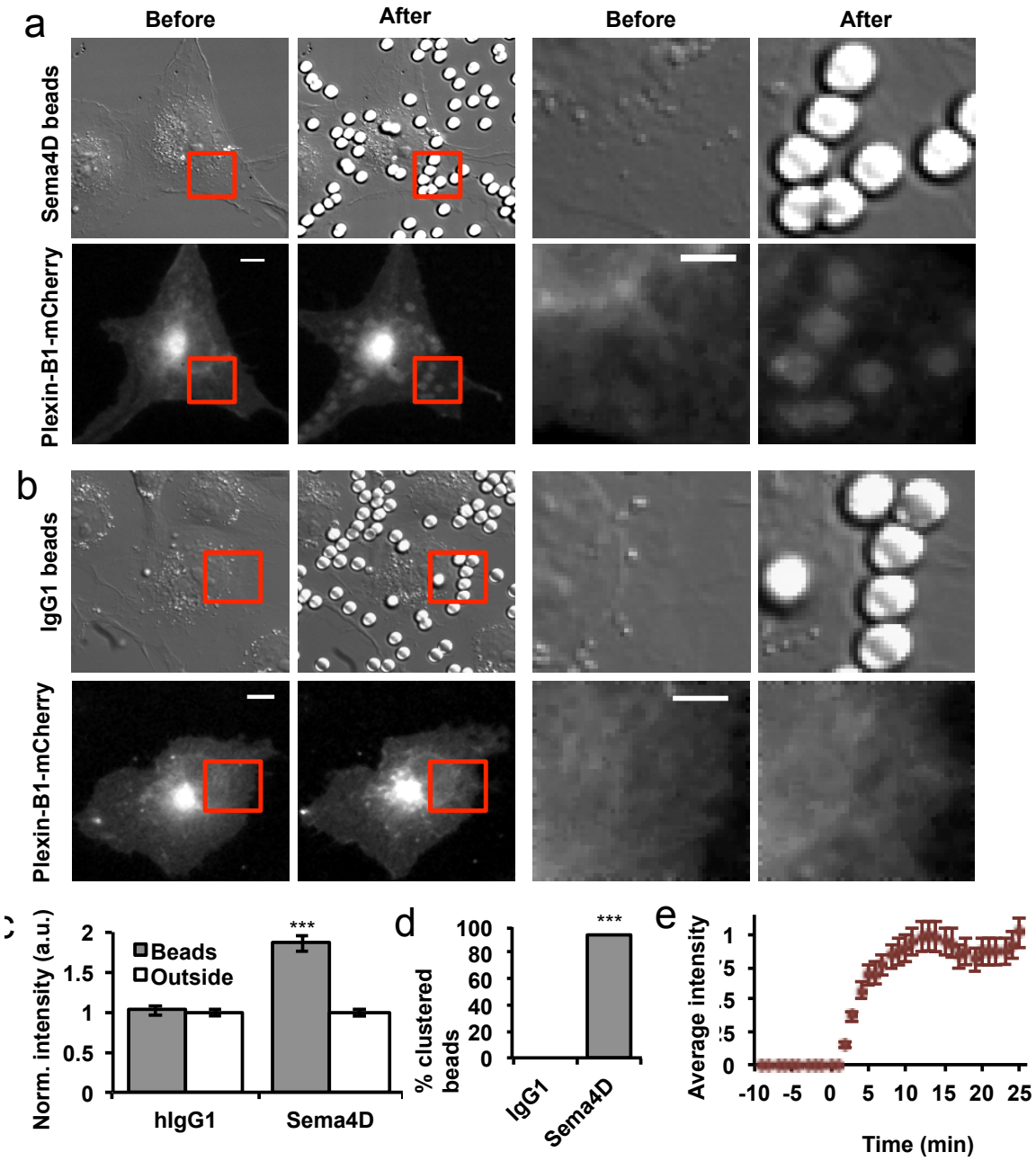

Figure 18. Sema4D immobilized on silica beads clusters Plexin-B1. DIC and wide-field fluorescent images showing changes in Plexin-B1-mCherry distribution in COS-7 cells before and 10 minutes after contact with Sema4D-Fc (a) or hIgG1 (b) immobilized on silica beads. Scale bar, 10 µm. The insets are magnified to show changes in distributionPlexin-B1-mCherry around Sema4D-Fc beads or hIgG1 beads. Scale bar, 5 µm. (c) mCherry intensity in 5 µm circle around beads and beads free cell body after 10 minutes of contact with beads, normalized to intensity in beads free regions. n ≥ 70 regions, mean ± s.e.m. are shown. (d) Percentage of beads that show clustering of mCherry around it. n ≥ 230 beads. (e) Temporal changes in Plexin-B1-mCherry clustering around Sema4D-Fc beads. n= 5 cells, mean ± s.e.m. are shown. ***

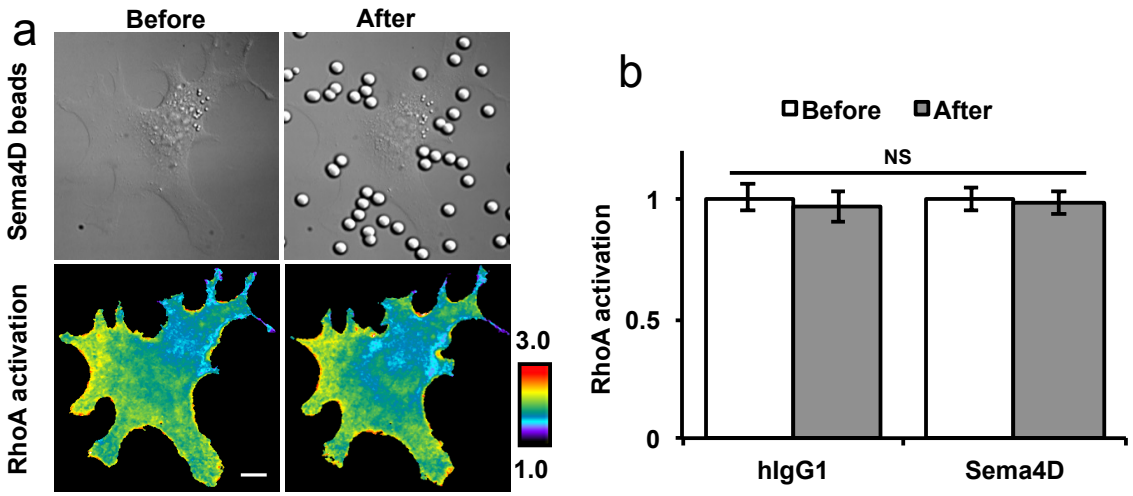

Figure 19. Sema4D immobilized on silica beads fails to activate RhoA (a) DIC and ratiometric images showing changes in morphology and RhoA activation in MC3T3-E1 cells expressing DORA-RhoA before and after contact with Sema4D-Fc beads. Scale bar, 10 µm. (b) Changes in RhoA activity of MC3T3-E1 cells after 10 minutes of contact with Sema4D-Fc of hIgG1 beads, normalized to activities before contact. n ≥ 7 cells, means ± s.e.m. are shown. *** $p<0.001$, * $p<0.05$, NS, not significant.

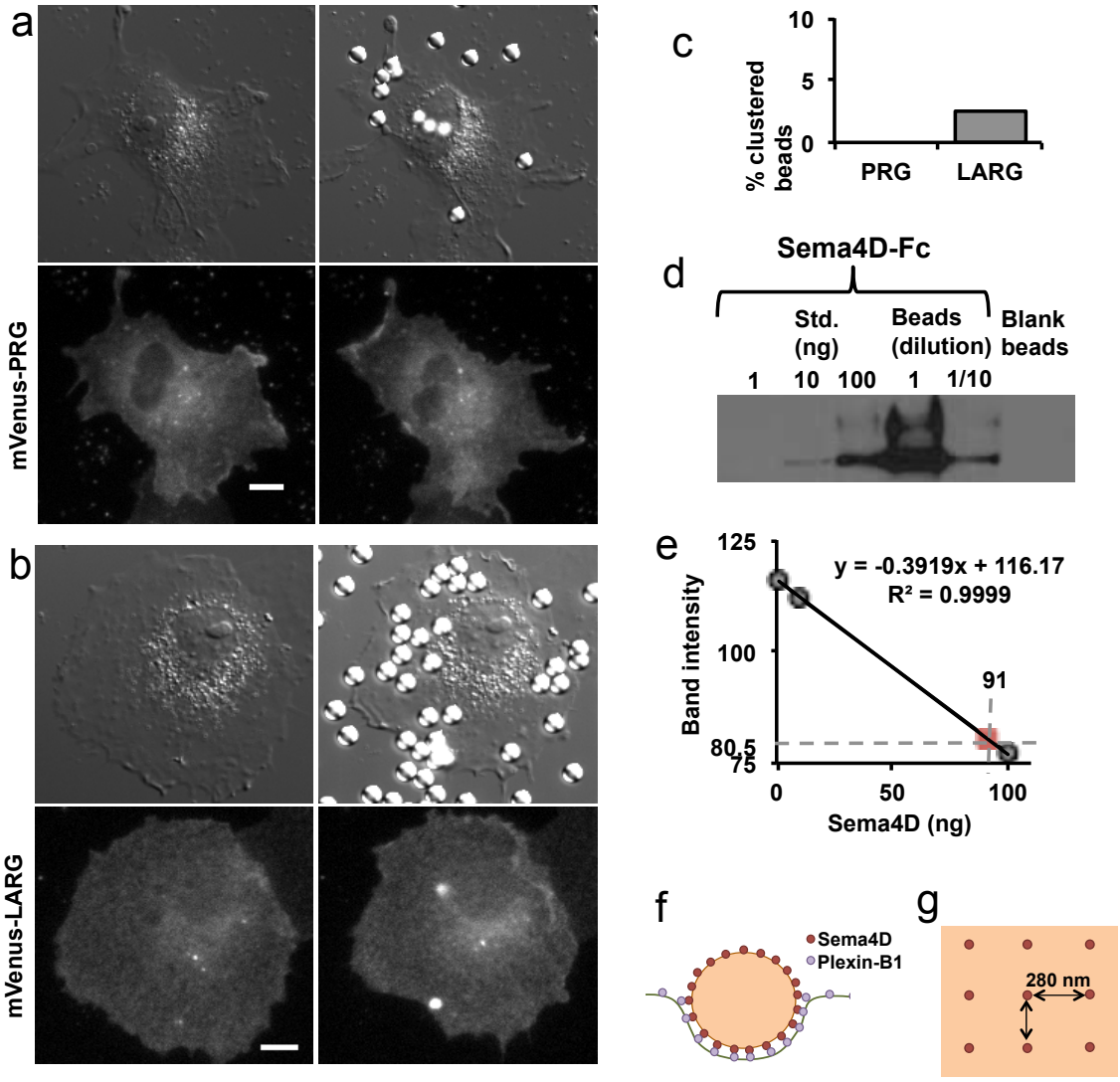

Figure 20. Sema4D immobilized on silica beads fails to recruit RhoGEFs. DIC and wide-field fluorescent images showing changes in mVenus-PRG (a) or mVenus-LARG (b) distribution around Sema4D-Fc beads in COS-7 cells exogenously expressing Plexin-B1 with mVenus-PRG or mVenus-LARG. Scale bar, 10 µm. (c) Percentage of beads that show mVenus clustering around it. n ≥ 90 beads. (d) Comparison of Sema4D-Fc bound to silica beads. (e) Analysis of the western blot in (c) to assess the amount of Sema4D-Fc bound to the silica beads. Gray circles indicate the standards. Red square corresponds to the intensity of the beads dilution 1/10. (f) Cartoon representation of hemisperic contact between Sema4D-Fc silica beads and cells and subsequent Plexin-B1 clustering around the beads. (g) Cartoon representation of the estimated distance between Sema4D-Fc molecules immobilized on a silica beads.

To mimic local initiation of Sema4D signaling, we used an optogenetic approach to activate the plexin receptor. We took advantage of the observations that both the RasGAP activity of Plexin-B1 and its activation of RhoA require its localization to the plasma membrane and that semaphorin-dependent clustering of plexin promotes its activation[71,141,142]. A recently characterized optogenetic module Cryptochrome-2 (Cry2) was used with a farnesylated Cryptochrome interacting basic helix-loop-helix 1 (CIB1-CAAX), to induce a plasma membrane translocation of cytosolic proteins in response to blue light[132]. Furthermore, Cry2 oligomerizes in light, and could be used to induce protein clustering[133]. We constructed a chimera protein containing Cry2 at the N-terminus, followed by a fluorescent protein (mCherry or mVenus), and finally the intracellular domain Plexin-B1 at the C-terminus (Figure 21), which preserved its interaction with PRG and LARG. Full-length Cry2 was used to minimize background activity in the dark[37]. Because the engineered Plexin-B1 was designed to be activated by light instead of Sema4D ligand, we named it optoPlexin (Figure 21, 22a).

To examine whether optoPlexin undergoes a plasma membrane translocation in response to light stimulation, we co-expressed mCherry-optoPlexin and CIB1-CAAX in COS-7 cells and used total internal reflection fluorescence (TIRF) microscopy to gauge the membrane association of optoPlexin. Upon blue light (440 nm LED) illumination over the entire cell, mCherry intensity increased immediately after the first pulse of illumination. The rate of increase appeared to be at a similar time scale as Cry2 alone and, with our illumination protocol of 10 second intervals, reached half maximal intensity within three pulses, indicating a

rapid recruitment of optoPlexin to the plasma membrane (Figure 22b top panel, 23, Supplementary Movie 9 left panel). The average increase in the intensity of optoPlexin and optoPlexin mutants (Figure 21) were close to two-fold, indistinguishable from that of Cry2 alone (Figure 22c, 24). Additionally, optoPlexin formed clearly visible fluorescent aggregates, indicating clustering of optoPlexin (Figure 22d, Figure 25). A flavin adenine dinucleotide (FAD)-deficient mutant of Cry2 (D387A) that does not absorb blue light[146] failed to recruit optoPlexin (Supplementary Movie 9 right panel). Since a lack of FAD may potentially compromise the folding of Cry2 or optoPlexin, we also examined an alternate mutation of Cry2 (D393A) which preserves the FAD-binding pocket but eliminates the proton donor (Asp^{393}) for FAD and blocks signal transduction of crytochrome in plants[147,148]. No membrane recruitment took place for either Cry2 alone or optoPlexin carrying the D393A mutation (Figure 22c), demonstrating that the observed effects were specific to the photoreaction of Cry2. More effective recruitment, an average induction of 4-fold within the region of illumination (Figure 22b,c), was observed when illumination was limited to a 5 μ c-diameter circle within the cells. These data demonstrated that optoPlexin can be efficiently recruited to the plasma membrane and cluster in response to light stimulation.

Robust activation of RhoA by optoPlexin on light stimulation

Upon Sema4D stimulation, Plexin-B1 interacts with and activates PRG or LARG through its C-terminal PBD and consequently activates RhoA[66,68,143]. To test whether optoPlexin could interact with PRG and LARG, we examined the membrane recruitment of these two RhoGEFs by co-expressing mVenus-PRG or

mVenus-LARG in COS-7 cells. Upon whole-cell illumination, we observed a rapid, concurrent co-recruitment of PRG (Figure 26a, b, Supplementary Movie 10) or LARG (Figure 26b) with optoPlexin to the plasma membrane. The kinetics of PRG recruitment and dissociation from the membrane closely followed that of optoPlexin. Co-recruitment of PRG was reversible upon pausing blue light illumination, and repeatable with a second round of illumination (Supplementary Figure 23). An increase in fluorescence of 26% ± 3% and 60% ± 6% (mean ± s.e.m.) relative to that of optoPlexin were observed for PRG and LARG respectively (Figure 26b), suggesting an efficient recruitment of RhoGEFs to the plasma membrane by optoPlexin. Since optoPlexin may also interact with endogenous PRG and LARG, the extent to which signals were transmitted from optoPlexin to these two RhoGEFs were most likely underestimated. When Cry2 alone was used as a control, no membrane recruitment of these two RhoGEFs was detected (Figure 26b). Illumination of cells expressing a PBD-truncated mutant (delPBD) (Figure 21) showed no increase of PRG levels on the plasma membrane (Figure 26c) indicating that PBD-PDZ interaction mediates RhoGEF association with optoPlexin. The interaction between optoPlexin and PRG did not appear to be constitutive. Upon illumination PRG formed quantifiable aggregates (see Methods for details) along with optoPlexin in addition to membrane recruitment (Figure 25). When we omitted the CIB-CAAX from optoPlexin, the clustering of optoPlexin remained visible using TIRF imaging but we did not detect any clustering of PRG (Figure 26d, e), suggesting that membrane translocation is critical for activation of optoPlexin.

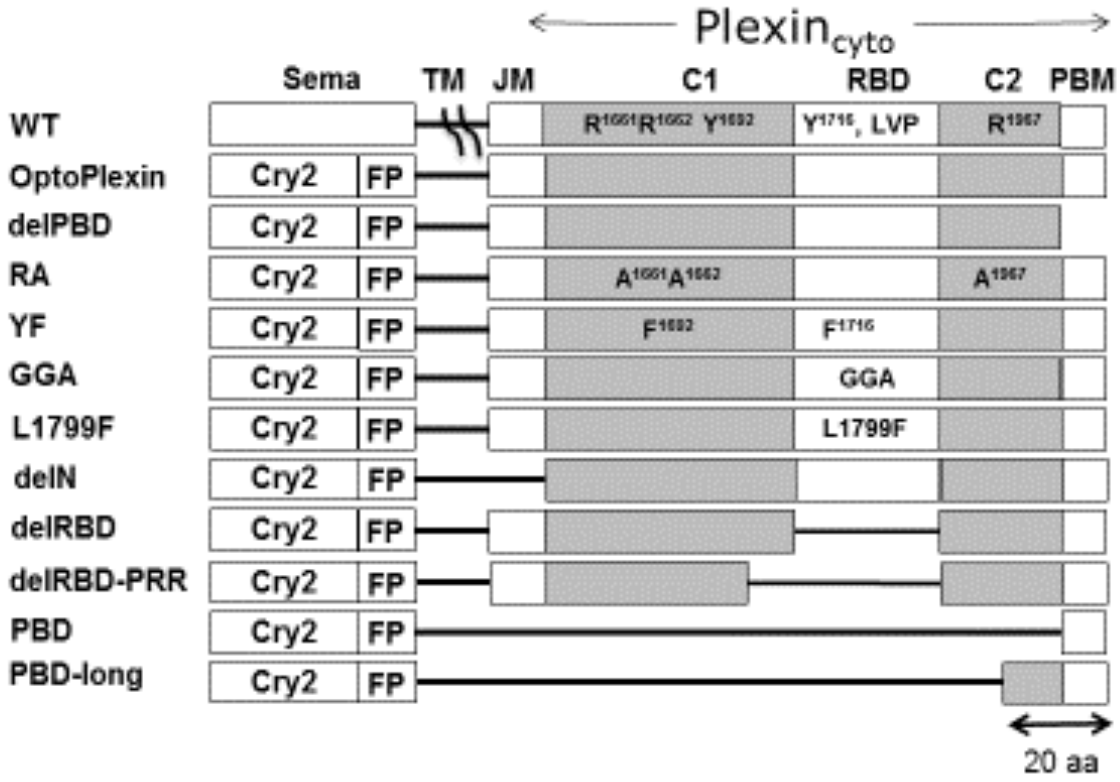

Figure 21. Functional domains of optoPlexin and its variants. A diagram depicting the domain organization of Plexin-B1, optoPlexin and its mutants. Plexin$_{cyto}$, intracellular domain of Plexin-B1. WT, wild type. Sema, Sema domain. TM, transmembrane region. JM, juxtamembrane region. C1 and C2, N and C-terminal halves of Plexin-B1 RasGAP domain. RBD, Rho GTPase binding domain that binds to Rac1 and Rnd1. PBD, PBZ binding domain. FP, fluorescent protein. PRR, proline rich region. aa, amino acids.

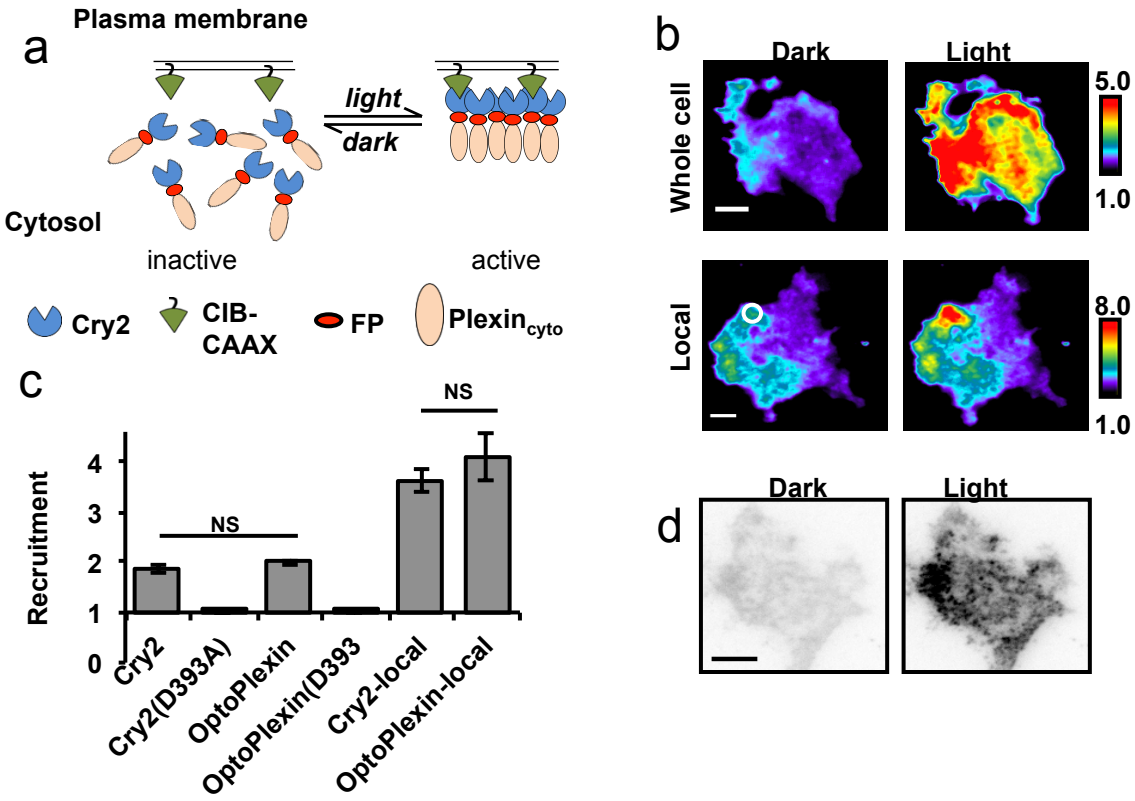

Figure 22. Design and characterization of optoPlexin. (a) Cartoon representation of the optoPlexin design (see main text). FP, fluorescent protein, Plexin$_{cyto}$, cytosolic domain of Plexin-B1. (b) TIRF images showing the plasma membrane recruitment of mCherry-optoPlexin in COS-7 cells after one minute of whole cell or local illumination (440 nm and 50 ms pulse at 0.1Hz, unless otherwise stated). Scale bar, 10 µm. White circle, region of illumination. (c) Quantification of the recruitment levels of Cry2, Cry2(D393A), optoPlexin and optoPlexin(D393A) on whole cell or localized blue light illumination in COS-7 cells. n = 12-20, means ± s.e.m. (d) TIRF images showing the clustering of mCherry-optoPlexin after one minute of whole cell illumination in COS-7 cells. Scale bar, 10 µm. NS, not significant, Student's t-test.

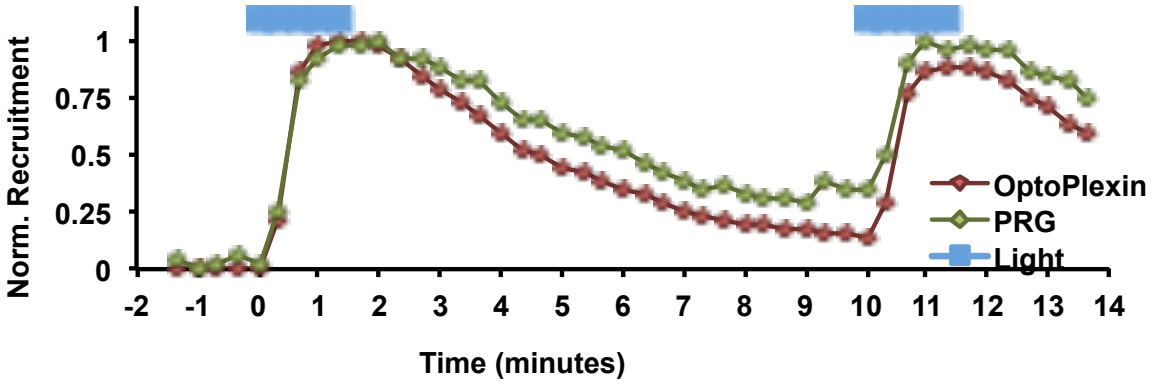

Figure 23. OptoPlexin and PDZ-RhoGEF recruitment kinetics. Temporal changes in membrane recruitment and dissociation of mCherry-optoPlexin and mVenus-PRG in response to intermittent whole cell illumination in a COS-7 cell. Blue line, illumination at 440 nm.

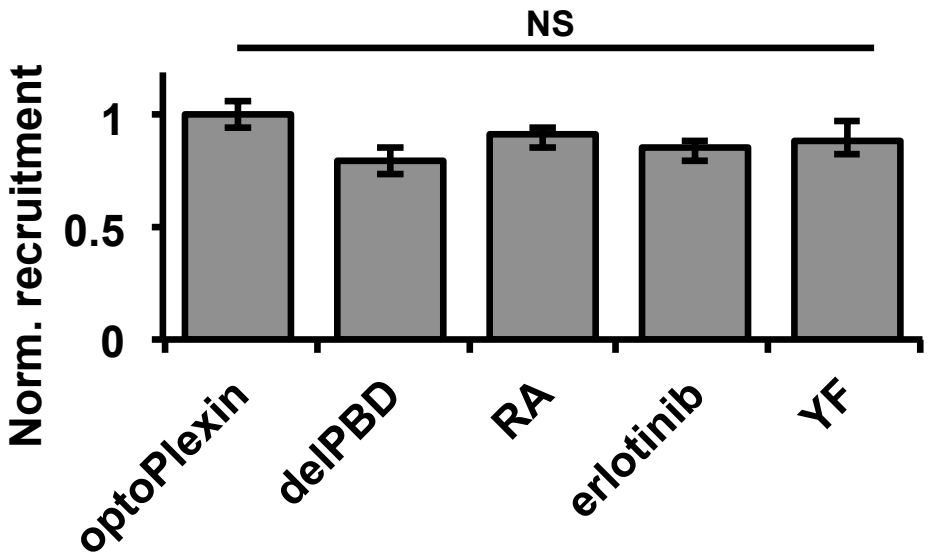

Figure 24. Recruitment levels of optoPlexin and its variants. Recruitment levels of optoPlexin, optoPlexin-delPBD, optoPlexin-RA, optoPlexin with 5 µM erlotinib and optoPlexin-YF on whole cell blue light illumination in COS-7 cells, normalized to recruitment level of optoPlexin. n ≥ 15, means ± s.e.m. are shown. *** p<0.001, * p<0.05, NS, not significant.

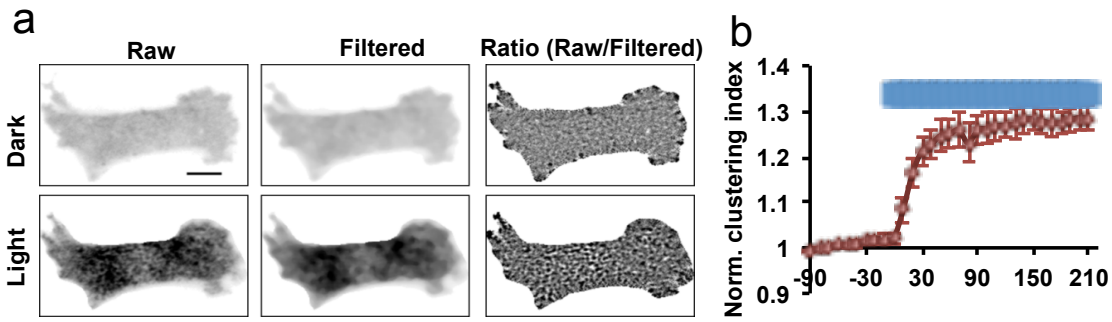

Figure 25. OptoPlexin and PDZ-RhoGEF clustering. (a) TIRF images showing changes in mCherry-optoPlexin clustering (left panels) in COS-7 cells before and after whole cell illumination. Images in right panel were passed through a 5X5 median filter to obtain 'smooth' images (middle panels). Changes in clustering upon illumination was visualized (right panels) by normalizing the raw images (left panels) to the filtered images (middle panels) to minimize effects of cell topology. Scale bar, 10 µm. (b) Temporal changes in optoPlexin clustering normalized to clustering levels prior to illuminination. Blue line, illumination. n=14 cells, mean ± s.e.m. are shown.

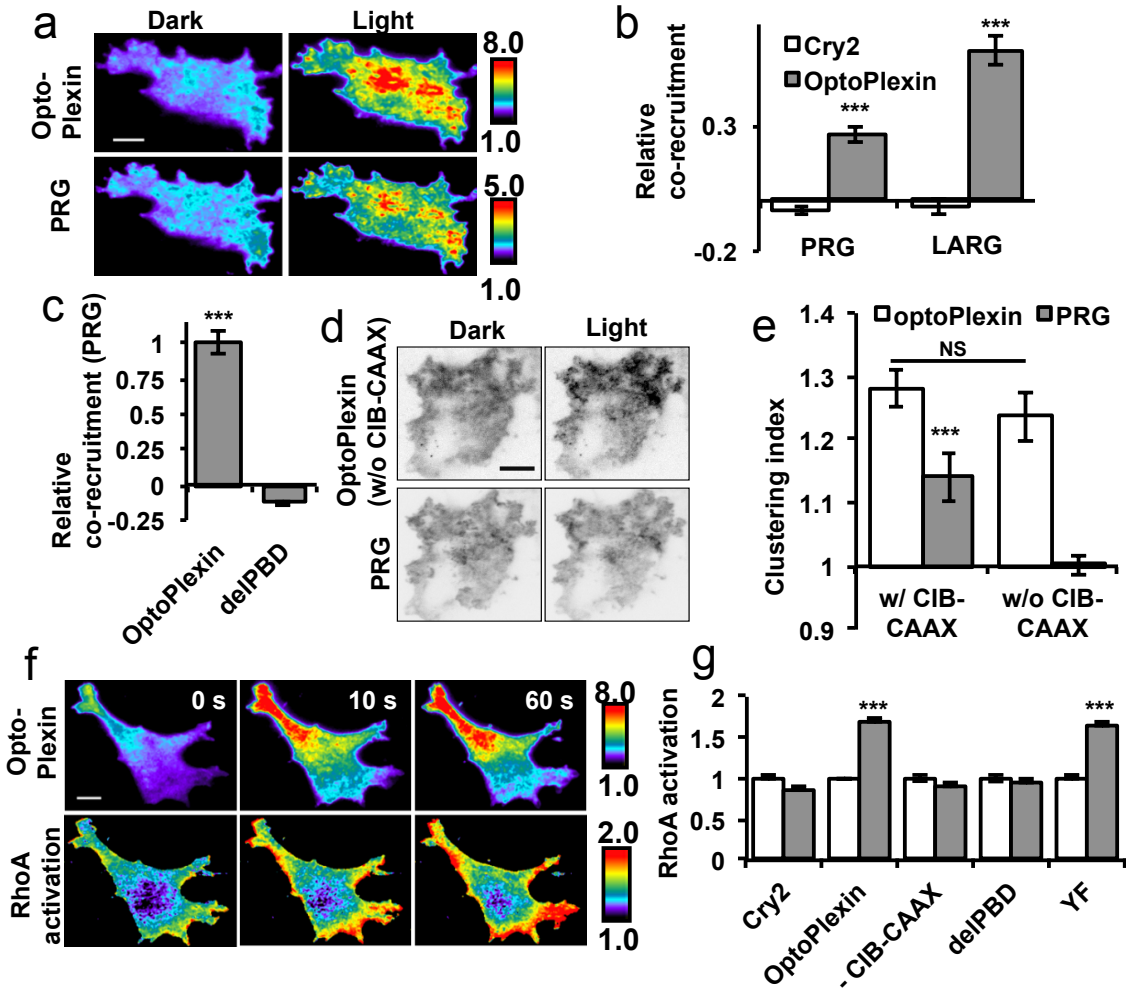

Figure-26. OptoPlexin activates RhoA through membrane recruitment of RhoGEFs. (a) TIRF images showing the membrane recruitment of mVenus-PRG along with mCherry-optoPlexin after one minute of whole cell illumination in COS-7 cells. Scale bar, 10 µm. (b) Relative co-recruitment of mVenus-PRG or LARG by Cry2 and optoPlexin upon whole cell illumination in COS-7 cells, n = 13-19. (c) Normalized relative co-recruitment of mVenus-PRG by optoPlexin (n = 19) and optoPlexin-delPBD (n=13). (d) TIRF images showing clustering of optoPlexin, and lack of that with mVenus-PRG, in the absence of CIB-CAAX after one minute of whole cell illumination in COS-7 cells. Scale bar, 10 µm. (e) Quantification of clustering of optoPlexin and PRG in the presence (n = 19) or absence of CIB-CAAX (n = 13). (f) Induction of mCherry-optoPlexin upon ratiometric imaging of DORA-RhoA biosensor using TIRFM. Scale bar, 10 µm. (g) RhoA activation in COS-7 cells expressing Cry2, optoPlexin, optoPlexin-delPBD or optoPlexin-YF upon whole cell illumination, n = 18-32 cells. For b, c, e & g, means ± s.e.m. are shown.*** p<0.001, * p<0.05, NS, not significant, Student's t-test

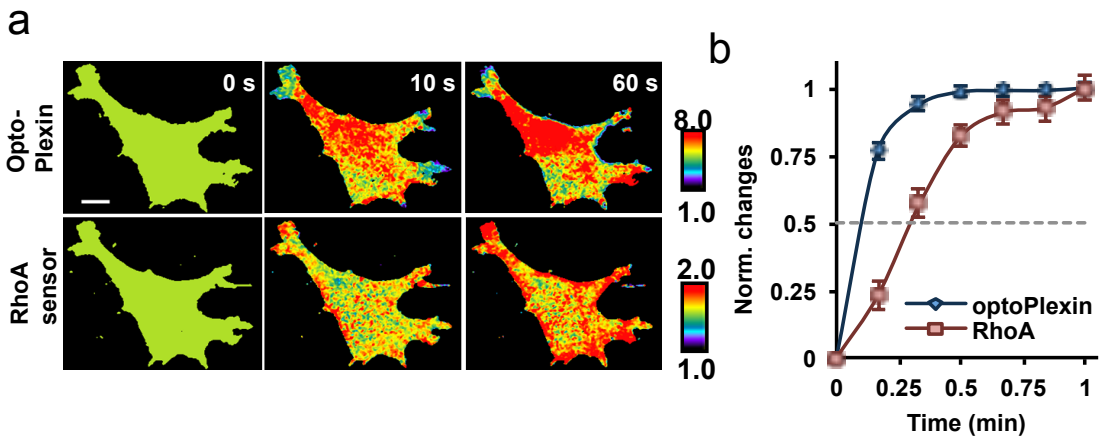

Figure 27. OptoPlexin activates RhoA. (a) TIRF images showing changes in mCherry-optoPlexin and Dora-RhoA biosensor induction in COS-7 cells normalized to the first frame. Scale bar, 10 µm. (b) Temporal changes in optoPlexin stimulation and Dora-RhoA biosensor activity in COS-7 cells. Excitation wavelengths used for donor (CFP) and FRET images were sufficient for whole cell induction of optoPlexin. Mean ± s.e.m are shown, n=32 cells.

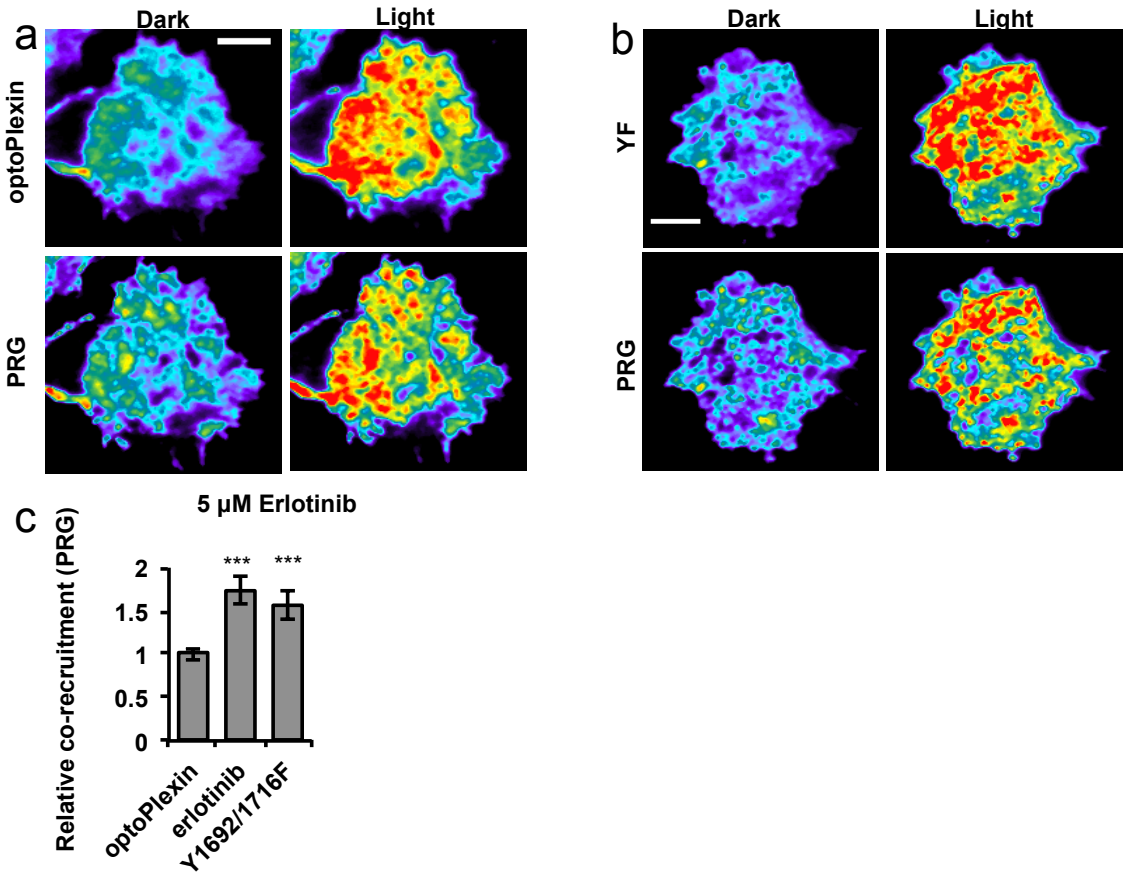

Figure 28. PRG recruitment by optoPlexin is not mediated by ErbB2 activation. TIRF images showing the membrane recruitment of mVenus-PRG and (a) mCherry-optoPlexin + 5 µM erlotinib or (b) mCherry-optoPlexin-YF after one minute of whole cell illumination in COS-7 cells. Scale bar, 10 µm. (c) Induction of mVenus-PRG relative to that of optoPlexin, optoPlexin + 5 µM erlotinib and optoPlexin-YF upon whole cell illumination in COS-7 cells, n ≥ 15 cells, mean ± s.e.m. are shown. *** $p<0.001$, * $p<0.05$, NS, not significant.

To directly test whether RhoA was activated upon optoPlexin stimulation, we employed the Dora-RhoA biosensor described previously[42,43]. Due to overlapping wavelengths, the excitation light for Dora-RhoA FRET sensor was sufficient to induce rapid membrane recruitment of mCherry-optoPlexin in COS-7 cells (Figure 25, 26f upper panel). Although this prevented us from accurately capturing the level of RhoA activation prior to illumination, a consistent increase of RhoA activation was readily detectable (Figure 3f lower panel, 27), with an average of 70% induction of RhoA activation within the first three acquisitions (Figure 26g, 27b). Spatial pattern of RhoA activation did not accurately match with optoPlexin recruitment levels, potentially due to spatial regulation of RhoA activation through other factors. Consistent with being further downstream of Plexin-B1, the activation of Dora-RhoA exhbited a delay (~20s) in comparison with the membrane recruitment of optoPlexin (Figure 27b). Importantly, the effects were specific because no RhoA activation was detected when Cry2 alone or optoPlexin-delPBD was used, or when CIB-CAAX was omitted (Figure 26g). Sema4D dependent ErbB2 association with Plexin-B1 mediates downstream RhoA activation in osteoblasts[15,86,149]. However, neither inhibiting ErbB2 with Erlotinib[150] nor mutations designed to abrogate ErbB2 regulation of Plexin-B1[149] (optoPlexin-YF) (Figure 21) had any negative impact on PRG co-recruitment (Fig 28a, b); in fact we observed increased PRG recruitment in both cases (Figure 28c). OptoPlexin-YF induced RhoA activation at levels comparable to optoPlexin-WT(Figure 26g). Based on these results, we concluded that optoPlexin exhibits minimal background activity in the dark and activates RhoA robustly upon illumination.

Induction of CIL upon local activation of optoPlexin

To precisely control where Plexin-B1 is activated, we expressed optoPlexin and CIB-CAAX in MC3T3-E1 cells, and illuminated a 5-μm circular region in protrusions to mimic contact with Sema4D-expressing osteoclasts. As optoPlexin continued to accumulate, the illuminated protrusion collapsed and started to retract (Figure 29a, indicated with an asterisk, Supplementary Movie 11). The effects of optoPlexin were better illustrated in kymograph analyses where the accumulation of optoPlexin and the sharp transition of the cell border became apparent (Figure 29c). Despite similar enrichment in the illuminated protrusions, optoPlexin-delPBD failed to induce retraction (Figure 29b, c, Supplementary Movie 13), suggesting RhoA activation is required for optoPlexin-induced retraction. Among the optoPlexin-expressing cells, the average delay from the start of illumination to initiation of retraction was 2.5±0.5 minutes (mean ± s.e.m., Figure 29d). Interestingly, in addition to retraction, we observed either formation of a new protrusion(s) (Figure 29a, indicated with an arrowhead) or enhancement of an existing protrusion(s) distal to the site of illumination. They appeared immediately after the initiation of retractions, with an average time delay of 75 seconds (Figure 29d, e), suggesting that they may be mechanistically coupled. Even though optoPlexin induced retraction locally (Figure 30a), the overall cell area remains unchanged (Figure 30b).

To quantify the effects of optoPlexin on motility, we superimposed images of the cell boundary before and 7.5 minutes after illumination, and determined the relative orientations of the illumination site, retraction and protrusion with respect to

the centroid of the cell immediately prior to illumination (Figure 30d). Retractions were closely aligned with the orientation of the illumination site (Figure 30e, g), whereas new protrusions were randomly distributed (Figure 30f, g). Since the centroid is dictated by the original cell shape, thereby influencing the relative orientations of protrusion and retraction, we also measured the linear distance between protrusive or retracting regions and the site of illumination (Figure 30d). Retractions took place within 10 microns of the site of illumination, as compared to protrusions, which were significantly farther from the site of illumination (Figure 30h). Persistent illumination in protrusions effectively repolarized the cells and and significantly altered their direction so that the cells migrated away from the region of illumination (Supplementary Figure 31a, Supplementary Movie 12). In some cases we had to change the region of illumination to new protrusions to effectively guide the cells. Tracing the displacements of the centroid and the nucleus of one such cell showed a gradual change in centroid direction preceding a sharp change in the direction of nuclear migration (Figure 31b, c). Consistent with our observations with osteoclast co-culture (Figure 13b), we did not observe significant changes in cell centroid or nuclear velocities in MC3T3-E1 cells upon optoPlexin stimulation (Figure 30c,32). By contrast, whole cell illumination of optoPlexin-expressing cells led to collapse of all existing protrusions and hindered motility (Movie 14), similar to the response on bath application Sema4D-Fc (Figure 16a, b). Thus, localized Plexin-B1 signaling through optoPlexin stimulation revealed a CIL-like phenotype in MC3T3-E1 cells that had not been demonstrated previously.

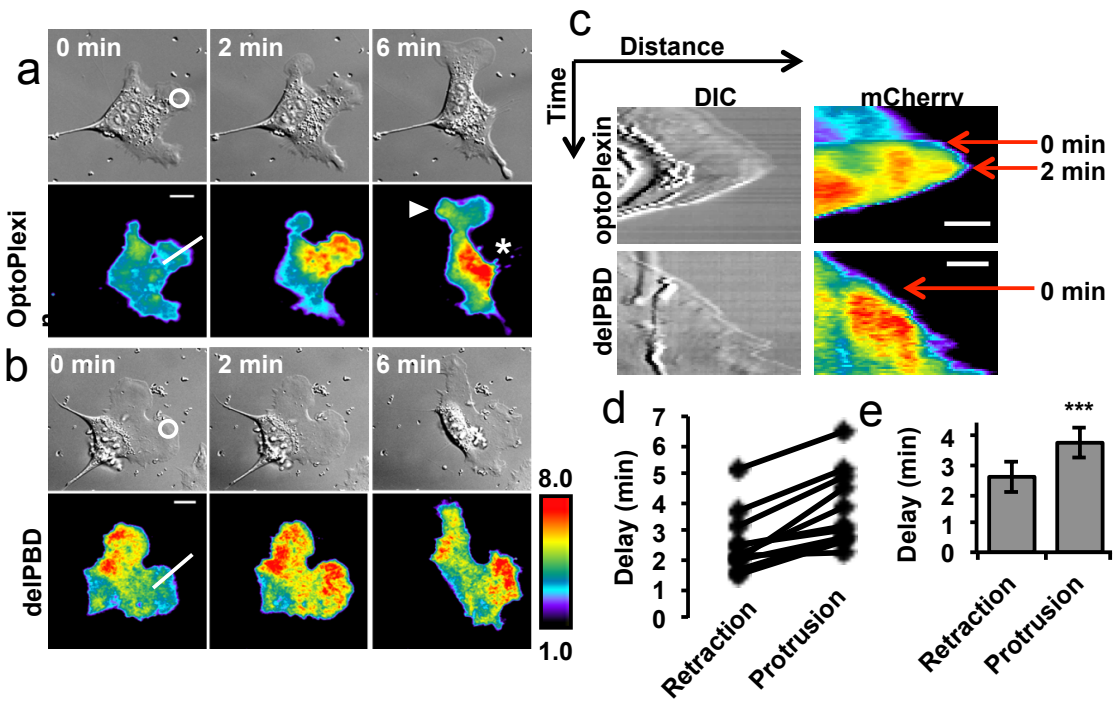

Figure 29. OptoPlexin induces CIL upon local activation. MC3T3-E1 cells expressing mCherry-optoPlexin (a) or mCherry-optoPlexin-delPBD (b) were locally illuminated as indicated (white circle). The DIC and TIRF images were shown to illustrate the morphological changes and local membrane recruitment. Scale bar, 10 µm. Asterisk, retraction. Arrowhead, induced protrusion. (c) Kymographs showing cell border progression upon local activation of optoPlexin or optoPlexin-delPBD. Reference lines for the kymographs are shown in white in (a) and (b). Scale bar, 10 µm. (d) Pairwise comparison of the delay in initiation of retractions and protrusions upon local optoPlexin activation. (e) Mean delay in initiation of local retractions and distal protrusions on local optoPlexin activation. n = 11 cells, means ± s.e.m. are shown. *** $p<0.001$, * $p<0.05$. NS, not significant, Student's t-test.

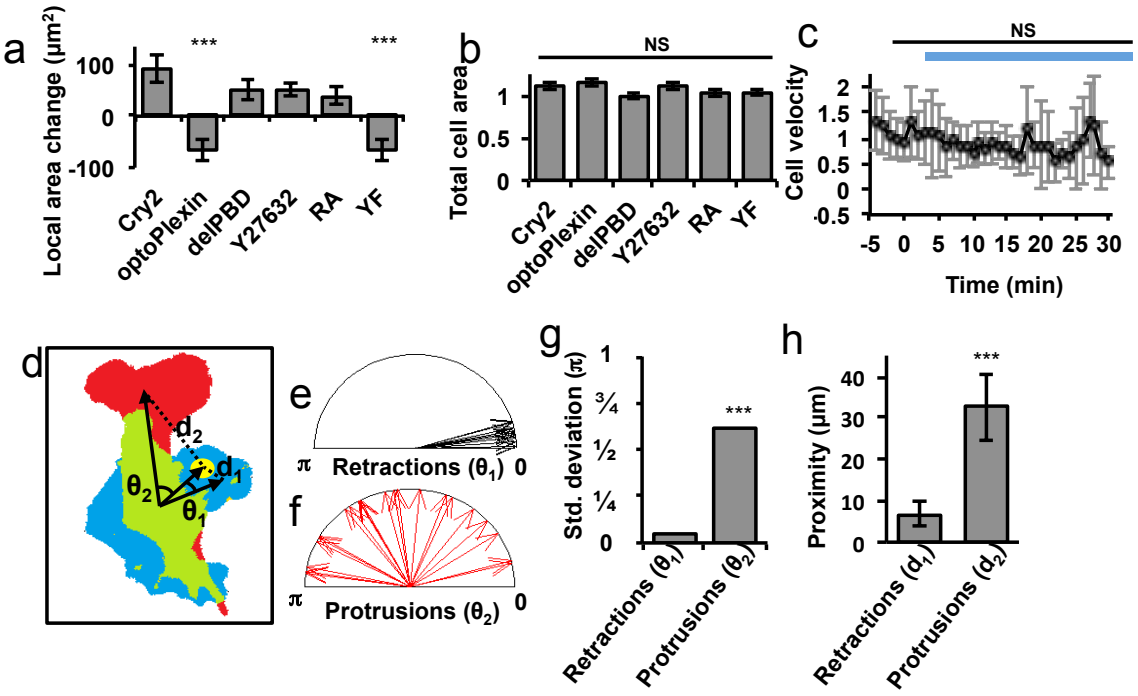

Figure 30. Effects of local activation of optoPlexin on cell morphology and motility. Effects on the illuminated protrusions (a), measured in a 50 μm diameter circle centered at the region of illumination, and total cell areas (b) after 7.5 minutes of local illumination in MC3T3-E1 cells expressing Cry2, optoPlexin, optoPlexin-delPBD, optoPlexin and pretreated with 10 μM Y-27632 ROCK inhibitor, and optoPlexin-RA, n = 9-14 cells. (c) Cell centroid velocities at different times upon local activation of optoPlexin in MC3T3-E1 cells. Blue line, illumination at 440 nm, n = 21 cells. (d) The locally induced retraction (blue) and the distal protrusion (red) after pulses of illumination (yellow) of an optoPlexin-expressing cell was illustrated in a morphology diagram. The overlapping cell area before and after illumination was labeled in green. Based on the centroids of these color-coded regions, θ_1 and θ_2 were used to describe the angles of retraction and protrusion relative to the direction from the centroid of the cell at time 0 to the center of illumination, respectively. Similarly, d_1 and d_2 indicated their centroid distances to the region of illumination, respectively. (e), (f) Angles of retraction and protrusion induced by local activation of optoPlexin in MC3T3-E1 cells and (g) standard deviation of their distribution, n = 14 cells. (h) Proximity of retractions and protrusions induced by local activation of optoPlexin in MC3T3-E1 cells to the region of illumination, n = 14 cells. For a, b, c & h, means ± s.e.m are shown, *** $p<0.001$, * $p<0.05$, NS, not significant, Student's t-test. For g, *** $p<0.001$, * $p<0.05$, NS, not significant, F-test.

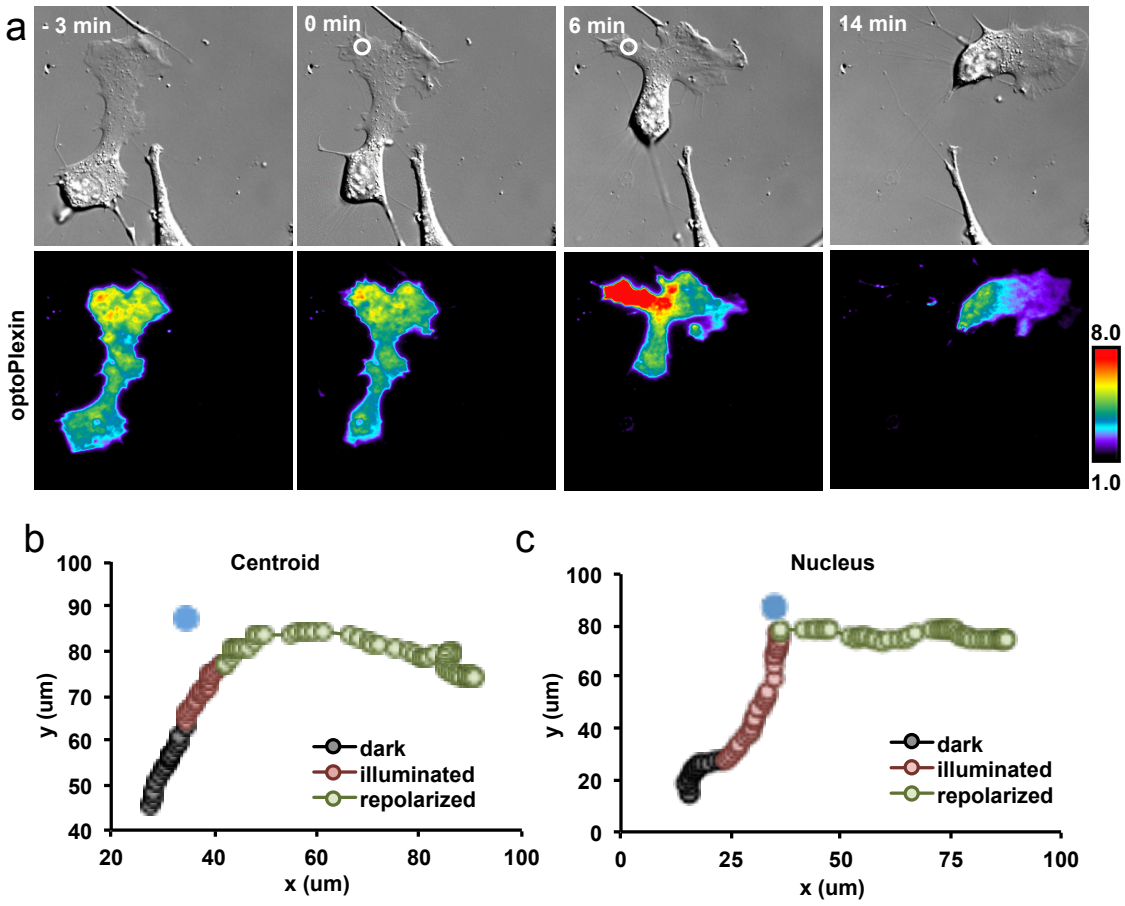

Figure 31. OptoPlexin induces cells to migrate away from the site of activation. (a) MC3T3-E1 cell expressing mCherry-optoPlexin was locally illuminated as indicated (white circle). The DIC and TIRF images were shown to illustrate the local membrane recruitment of mCherry-optoPlexin, and change in direction of migration. Scale bar, 10 µm. Asterisk, retraction. Arrowhead, induced protrusion. Changes in the direction of migration of the cell is illustrated by the changes in the centroid (b) and nucleus (c) of the cell. The change in direction of migration of the cenroid appears to be more gradual and precedes that of the nucleus. Blue circle, initial region of illumination.

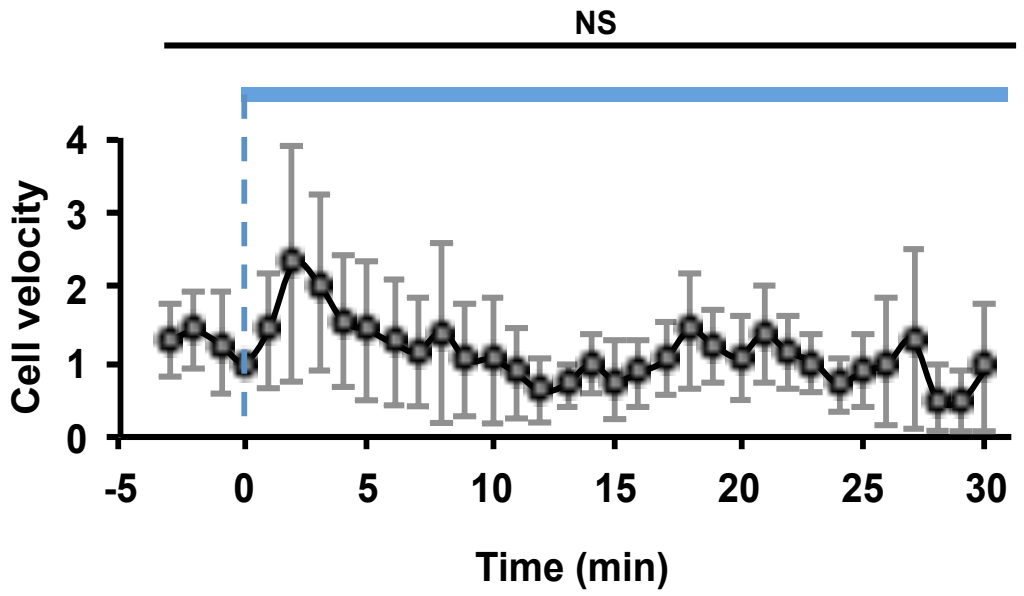

Figure 32. Changes in cell motility upon optoPlexin activation. Cell nucleus velocities at different times upon local activation of optoPlexin in MC3T3-E1 cells. Blue line, illumination at 440 nm. n=21 cells, mean ± s.e.m. are shown. *** $p<0.001$, * $p<0.05$, NS, not significant.

Both RhoA and RasGAP pathways are required for CIL

To determine which pathway(s) downstream of optoPlexin mediates CIL, we quantified the changes in protusive areas induced by optoPlexin activation. We already showed that the delPBD mutant failed to inhibit protrusion (Figure 29b, 30a, Supplementary Movie 13). A specific ROCK inhibitor Y-27632 also abrogated optoPlexin mediated retractions (Figure 30a), further validating the role of RhoA-ROCK signaling in Plexin-B1 mediated retractions. In addition, we tracked the signaling molecules upstream or downstream of RhoA. We locally activated mCherry-optoPlexin in cells coexpressing mVenus-PRG, and found PRG was recruited immediately to the spot where optoPlexin accumulated (Figure 33a, Movie 15). The line-scan profile of PRG resembled that of optoPlexin very closely (Figure 33b), which is consistent with a physical interaction between these two proteins. Myosin II regulatory light chain (MyoRLC) is phosphorylated by ROCK downstream of RhoA, which leads to its association with actin filaments. We used mCherry-MyoRLC in TIRF imaging to track the immobilized myoRLC as an indicator of myosin II activation[151]. Upon local activation of mVenus-optoPlexin, we observed accumulation of mCherry-myoRLC at the site of illumination, but with an apparent delay (Figure 33c, d, Supplementary Movie 16). Interestingly, the distal protrusions induced were associated with substantially decreased myoRLC, suggesting a depletion of myosin activity in these nascent protrusions (Figure 33c, e). An optoPlexin mutant (optoPlexin-RA) (Figure 21) lacking RasGAP activity also failed to induce retraction (Figure 30a, 34, Supplementary Movie 17). The response of MC3T3-E1 cells upon local activation of optoPlexin-YF mutant was

indistinguishable from that of optoPlexin (Figure 30a, 35, Supplementary Movie 18). In all cases where retraction was not induced, protusions also failed to form in distal regions. Thus both RhoA and RasGAP pathways are required for optoPlexin to induce CIL.

Local activation of optoPlexin repolarizes PIP_3

Phosphoinositides, in particular phosphatidylinositol(3,4,5)P_3 (PIP_3), are extensively involved in regulation of cell polarity and motility[152,153]. To examine whether PIP_3 is regulated in migration of MC3T3-E1 cells, we employed the PH domain of Akt (PH-Akt) to monitor the spatial distribution of PIP_3[51]. Ratiometric imaging of mVenus-PH-Akt and a cytosolic mCerulean volume maker were imaged using TIRF microscopy and their ratio (mVenus/mCerulean) was used to indicate the levels of PIP_3 enrichment. Consistent with a role of PIP_3 in migration, we observed accumulation of PIP_3 at the leading edge and low levels in retracting areas of migrating MC3T3-E1 cells (Figure 36a, b). Because of the overlapping wavelengths between optoPlexin activation and mCerulean excitation, to investigate spatial regulation of PIP_3 during optoPlexin mediated CIL, we activated mCherry-optoPlexin at protrusions first and acquired a pair of mVenus and mCerulean images upon induction of distal protrusions. In contrast to an elevated PIP_3 seen in unperturbed protrusions, a substantial reduction of PIP_3 was observed in the area of optogenetic illumination. Furthermore, we observed an acute accumulation of PH-Akt in the newly formed distal protrusions (Figure 36c, d). Neither optoPlexin-delPBD nor optoPlexin-RA induced significant decrease of local PIP_3 (Figure 36d) upon at least 7.5 minutes of local activation. Thus our data

supported the requirement of both RhoA activation and RasGAP activity of Plexin-B1 in regulating PIP_3 in osteoblasts.

OptoPlexin spatially coordinates Cdc42 activity in CIL

Small GTPases Rac1 and Cdc42 are potent inducers of actin polymerization and migration. Employing Dora-Cdc42 and Dora-Rac1 biosensors[154], we observed elevated Cdc42 activation at protrusions in migrating MC3T3-E1 cells, whereas Rac1 activity was less polarized (Figure 37). To examine how optoPlexin may affect Cdc42 and Rac1 activities, we co-expressed mCherry-optoPlexin with a Dora-Cdc42 or Dora-Rac1 sensor in MC3T3-E1 cells. We activated optoPlexin exclusively in a protrusion where Cdc42 was expected to be active. In order to avoid activating optoPlexin globally, we acquired sensor images when distal protrusion(s) were induced (Figure 38a, b). We did not detect any active Cdc42 in the illuminated and retracting area, suggesting local inhibition of Cdc42 activity (Figure 38b, e). In contrast, the new protrusions in distal regions showed marked activation of Cdc42. Moreover, a non-binding control sensor exhibited low ratio values and minimal variation across the cell (Figure 38c-e), suggesting that the Cdc42 polarization was not due to a volume artifact. Using the Dora-Rac1 sensor, we found that Rac1 was also activated in the distal protrusion(s), albeit to a substantially reduced level (Figure 38e, 39). Thus, our data indicated that spatial and temporal activation of Cdc42 and possibly Rac1 may coordinate the opposing effects between local and distal regions upon optoPlexin activation.

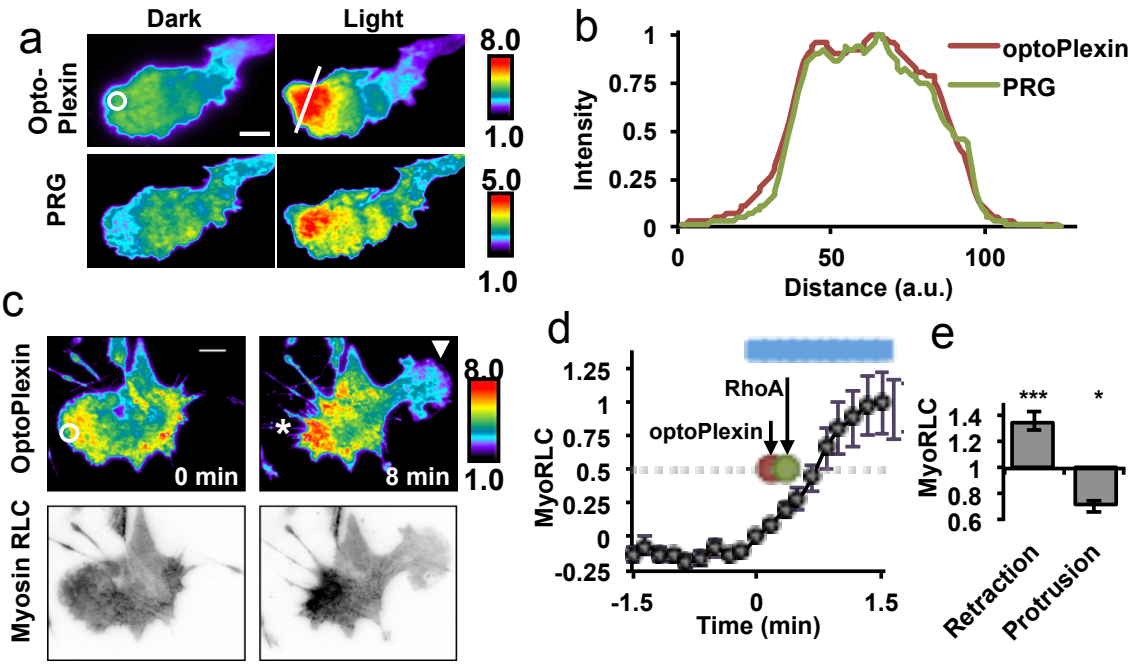

Figure 33. OptoPlexin induces CIL through RhoA mediated pathways. (a) TIRF images showing localized membrane recruitment of mVenus-PRG with mCherry-optoPlexin in MC3T3-E1 cells upon local illumination. White circle, region of illumination. Scale bar, 10 µm. (b) Normalized intensities of mCherry-optoPlexin and mVenus-PRG after local illumination in a linescan analysis. Reference line for the linescan is shown in the right top panel of (a). (c) TIRF images showing a polarized distribution of mCherry-MyoRLC upon local activation of mVenus-optoPlexin in MC3T3-E1 cells. White circle, region of illumination. Asterisk, induced retraction. Arrowhead, induced protrusion. Scale bar = 10 µm. (d) Temporal changes in average mCherry-MyoRLC intensity in a 50 µm diameter circle around the region of illumination (white circle) in MC3T3-E1 cells upon localized activation of mVenus-optoPlexin. Red and green circles indicate $t_{1/2}$ for optoPlexin and RhoA inductions respectively as estimated from Fig. S4b. Blue line, illumination at 440 nm. (e) Relative intensities of mCherry-MyoRLC in retractions and new protrusions induced by local activation of mVenus-optoPlexin, normalized to the whole cell average. For (d) and (e) n = 12 cells, means ± s.e.m. *** $p<0.001$, * $p<0.05$, NS, not significant, Student's t-test.

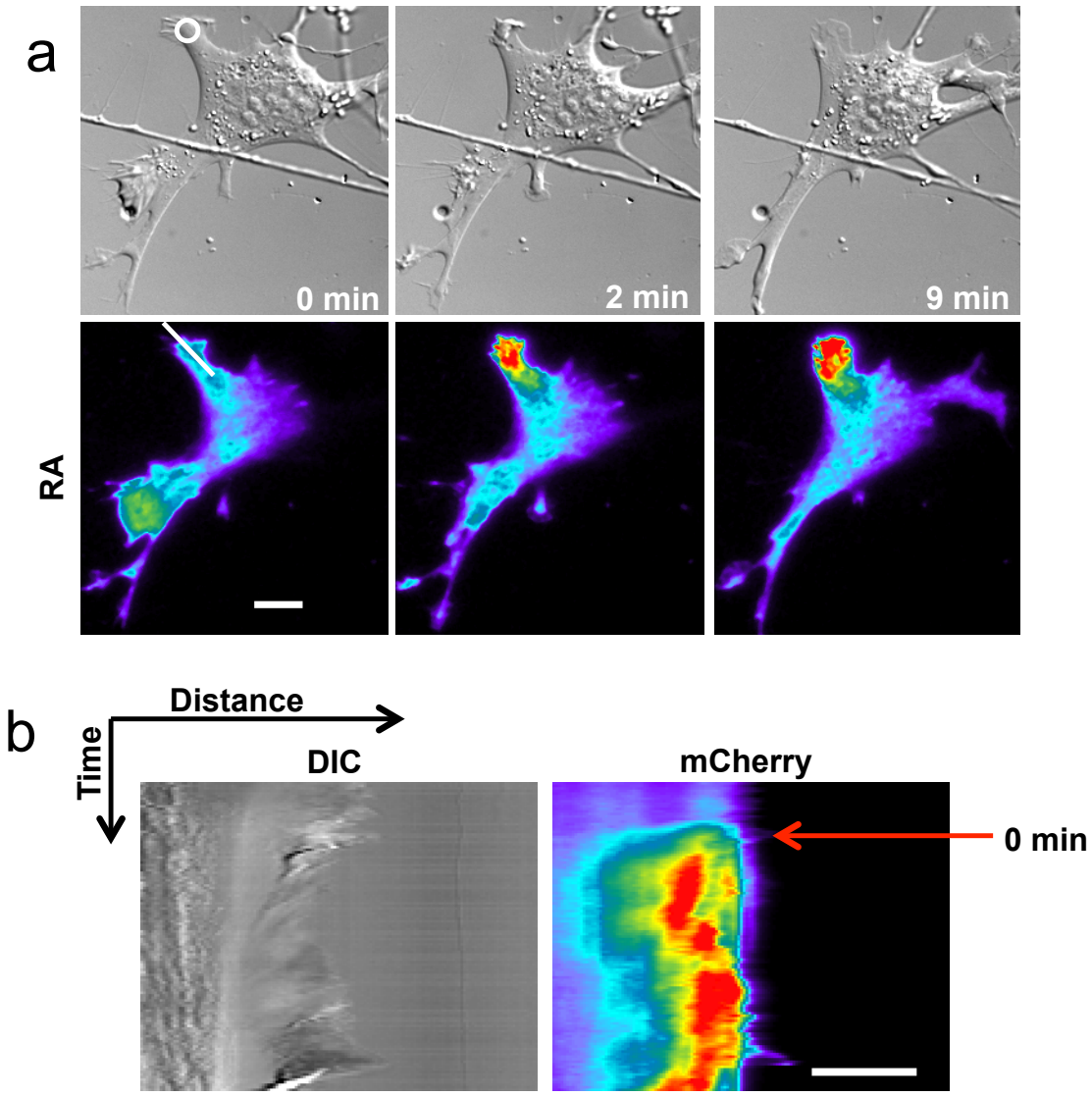

Figure 34. RasGAP deficient optoPlexin fails to induce CIL. (a) MC3T3-E1 cells expressing mCherry-optoPlexin-RA were locally illuminated as indicated (white circle). The DIC and TIRF images were shown to illustrate the morphological changes and local membrane recruitment. Scale bar, 10 µm. (b) Kymograph showing cell border progression upon local activation of optoPlexin-RA. Reference line for the kymograph is shown in white in (a). Scale bar, 10 µm. n ≥ 10.

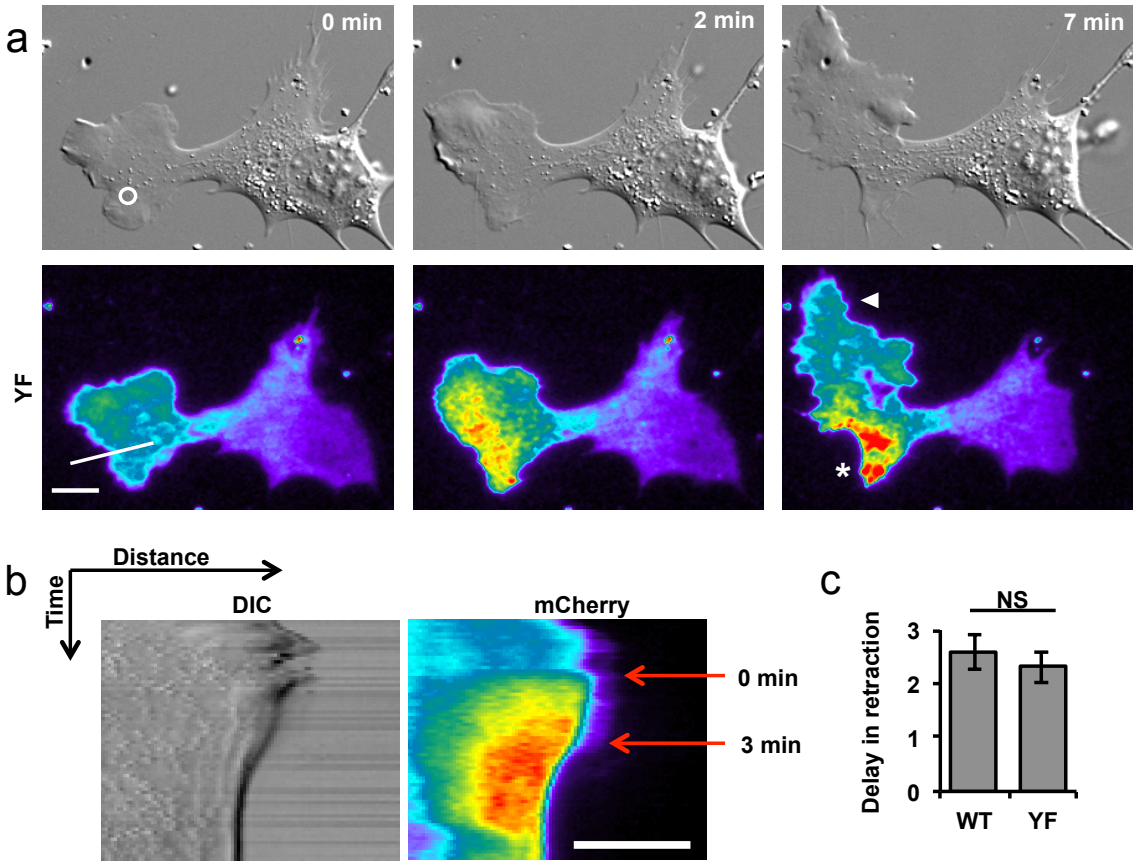

Figure 35. ErbB2 does not mediate optoPlexin-induced cell repolarization. (a) MC3T3-E1 cells expressing mCherry-optoPlexin-YF were locally illuminated as indicated (white circle). The DIC and TIRF images were shown to illustrate the morphological changes and local membrane recruitment. Scale bar, 10 µm. Asterisk, retraction. Arrowhead, induced protrusion. (b) Kymograph showing cell border progression upon local activation of optoPlexin-YF. Reference line for the kymograph is shown in white in (a). Scale bar, 10 µm. (c) Comparison of delay in initiation of local retractions on local optoPlexin and optoPlexin-YF activation. n ≥ 10, means ± s.e.m. *** p<0.001, * p<0.05. NS, not significant.

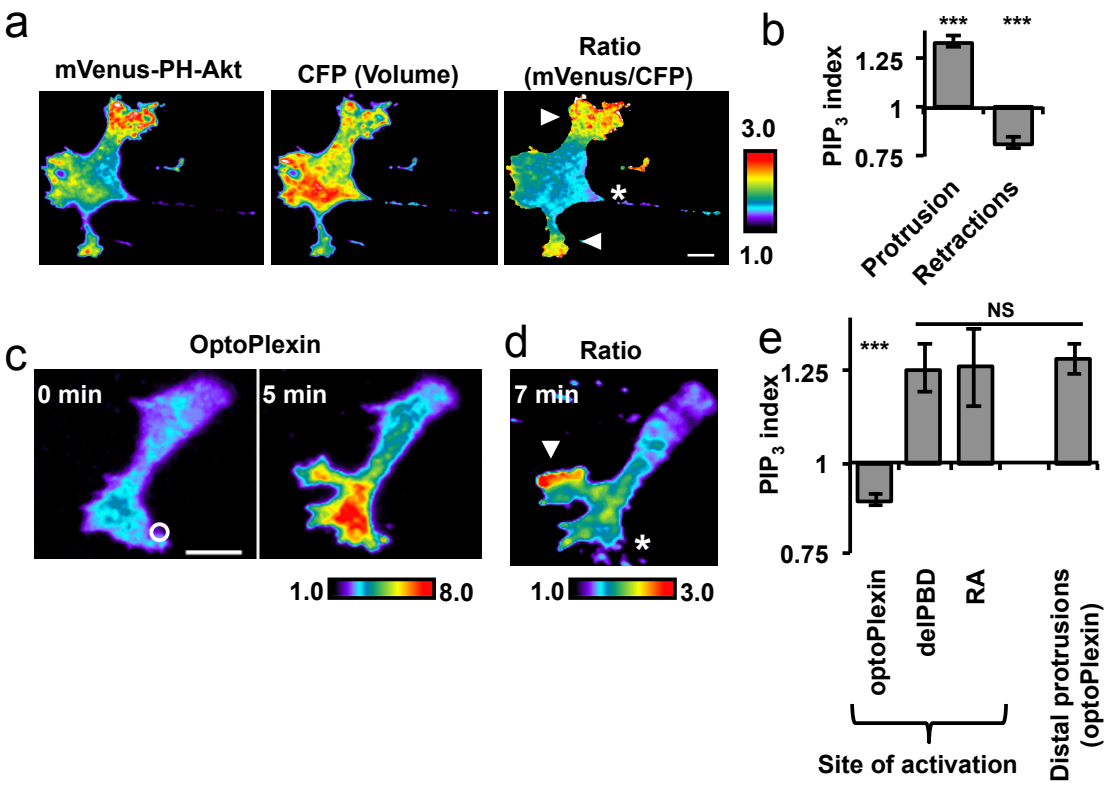

Figure 36. Local activation of optoPlexin repolarizes PIP_3. (a) TIRF images of mVenus-PH-Akt and CFP (volume marker) in an MC3T3-E1 cell were processed to generate a ratiometric image (mVenus/CFP) that displays the membrane enrichment of mVenus-PH-Akt, indicative of PIP_3 concentration. Asterisk, retraction. Arrowheads, protrusions. Scale bar, 10 µm. (b) PIP_3 distribution in protrusions and retractions in MC3T3-E1 cells, as measured by membrane enrichment mVenus-PH-Akt normalized to the whole cell average, n =9 cells (c) TIRF images showing local induction of mCherry-optoPlexin in a MC3T3-E1 cell expressing mCherry-optoPlexin, mVenus-PH-Akt and CFP. Upon induction of CIL, mVenus and CFP images were obtained and processed to generate ratiometric image (d) indicating PIP_3 distribution. White circle, region of illumination. Scale bar, 10 µm. Asterisk, induced retraction. Arrowhead, induced protrusion. (e) Quantification of PIP_3 indices in a 50 µm diameter circle centered at the region of illumination upon local activation of optoPlexin, optoPlexin-delPBD and optoPlexin-RA; and in distal protrusions induced by local activation of optoPlexin, normalized to whole cell average, n = 8-12 cells. For b and e means ± s.e.m. are shown. *** $p<0.001$, * $p<0.05$, NS, not significant, Student's t-test.

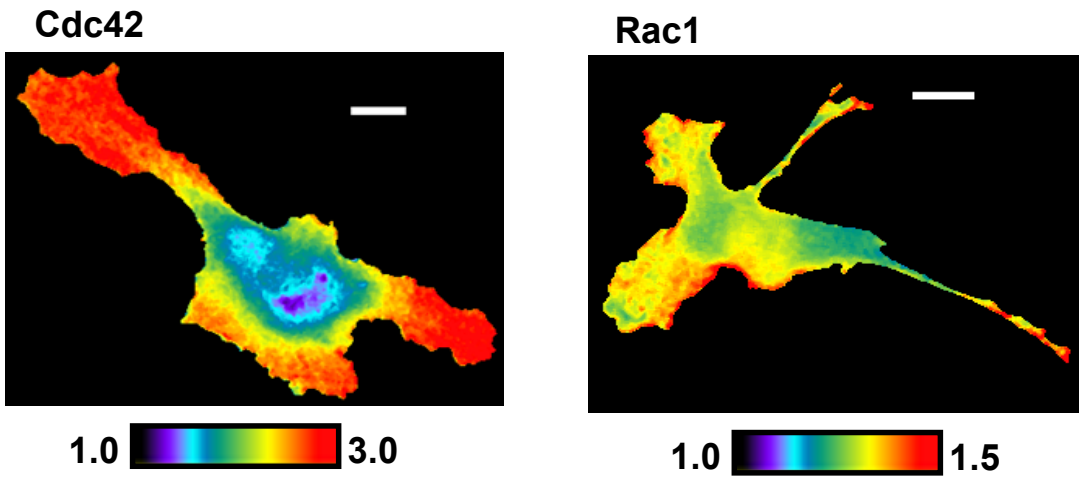

Figure 37. Spatial regulation of Rac1 and Cdc42 in migrating MC3T3-E1 cells. Ratiometric images showing spatial distribution of Rac1 and Cdc42 activities as measured using DORA biosensors in migrating MC3T3-E1 cells. Scale bar, 10 µm.

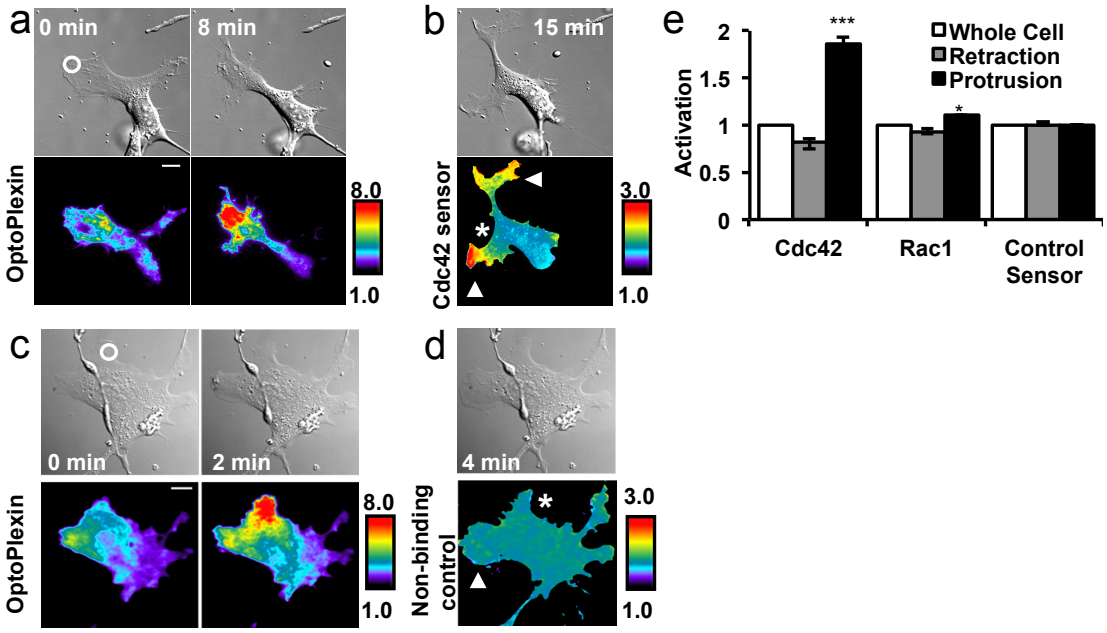

Figure 38. Local activation of optoPlexin spatially coordinates Cdc42 and Rac1 activities. DIC and TIRF images showing local accumulation and activation of mCherry-OptoPlexin in MC3T3-E1 cells co-expressing a Dora-Cdc42 biosensor (a) or its non-binding control (c). Upon induction of CIL, a pair of FRET and CFP images were acquired using TIRFM and processed to generate a ratio image for the Dora-Cdc42 sensor (b) and its non-binding control (d). White circle, region of illumination. Scale bar, 10 µm. Asterisk, induced retraction. Arrowhead, induced protrusion. (e) Quantificaiton of the spatial distribution of active Cdc42 and Rac1 in MC3T3-E1 cells after induction of CIL, n = 9-12 cells, means ± s.e.m. are shown. *** $p<0.001$, * $p<0.05$, NS not significant, Student's t-test.

Figure 30. OptoPlexin alters Rac1 polarization. DIC and TIRF images showing

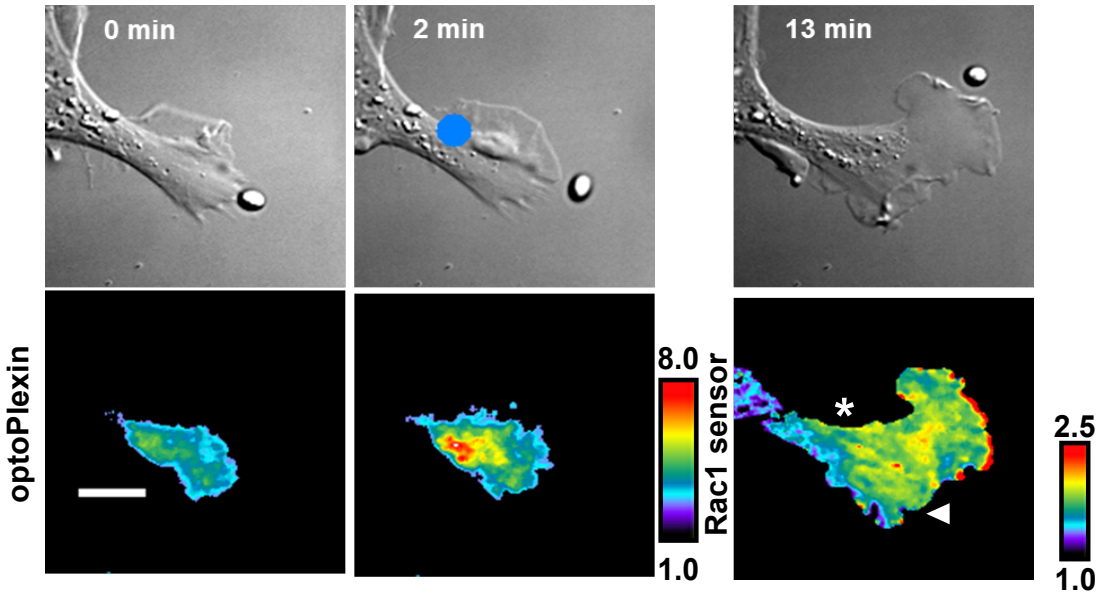

OptoPlexin redistributes β-Pix to distal regions during CIL

To understand how optoPlexin may regulate Cdc42 and Rac1, we focused on a ubiquitously expressed RhoGEF β-Pix, which activates Cdc42 and Rac1[155,156] and mediates crosstalk between RhoA and Cdc42/Rac1. In migrating MC3T3-E1 cells, β-Pix is predominantly associated with nascent adhesions and focal complexes in protrusions rather than with focal adhesions in stationary or retracting areas (Figure 40 a-c). Consistent with previous reports[157], inhibition of RhoA-ROCK signaling using ROCK inhibitor Y-27632 promoted association of β-Pix with adhesions (Figure 40d). To examine how optoPlexin may affect β-Pix locally, we co-expressed mVenus-Venus-fecmCherry-Paxillin with optoPlexin in MC3T3-E1 cells and tracked their changes upon optoPlexin activation in separate experiments. Upon activating optoPlexin, β-Pix was rapidly depleted in illuminated region (Figure 41a, b top panel, 42a, Supplementary Movie 19). This depletion was not due to a loss of adhesions as we observed an increase in the intensity of paxillin around sites of illumination (Figure 41c, d top panel, 42b, Supplementary Movie 20). The opposite changes in β-Pix and paxillin accumulation indicate dissociation of β-Pix from the adhesion molecular complex (Figure 41e, 42). The decrease of β-Pix around the region of illumination preceded or coincided with the initiation of retraction (Figure 41b top panel, 42c). Moreover, we observed a concurrent accumulation of β-Pix and nascent adhesions in distal regions where new protrusions were produced (Figure 41b, d bottom panels). In support of the involvement of RhoA signaling, optoPlexin-delPBD failed to deplete β-Pix locally, and addition of ROCK inhibitor Y-27632 also abrogated the effects of optoPlexin

on Plexin on β-Pix redistribution (Figure 41f, 43). The presence of exogenous β-Pix caused a delay in retraction that was proportional to the level of β-Pix expression (Figure 41g), suggesting that a local depletion of β-Pix may be required for the initiation of retraction. Taken together, these data revealed a novel mechanism in which a redistribution of β-Pix mediated by Plexin-B1-RhoA pathway coordinates CIL.

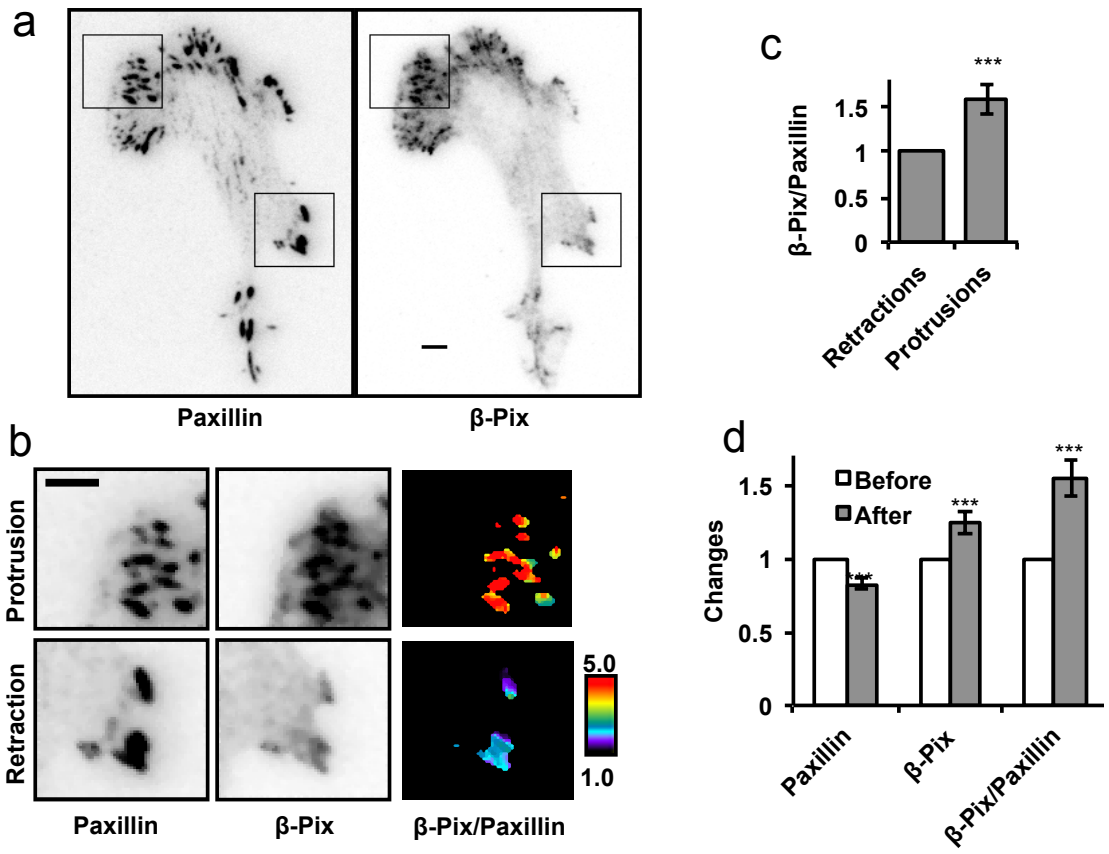

Figure 40. Spatial regulation of β-Pix in migrating MC3T3-E1 cells. (a) Representative TIRF images showing spatial distribution of mCherry-Paxillin and mVenus-β-Pix in a migrating MC3T3-E1 cell. (b) Inset squares at a protrusion and a retraction in (a) are magnified, and processed to generate a ratiometric image (mVenus-β-Pix/mCherry-Paxillin), which illustrates the differences in mVenus-β-Pix and mCherry-Paxillin association withnascent and mature adhesions at protrusions and retractions respectively. For (a) and (b) scale bar, 5 µm. (c) Normalized ratio of mVenus-β-Pix to mCherry-Paxillin signal in migrating MC3T3-E1 cells at retractions and protrusions. (d) Changes in mCherry-Paxillin, mVenus-β-Pix and mVenus-β-Pix/mCherry-Paxillin ratio in MC3T3-E1 cells on 10 µM Y-27632 ROCK inhibitor treatment, normalized to values prior to treatment. n = 7 cells, mean ± s.e.m. *** $p<0.001$, * $p<0.05$.

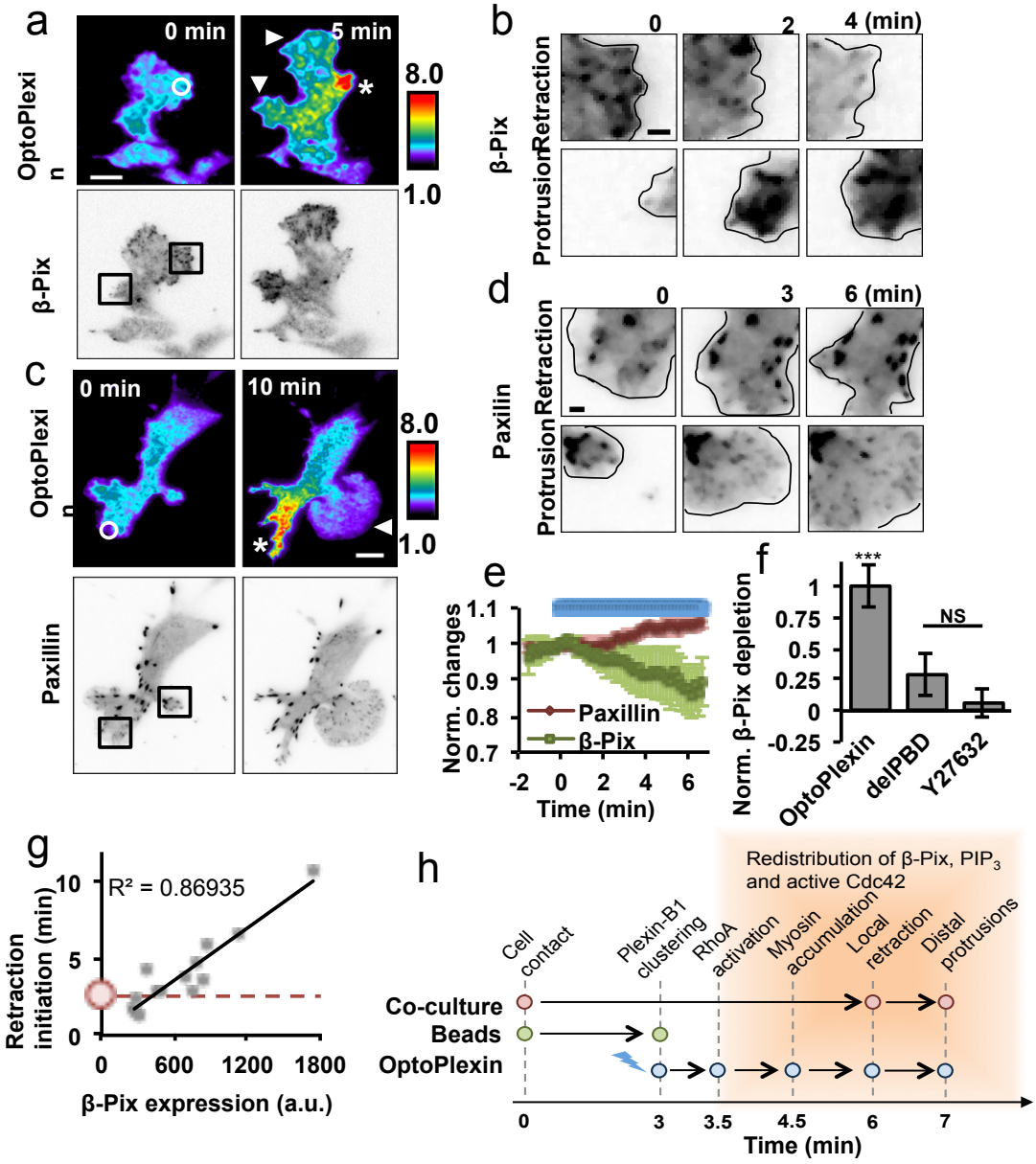
a
0 min
5 min
OptoPlexin
β-Pix
8.0
1.0
b
0
2
4 (min)
β-Pix
Retraction
Protrusion
c
0 min
10 min
OptoPlexin
Paxillin
8.0
1.0
d
0
3
6 (min)
Paxilin
Retraction
Protrusion
e
Norm. changes
1.1
1
0.9
0.8
0.7
Paxillin
β-Pix
-2
0
2
4
6
Time (min)
f
***
NS
Norm. β-Pix depletion
1
0.75
0.5
0.25
0
-0.25
OptoPlexin
delPBD
Y27632
g
R² = 0.86935
Retraction initiation (min)
10
5
0
0
600
1200
1800
β-Pix expression (a.u.)
h
Redistribution of β-Pix, PIP3 and active Cdc42
Cell contact
Plexin-B1 clustering
RhoA activation
Myosin accumulation
Local retraction
Distal protrusions
Co-culture
Beads
OptoPlexin
0
3
3.5
4.5
6
7
Time (min)

Figure 41. OptoPlexin mobilizes and redistributes β-Pix to distal regions. TIRF images showing intensity changes of mCherry-optoPlexin and mVenus-β-Pix (a), or mVenus-optoPlexin and mCherry-Paxillin (c) in MC3T3-E1 cells upon local illumination. White circle, region of illumination. Scale bar, 10 µm. Asterisk, induced retraction. Arrowhead, induced protrusion. Inset squares in (a) and (c) are magnified to show temporal changes in mVenus-β-Pix (b) or mCherry-Paxillin (d) at induced retractions (b,d, top panels) or protrusions (b, d, bottom panels). Scale bar, 2 µm. (e) Quantification of fluorescence intensities of mCherry-Paxillin (n = 10 cells) and mVenus-β-Pix (n = 18 cells) in a 50 µm diameter circle centered at the region of illumination on local optoPlexin activation in MC3T3-E1 cells. Blue line, illumination at 440 nm. (f) Quantification of mVenus-β-Pix depletion in a 50 µm diameter circle centered at the region of illumination upon local illumination of MC3T3-E1 cells expressing optoPlexin, delPBD, or optoPlexin with addition of 10 µM Y-27632 (n = 10-18 cells). (g) Delay in initiation of retraction upon local activation of mCherry-optoPlexin with exogenous β-Pix expression levels in MC3T3-E1 cells. Red circle indicates mean delay in initiation of retraction by local activation of mCherry-optoPlexin in MC3T3-E1 cells with exogenous β-Pix expression as measured in Fig. 3e. n = 14 cells. (h) Correlation coefficient (R^2) between delay in initiation of retraction by local activation of mCherry-optoPlexin and exogenous β-Pix expression level as measured in Fig. 3e. n = 14 cells. (i) Model of Semaphorin-Plexin-B1 mediated CIL between osteoclasts and osteoblasts. MC3T3-E1 cells are shown. *** p<0.001, * p<0.05, NS, not significant, n=8 cells (c-e).

Figure 42. Spatial and temporal changes in β-Pix and paxillin upon optoPlexin activation. (a) Changes in mVenus-β-Pix in a 50 µm diameter circle centered around the region of illumination in MC3T3-E1 cells upon local activation of mCherry-optoPlexin. Mean ± s.e.m. (b) Changes in mCherry-Paxillin in a 50 µm diameter circle centered around the region of illumination in MC3T3-E1 cells upon local activation of mVenus-optoPlexin. Mean ± s.e.m., n=8 cells (c) Delay in initiation of mVenus-β-Pix depletion in a 50 µm diameter circle centered around the region of illumination, and that of retraction upon local activation of mCherry-optoPlexin activation. *** p<0.001, * p<0.05.

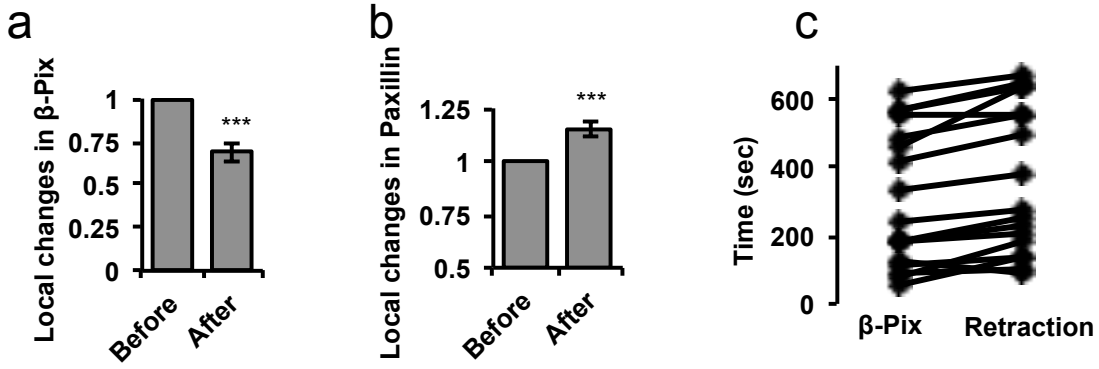

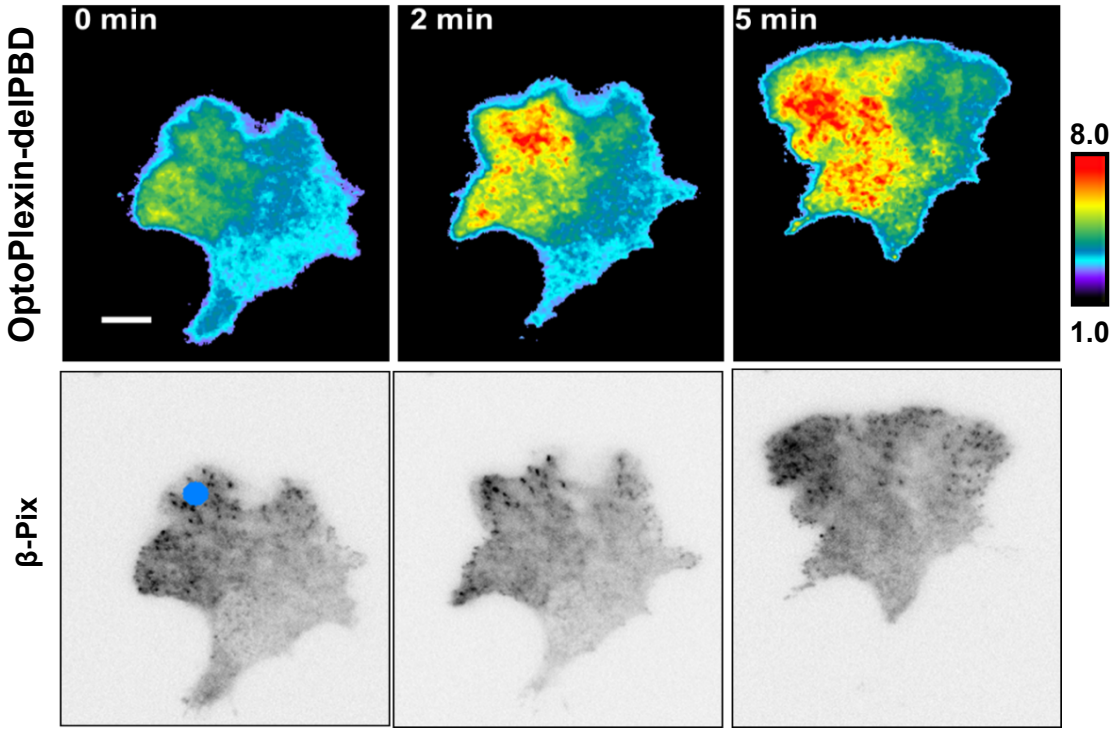

Figure 43. β-Pix redistribution by optoPlexin requires RhoA activation. Representative TIRF images showing lack of mVenus-β-Pix depletion from the region of localized mCherry-optoPlexin-delPBD activation in MC3T3-E1 cells. Blue circle, region of illumination. Scale bar, 10 µm.

Discussion:

Semaphorin-Plexin signaling attracts a lot of research interest because of its important functions in development and diseases. *In vivo* semaphorins are often present as directional cues for cell migration, and thus experimental perturbations with spatial control at the subcellular scale can offer unique insight into their signaling mechanisms. One of the technical challenges in spatial control is that existing ligand-based methods may not be optimal for localized stimulation. Here we describe a novel approach to precisely control the location and time of Plexin-B1 activation with light. We validated this new optogenetic reagent by tracking its binding with two known interacting RhoGEFs, PRG and LARG, and by visualizing its activation of RhoA. We named the new tool optoPlexin, following the naming convention of many optogentic reagents developed in recent years[158–161]. To our knowledge, optoPlexin is the first optogenetic tool for the receptors of repulsive guidance molecules.

The optogenetic module Cry2 has two independent[134] modes of action, i.e. inducible translocation mediated by CIB1[132] and homo-oligomerization[133], which benefitted optoPlexin design to reduce dark background. We found that mere oligomerization (by omitting CIB-CAAX) is not sufficient for inducing binding of PRG, a GEF for RhoA (Figure 26d,e) or RhoA activation (Figure 26g). It is likely that additional factors such as Rnd1 or Rac1 on the plasma membrane may participate in recruiting PRG[63,69,70]. Additionally, the slow off-rate of Cry2-CIB1 binding helped to maintain the Plexin-RhoGEF complex locally, mimicking sustained contact between osteoblasts and osteoclasts. Using optoPlexin, we

demonstrated spatial modulation of different regulators of cell migration to understand the signaling mechanism involved in CIL between osteoclasts and osteoblasts. Since plexins share high sequence homology in their intracellular regions[62], optoPlexin design should be extendable to other plexins as well.

Upon Sema4D stimulation ErbB2 associates with and is transactivated by Plexin-B1 and regulates RhoA activation through Phospholipase C-γ (PLC-γ)[86,149]. Given that the interaction with ErbB2 is mediated by the extracellular domain of Plexin-B1, it is unlikely that optoPlexin can associate with or activate ErbB2, which could be a limitation of optoPlexin. However, clustering of the cytosolic domain of Plexin-B1 on the membrane was shown to be sufficient for RhoA activation[141]. Our results also demonstrated that optoPlexin sufficiently recruits RhoGEF and activates RhoA. Mutations designed to abrogate PLC-γ association (optoPlexin-YF) did not affect RhoGEF recruitment, RhoA activation or the repulsion phenotype induced by optoPlexin. It is possible that ErbB2 mediated tyrosine phosphorylation of Plexin-B1 and consequent association with PLC-γ promotes clustering of the endogenous protein, which is compensated by light induced clustering of optoPlexin.

In interrogating Plexin-B1 signaling, we probed the RhoA-ROCK-Myosin pathway, and observed accumulation of MyoRLC and maturation of nascent adhesions in the protrusions where optoPlexin was activated. Local activation of optoPlexin repolarized active Cdc42 and active Rac1 away from the retracting area to new distal protrusions. We attribute these effects to mobilization and a redistribution of β-Pix. Crosstalk among Rho GTPases are known to facilitate cell

migration and polarity[55]. β-Pix is one of the molecules that mediate cross-talk between RhoA and Cdc42 or Rac1. Myosin II-mediated contractility, downstream of RhoA/ROCK signaling, has been shown to induce dissociation of β-Pix from adhesions and decrease Rac1 activation[157]. While we identified RhoA/ROCK activity being critical for local depletion of β-Pix, the exact molecular mechanism by which β-Pix is regulated demands further investigation. Our observations of opposite repolarization of MyoRLC and adhesion maturation compared to β-Pix are consistent with a model of mechanical regulation, although we cannot rule out a role of ROCK mediated phosphorylation of β-Pix[155,162] in its redistribution. Importantly, localized Plexin-B1 signaling did not simply deplete β-Pix, but induced redistribution to distal regions and activated Cdc42 and Rac1 to promote new protrusions. While we also observed repolarization of PIP_3, the underlying signaling mechanism remains to be explored. Plexin-B1 may inhibit PIP_3 by activating Phosphatase and tensin homolog (PTEN) via its RasGAP domain[163]. RhoA activation by Plexin-B1 may also activate PTEN and SH2 domain containing inositol 5'-phosphatase 2 (SHIP2)[57,164]. In other studies, Plexin-B1 has been reported to promote PIP_3 production through activation of phosphoinositide 3-kinases (PI3Ks)[90,165]. R-Ras is another important target that regulates CIL, as evident from the inability of optoPlexin-RA to induce CIL or PIP_3 redistribution. All plexins contain a RasGAP domain[16,56] and other repulsive guidance molecules such as ephrins also inhibit R-Ras[65,66], suggesting that R-Ras may play a critical role in mediating repulsion between cells.

Optogentic approach offers spatial and temporal control in initiating

signaling pathways in subcellular regions. This is particularly lucrative in studying CIL since the underlying signaling is initiated specifically at the site of cell-cell contact. Precise activation of optoPlexin in leading protrusions steered MC3T3-E1 cells away in a manner reminiscent of osteoclast-mediated CIL and followed similar timelines of retractions and protrusions (Figure 41h). While CIL has been proposed to transiently promote cell motility[166], both osteoclasts and localized optoPlexin stimulation induced CIL without affecting the overall motility of MC3T3-E1 cells (Figure 13b, 30c, 32). Previous studies have reported formation of transient cadherin-mediated cell-cell adhesions that generate mechanical tension across cells undergoing CIL[47,56,59,167,168]. We observed a sustained contact between osteoclasts and osteoblastic cells before separation (Supplementary Movie 2, 3, 5), which may potentially be critical for Plexin-B1 clustering. Whether osteoblasts and osteoclasts form any cadherin-mediated inter-cellular adhesions and their role in heterotypic CIL remains to be investigated. Our experiments with optoPlexin cannot decipher the nature and duration of such cell-cell contact. Nevertheless, we observed cellular response comparable to CIL induced by osteoclasts with similar kinetics (Figure 41h), suggesting that localized activation of Plexin-B1 was sufficient to generate similar behavior. Furthermore, our observations on spatial redistribution of PIP_3, active Cdc42 and active Rac1 suggest that although different signaling mechanisms may initiate homotypic and heterotypic CIL, their effects converge to induce similar spatial changes in factors that regulate cell migration.

In recent years, repulsion between cells has been implicated in many physiological and pathological processes[37]. Our data demonstrate CIL between osteoblasts and osteoclast. In the bone microenvironment, resorption by osteoclasts is followed by deposition of matrix by osteoblasts. Osteoclasts are generally thought to attract osteoblasts to the site of resorption through release of chemoattractants[8,9,144,145]. However, a simple chemotaxis model does not explain spatial segregation of osteoclasts and osteoblasts on the bone surface[15], which is consistent with their opposing functions. Our observation of CIL between osteoclasts and osteoblasts explains the spatial segregation between osteoblasts and osteoclasts[15,58]. Additionally, loss of Sema4D has been reported to impact bone resorption[119]. Whether osteoclasts utilize similar signaling mechanisms to repel osteoblastic bone lining cells and gain access to the bone matrix to initiate resorption remains to be investigated. A combination of CIL and chemotaxis might facilitate osteoblasts occupying sites of resorption only after the short-lived osteoclasts disappear. Considering the multitude of coupling factors between osteoclasts and osteoblasts, further research is necessary to gain a complete understanding of how osteoclasts modulate osteoblast migration and function.

Materials and methods

Cell culture and transfection Primary calvarial osteoblasts (POB) were obtained as described previously[169] from two month old inbred C57BL/6 male mice. Briefly, calvariae from 5-6 neonatal mice were minced, washed with Phosphate-buffered saline (PBS) and digested with 0.5 mg/ml collagenase P (Roche Diagnostics, Indianapolis, IN) and 0.5 mg/ml Trypsin/EDTA in PBS at 37°C four times for 10 minutes each and a final digest for 90 minutes. Cells isolated from digests 2-5 were combined and plated at a cell density of 4×10^4 cells/well in 6 well dishes for imaging experiments. For coculture experiments, POBs were lifted at day 5-7 after isolation. For real-time quantitative PCR, MC3T3-E1 and POBs were plated at $5X10^4$ cells /well in 6-well dishes and cultured in osteoblast differentiation media for 7 or 14 days. Osteoblast differentiation medium consisted of basic medium plus 50 μg/ml phosphoascorbate (Wako Pure Chemical Industry, Osaka, Japan). Media were changed every 3 days. 5 mM of β-glycerophosphate (Sigma-Aldrich, Saint-Louis, MO) was added on day 7 of these cultures. Bone marrow macrophages (BMMs) were made as described previously[169] following the protocols of R. Faccio (www.orthoresearch.wustl.edu/content/Laboratories/2978/Roberta-Faccio/Faccio-Lab/Protocols.aspx) from 5-6 two month old inbred C57BL/6 and outbred CD1 male mice. For osteoclastic differentiation, recombinant mouse macrophage-colony stimulating factor (M-CSF) and receptor activator of nuclear factor κ B ligand (RANKL) were purchased from R & D systems (Minneapolis, MN, USA). BMMs were plated at $6X10^4$ cells/well in 12-well dishes in basic medium plus 30 ng/ml M-CSF with or without RANKL (30 ng/ml) for 3 days. Vehicle for RANKL and

M-CSF was 0.1% bovine serum albumin (BSA) in phosphate buffered saline (PBS).

All studies were conducted in accordance to the approved protocols by the Institutional Animal Care and Use Committee of the University of Connecticut Health Center.

COS-7 and MC3T3-E1 cells were obtained from American Type Culture Collection (ATCC) and were cultured in DMEM and α-MEM (Lonza, Basel, Switzerland) basal media respectively, and were passaged every third day of culture. For optimal growth, the media were supplemented with 10% (v/v) FBS (Gibco, Billings, MO) and Penicillin/Streptomycin (Lonza), and the cells were maintained under standard cell culture conditions (37°C and 5% CO_2). The cell lines were regularly checked for mycoplasma contamination. FuGENE 6 reagent (Promega, Madison, WI) was used for transient transfections according to manufacturer's instructions. Lentiviral transductions for shRNA and CRISPR-Cas9 approaches were performed as previously described.

DNA plasmids pLKO.1 puro vector (Addgene plasmid # 8453) was a gift from Dr. Bob Weinberg. lentiGuide-Puro (Addgene plasmid # 52963) and lentiCas9-Blast (Addgene plasmid # 52962) were gifts from Dr. Feng Zhang (Massachusetts Institute of Technology, Cambridge). The farnesylated CIB (CIB-CAAX) and full-length Cry2 expression plasmids (same as addgene plasmids 28240 and 26871 respectively) were gifts from Dr. Chandra Tucker (University of Colorado, Denver). The source cDNAs of mouse Plexin-B1, Plexin-B1-RA, and Plexin-B1-delPBD (Fig. S1) were from Dr. Hiroshi Takayanagi (Tokyo Medical and Dental University,

Japan). The cDNAs of PRG and LARG were from Dr. Keith Burridge (University of North Carolina at Chapel Hill), of PRG and LHordijk (University of Amsterdam, the Netherlands), myosin regulatory light chain (MRLC) from Dr. Rex Chisholm (Northwestern University), and PH-Akt from Dr. Craig Montel (University of California,Santa Barbara). These constructs were initially subcloned into the pTriEx-4 vector (Novagen) using polymerase chain reaction (PCR) and restriction digestion. Cry2 was positioned at the N-terminus and Plexin-B1 at the C-terminus to minimize interference with PRG and LARG. As indicated in the results and figure legends, tags of compatible fluorescent proteins including mCerulean, mVenus and mCherry were appended to facilitate detection. Unless specified otherwise, the termini of tagging were positioned as in the orders they were written. Additional point mutations in the Cry2, D387A and D393A, were generated using overlapping PCR. The open reading frames of all DNA plasmids were verified by DNA sequencing.

Co-culture migration assay Cell culture inserts (Ibidi, Germany) were used according to manufacturer's instructions. Briefly, the culture inserts were placed on tissue culture dishes and BMMs were cultured and differentiated into osteoclasts inside one of the insert chambers. Upon appearance of multinucleated osteoclasts, osteoblasts or MC3T3-E1 cells were added to the empty adjacent chamber. After 5-6 hours of incubation allowing the cells to adhere to the tissue culture dish, the inserts were gently lifted using tweezers enabling the cells to migrate towards the osteoclasts. Delay in retraction and protrusions upon contact were determined by visual inspection. Initiation of

retraction was identified as the time point when a protrusion in contact with osteoclasts began to contract. Initiation of protrusions was identified as the time point of formation of the persistent protrusions that enabled the cell to migrate away from the site of contact. Cell velocities were computed by measuring the displacement of the cell nuclei.

Quantification of CIL Whether a protrusion collapsed at the site of cell-cell contact was determined by visual inspection using time lapse images within 30 minutes after contact. Previous studies have quantified CIL by measuring spatial separation between cells undergoing CIL[42,47,59]. Since osteoclasts are large cells with multiple nuclei, we determined the spatial separation between osteoclasts and osteoblasts by computing the difference in distances between the osteoblastic nucleus and the site of contact at the time of and 40 minutes after contact. Positive and negative values respectively indicate spatial separation or lack of it. Changes in direction of migration of osteoblasts after contact were assessed by measuring contact acceleration indices (Cx) using vector analyses as described previously[42–44]. Briefly, the displacement of a migrating osteoblast for 40 min before contact (vector A) and 40 min after contact (vector B) were determined by tracking the nuclei. The Cx component of the vector (B-A) is a measure of how much the cell has deviated from its original trajectory (vector A') in the migration axis after contact (Figure 12h). Cx values for MC3T3-E1 cells that did not come in contact with osteoclasts were also determined for 40 minute intervals. Positive and negative values of Cx respectively indicate persistence

and reversal of direction of motion. In the absence of CIL, Cx approaches zero, whereas higher magnitudes indicate significant deviation from expected path.

Real-time quantitative PCR Total RNA was extracted using Trizol (Invitrogen) following manufacturer's instructions. 4 µg of total RNA was DNase treated (Ambion Inc., Austin, TX) and converted to cDNA by the High Capacity cDNA Archive Kit (Applied Biosystems, Foster City, CA). PCR was performed in 96-well plates. Assays-on-Demand Gene Expression Taqman primers (Applied Biosystems) were used for PCR (Mm99999915_g1 for *Gapdh*; Mm00443147_m1 for *Sema4d*; Mm00555359_m1 for *Plxnb1*). *Gapdh* served as endogenous control. All primers were checked for equal efficiency over a range of target gene concentrations. Each sample was amplified in duplicate. PCR reaction mixture was run in Applied Biosystems Prism 7300 Sequence Detection System instrument utilizing universal thermal cycling parameters. Data analysis was done using relative quantification (RQ, $\Delta\,\Delta\,C_t$) or the relative standard curve method. As per manufacturer's recommendation, any cycle threshold (C_t) values obtained below 33 were considered undetectable for that particular target gene.

Western blot analysis MC3T3-E1 and POBs prior and after addition of β-glycerophosphate were washed three times with phosphate-buffered saline, and lysed on ice in a buffer containing 1% Triton X-100, 50 mM monobasic sodium phosphate (pH 7.4), 150 mM NaCl, 5 mM EDTA and Halt^{TM} Protease inhibitor cocktail (Thermo Scientific, Rockford, IL, USA). The cell lysates were fractionated using 4-12% NuPAGE gels (Invitrogen), immobilized on to PVDF membranes (Millipore), followed by immunoblotting using anti-Plexin-B1 monoclonal antibody

(A-8, Santa Cruz Biotechnology, Dallas, TX, USA) or anti-alpha-tubulin monoclonal antibody (DM1A, Cedarlane laboratories, Burlington, Ontario, Canada) and horseradish peroxidase-coupled secondary antibody (Millipore, Germany). Enhanced chemiluminescence detection (Pierce, Waltham, MA, USA) and autoradiography were used to detect the signals. For detection of Sema4D-Fc horseradish peroxidase-coupled Protein-A was used. The blot images were cropped to show relevant bands. For Figure 12c, the uncropped scan is shown in Figure 44.

RNAi approaches and CRISPR-Cas9 mediated Plexin-B1 knock out

siGENOME non-targeting (D-001206-13-05) and Plexin-B1 (M-040982-01-0005) siRNA pools (GE Dharmacon, Colorado, USA) were used according to manufacturer's instructions.

shRNA target sequences for luciferase (Luc, TRCN0000072254) and Plexin-B1 (sh1 - TRCN0000078913, sh2 - TRCN0000078917 and sh3 - TRCN0000078916) were identified using Broad Institute Genetic Perturbation Platform web portal (http://broadinstitute.org) and were cloned into pLKO.1 puro vector.

To identify target sites for CRSPR-Cas9 mediated knock-out, the genetic sequence of Plexin-B1 was obtained from UCSC genome browser (http://genome.ucsc.edu) using the mouse assembly GRCm38/mm10 (December, 2011). The gene encoding Plexin-B1 has 38 exons, with the start codon located within the third exon. Two sgRNAs were designed flanking the start codon (Figure 14f,Table 1) using CRISPR design tool by Zhang lab

(http://crispr.mit.edu) so that Cas9 mediated cleavage was expected to delete a 100 bp region including the start codon. The sgRNAs were cloned into lentiGuide-Puro vector[68]. Cas9 and the sgRNAs were stably expressed in MC3T3-E1 cells using lentiviral transduction. Genomic DNA from 24 clones of the transduced MC3T3-E1 cells were extracted using Quick-gDNA™ kit (Zymo Research, Irvine, CA, USA) as per manufacturer's instructions. Upon PCR screening we identified two clones that showed deletion at the expected site (Figure 14g, Table 1). DNA sequencing validated the loss of Plexin-B1 start codon in both of these clones. Loss of Plexin-B1 expression was further confirmed using western blot (Figure 12d).

Immobilization of Sema4D-Fc and IgG1 on silica beads Sema4D-Fc and hIgG1 were immobilized on 5 μm diameter Silica Bind-IT™ pre-activated microspheres (Catalog # SB06N) from Bangs Laboratories (Fishers, IN, USA) by following the manufacturer's instructions with minor modifications. Briefly, 50 μl of the 2.5% bead suspension was centrifuged at 1000 X G for 5 minutes. The supernatant was removed and the beads were washed thrice in 100 μl coupling buffer (50 mM MES buffer, pH 5.2). After the final wash, the supernatant was removed and 25 μl coupling buffer. 25 μl of Sema4D or hIgG1 solution (0.1 μg/ml) were added to the bead suspension and incubated for 2 hours at 4℃ for 2 hours on a rotator. The suspensions were centrifuged, the supernatant was removed and the beads were washed thrice in 100 μl storage solution (150 mM NaCl, pH 7.0). After the final wash, the beads were resuspended in 50 μl storage solution and this suspension was used for further experiments. To assess the

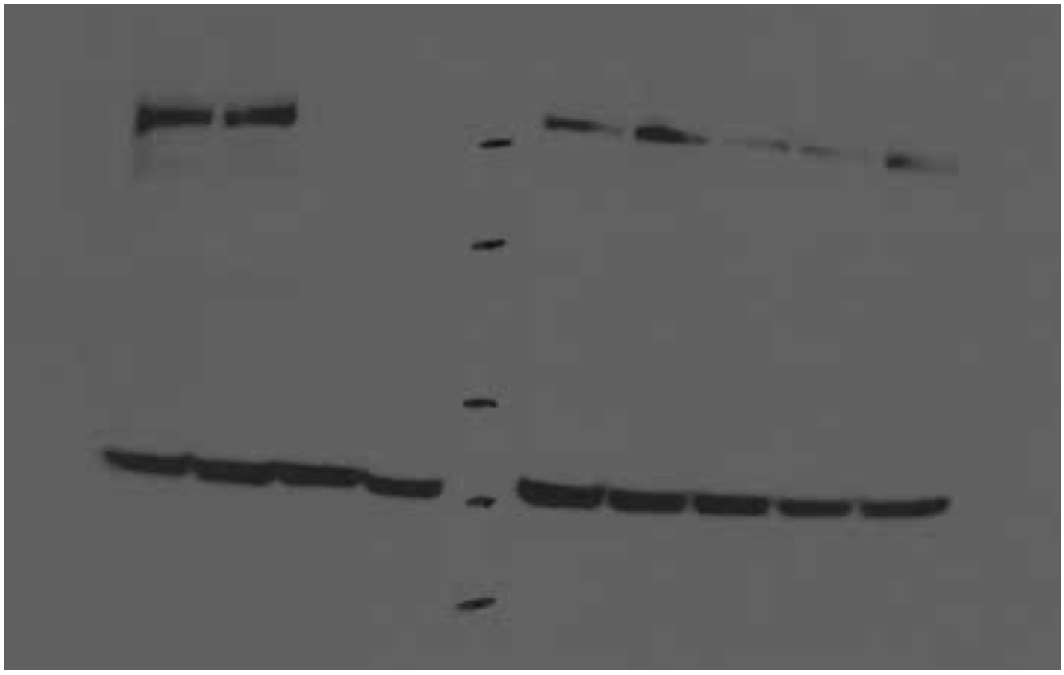

Figure 44. Full blot for Figure 12c.

amount of Sema4D immobilized on the beads, western blot was performed under non-reducing conditions. The samples 1X and 1/10X dilutions were equivalent to 25 µl and 2.5 µl of the bead suspension. From the western blot (Supplementary Figure 20d, e) we estimated that 80.5 ng Sema4D-Fc was present in the 1/10X sample. The density of the beads as provided by the manufacturer is $2g/cm^3$. Assuming no loss of beads or Sema4D-Fc during the sample preparation and assuming perfectly spherical beads, we calculated that the average number of Sema4D-Fc molecules bound to each silica bead was around 1000. Assuming a hemispheric contact (Figure 20f), each bead would provide 500 Sema4D-Fc molecules to come in contact with the cells. Furthermore, an even distribution of Sema4D-Fc is equivalent to a surface density of 12.73 molecules/μm^2, which amounts to a distance of 280 nm between each molecule (Figure 20g). It is possible that by using a significantly higher surface density of Sema4D-Fc, or enabling diffusion of Sema4D-Fc on such beads by using lipid layers may solve this problem; however such approaches would still not allow sufficient spatial and temporal control since it is difficult to manipulate the specific time and location of contact between cells and the beads.

Imaging setup. All time-lapse imaging were performed on a customized Nikon Ti-E inverted microscope. Phase contrast images for osteoclast co-culture experiments were captured using a 10x objective (NA 0.30) and Andor Neo 5.5 sCMOS camera. Wide field fluorescence imaging was performed using 40x oil objective (NA 1.30) using LED sources for excitations at 438, 513 and 575 nm (CoolLED) for imaging mCerulean, mVenus, and mCherry respectively. TIRF

imaging was performed using a 60x oil TIRF objective (NA 1.49). The microscope was modified with a “stage-up” design which enables an insertion of two independent, motorized dichroic mirrors/filter cubes in the microscope infinity space. A dichroic mirror in the bottom cube was used to reflect excitation laser lines at 442, 514, 594 nm for imaging of mCerulean, mVenus, and mCherry respectively. The laser lines were lunched from a fiber-coupled LMM5 system (Andor) equipped with an acousto-optic tunable filter (AOTF) for shutter and intensity control. Another dichroic mirror (495LP) in the top cube was used to bring in optogenetic illumination originated from a LED source at 440 nm (CoolLED). The 495LP mirror permitted immediate acquisition of mVenus or mCherry after optogenetic illumination. Alternatively, the top mirror can be rotated out to a blank position for Patterned illumination was generated using a commercial digital mirror device (Mosaic, Andor). The fluorescent emission was captured with an EMCCD camera (iXon Ultra, Andor). Metamorph software was used to control the imaging set up. Live cell imaging was performed at 37°C in a heated chamber (Bioptechs) with humidified 5% CO_2 supply. Vitamin and phenol red-free media (US Biological) supplemented with 2% FBS were used in imaging to reduce background and photobleaching.

Membrane recruitment assay COS-7 or MC3T3-E1 cells were transiently transfected with mVenus- or mCherry-optoPlexin along with CIB-CAAX. The recruitment of optoPlexin to the plasma membrane was induced with a short pulse (50 ms) 440 nm illumination at 10 s intervals, shortly (typically 10-15 frames) after acquisition of base lines of fluorescent intensities. For localized activation, a 5 μ a-

diameter circular region near the cell periphery was chosen for each cell. TIRF imaging of mVenus and/or mCherry channel was used to gauge the amount of optoPlexin that became excitable by the evanescent wave (~200 nm from the coverslip surface) presumably due to association with the plasma membrane. Because a robust translocation of optoPlexin could be induced in the assay (Fig. 1c), proteins associated with optoPlexin, labeled with different fluorescent proteins for example, mVenus-PRG and mCherry-optoPlexin for example, may also 'precipitate' into the TIRF imaging plane due to association. After conducting background subtraction using the mean fluorescence intensities of cell-free regions, the fluorescence intensities after 10 blue light pulses were normalized to that before blue light illumination, and the changes were used to estimate the recruitment of optoPlexin and its associated proteins to the plasma membrane. The results of membrane recruitment assay were quantified as follows,

$$R_C = \frac{\Delta F/_F\,(mVenus)}{\Delta F/_F\,(mCherry)}$$

where R_C = relative co-recruitment and F = fluorescence intensity.

To minimize effects of noise in measurement of binding, only cells with at least 30% fractional increase in optoPlexin signal were considered.

Quantification of optoPlexin clustering The local variance of fluorescence intensities was used to estimate the extent of molecular clustering of optoPlexin and its associated proteins. Briefly, TIRF imaging was used to sample the basal focal plane of cell, thereby rejecting most of the out-of-focus fluorescence. The raw images were first background subtracted using cell-free regions. To eliminate effects of changes in cell topology on changes in variance of fluorescence

intensities, a ratio image was then calculated using the original image divided by a processed one, which was passed through an empirically determined 5x5 median filter. Clustering index was defined as the fractional changes in standard deviation of the ratiometric image (Figure 25).

Analysis of cell repolarization Fluorescence images of MC3T3-E1 cells expressing optoPlexin (or its mutants) were thresholded based on intensity to produce binary images. Cell velocity at each frame was measured by tracking the displacement of the centroids of these binary images, and average of such velocities was used to assess the cell velocity. Changes in cell shape were identified by subtracting the binary images in a time series from the image at time 0. Pixels of areas in positive values were identified as protrusions. Conversely ones in negative values were identified as retractions. Areas where the images overlapped since time 0 were designated as neutral regions. An arbitrary floor was added to the image to display these regions in color: red for protrusion, blue for retractions and green for regions occupied by the cell at both time points, whereas cell free regions were shown in white. The region of blue light illumination is shown in yellow (Figure 30d). Only regions exceeding 50 pixels (3.52 μm^2) were considered in the quantification of protrusions and retractions, and only regions that were converted from protrusions to retractions were used to measure induction of retractions by optoPlexin.

To measure the angle of retraction (θ_1) or protrusion (θ_2) with respect to the region of illumination, a straight line joining the centroid of the cell at time 0 was used as the horizontal axis. The angle between the straight line joining the centroid

of protrusions (or retractions) and the centroid of the cell at time 0 and the horizontal axis was defined as the angle of protrusion (or retraction). The proximity of retraction (d_1) and protrusion (d_2) to the region of illumination was measured by the linear distance between the centroid of protrusion (or retraction) and the centroid of the region of illumination. Delay in initiation of retraction was determined by identifying the time point when the cell area in a 50 μm diameter circle centered around the region of illumination (as defined for Figure 30d) began to contract. Metamorph (Molecular Devices, Sunnyvale, CA) and Matlab (Mathworks, Natick, MA) softwares were used for image processing and data analyses.

Imaging and analysis of FRET sensors For FRET imaging, donor (mCerulean) images were captured sequentially after the FRET (mVenus) image. The Dora-RhoA sensor uses an intra-molecular effector fragment derived from the RhoA effector Protein Kinase N (PKN) to detect the nucleotide states (GDP or GTP) of RhoA. Upon GTP-loading or activation of RhoA, Dora-RhoA interacts with the effector fragment and adopts a closed conformation. The conformational change leads to an increase of FRET signal, the extent of which is quantifiable using the ratio of FRET/CFP. For RhoA sensor imaging in MC3T3-E1 cells upon Sema4D-Fc or hIgG1 treatment mCerulean and FRET images were acquired every minute. For RhoA sensor imaging in COS-7 cells on optoPlexin activation, sequential images of mCherry, mCerulean and FRET images were acquired every 10 s using TIRF excitation with 594 nm and 442 nm lasers. Since the excitation wavelength for CFP and FRET was sufficient to activate Cry2 recruitment, no additional blue light

illumination was employed. Ratiometric images of FRET and mCerulean were generated and changes in the average intensity of these ratiometric images were used to measure changes in RhoA activity. The first image in each of these time series was used for baseline measurement of RhoA activity before optoPlexin activation. Changes in ratiometric measurements for a binding deficient RhoA control sensor in response to mCherry tagged Cry2 recruitment was used to correct for optical artifacts of mCherry and Cry2 recruitment to the TIRF plane. DORA-Rac1 and DORA-Cdc42 sensors share a similar design as the Dora-RhoA sensor except using a Cdc42/Rac interactive binding (CRIB) domain of p21-activated kinase (PAK) as the binding domain. The non-binding control Cdc42 sensor control harbours a mutated (H83,86D) effector domain in Dora-Cdc42 and does not alter FRET in response to activation. For Cdc42 sensor, Cdc42 control sensor and Rac1 sensor imaging in MC3T3-E1 cells, optoPlexin was locally activated using the Mosaic illumination system as mentioned above until we observed local retraction and distal protrusions, at which point the time lapse imaging was ended and FRET and mCerulean images were obtained immediately afterwards. Ratiometric images from each of these FRET and mCerulean image pairs were processed as described previously[69] and used to visualize the spatial distribution of Rac1 and Cdc42 activities in individual cells.

Statistical analyses Microsoft Excel and Matlab were used for statistical analyses. Sample sizes for different experiments were chosen based on the commonly used range in the field without conducting any statistical power analysis. Normal

probability plot function of Matlab was utilized to confirm normal distribution of the data. Similarity of variance across all the groups (or before and after stimulation) being compared were tested using F-test in Matlab. For RT-PCR data, one way ANOVA was performed using Sigmaplot 11.0 (Systat Inc., Chicago, IL). Sample means and standard error of mean was calculated and shown on the graphs. P values were obtained from one-tailed Students t-test.

Data availability: All relevant data are available in the article and the supplementary information, or upon request from the authors.

Chapter III

Molecular mechanisms of Plexin-B-mediated activation of PDZ-RhoGEF and LARG

Introduction: As described in Chapter I and II, B-family plexins activate RhoA through two PDZ-domain containing RhoGEFs, PRG and LARG. These two RhoGEFs, along with p115, share a regulator of G protein signaling (RGS)-like domain and are classified as RGS-RhoGEFs[172] (Figure 45). Although it is largely understood how RGS-RhoGEFs are activated by $G\alpha_{12/13}$ of heterotrimeric G proteins--activated $G_{\alpha 12/13}$ binds with the RGS domain and stimulates GEF activity[173,174]; how the B family of plexins activate PRG and LARG remains elusive. It is thought that Plexin-B1 interacts with PRG or LARG solely via its C-terminal PDZ-binding motif (PBD). However, the PBD-PDZ interaction has been proposed to be constitutive and thus cannot explain how the RhoGEF activity is regulated downstream of Plexin. Previous studies have shown that Rnd1 binding to the RBD of Plexin promotes PRG recruitment and RhoA activation[69], suggesting that 1) an additional interaction(s) may exist between Plexin-B1 and PRG and 2) such an interaction may involve or be regulated by the RBD of Plexin. Here, I will discuss some results from ongoing investigations into these molecular mechanisms. My data demonstrate that Plexin-B1 RBD acts as an autoinhibitory domain in PRG recruitment: deletion or mutation of the RBD can relieve the inhibition. Furthermore, we identify the RGS domain of PRG to play a critical role in Plexin-B1 binding. Our data sheds new light into the mechanism of Rac1 regulation of Plexin-B1 signaling and identifies an unexpected role of the RGS domain in PRG binding to Plexin-B1.

Results: As discussed in Chapter II, I had developed an optogenetic tool named optoPlexin to initiate Plexin-B1 signaling upon blue light illumination, which efficiently recruited PRG and LARG to the plasma membrane. We utilized co-recruitment of PRG by optoPlexin to investigate how Rac1 might regulate PRG recruitment by Plexin-B1 (Figure 46). Consistent with the critical role of PBD-PDZ interaction, we had observed that an optoPlexin mutant lacking the PBD (optoPlexin-delPBD) failed to recruit PRG. Another optoPlexin mutant lacking RasGAP activity (optoPlexin-RA) efficiently recruited PRG, suggesting that RasGAP activity may not indirectly affect PRG recruitment.

GTPase binding to Plexin-B1-RBD is critical for RasGAP activity and has been reported to promote PRG recruitment and RhoA activation[69,63]. To test whether GTP-loaded Rac1 regulates PRG recruitment by optoPlexin, we co-expressed a constitutively active mutant of Rac1 (caRac1) tethered to mCerulean with optoPlexin and PRG or LARG. Co-expression of caRac1 significantly increased recruitment of PRG and LARG by optoPlexin (Figure 47a, b). Illuminating photoactivatable Rac1 (paRac1) or plasma-membrane recruitment of Cry2-caRac1 did not recruit PRG to the membrane (Figure 47c). Our observations indicate that the increased PRG recruitment was not due to direct association between caRac1 and PRG. These data suggest that Rac1 binding to Plexin-B1-RBD promotes its interaction with PRG. GTP-Rac1 binds to Plexin-B1-RBD and to investigate the role of Plexin-B1 RBD in PRG recruitment, we utilized a previously described mutation in the RBD domain (optoPlexin-GGA, figure 21) that is known to destabilize it and abrogate Rac1 binding as well as RasGAP

activity[62,63,175]. Despite the presence of the C-terminal PBD, optoPlexin-GGA failed to recruit PRG. This defect was not rescued by co-expression of caRac1 (Figure 48a), further excluding the possibility that caRac1 may independently recruit PRG. We further investigated the role of RBD by utilizing an oncogenic mutation in the RBD (OptoPlexin-L1799F, figure 21) that was detected in solid tumours[176,177]. The L1799F mutation increases the RBD stability, abrogates Rac1 binding, but has no impact on RasGAP function of Plexin-B1[176]. OptoPlexin-L1799F recruited PRG very efficiently, at levels comparable to optoPlexin with co-expression of caRac1. Co-expression of caRac1 with optoPlexin-L1799F did not further promote recruitment (Figure 48a). These opposite effects of GGA and L1799F mutants on PRG recruitment prompted us to speculate that these two mutants mimic an off and on state of a regulatory switch respectively. We hypothesized that either the GTPase-bound RBD provided additional binding sites between Plexin-B1 and PRG, or that it inhibited binding between Plexin-B1 and PRG, with the inhibition relieved upon GTPase binding. To test these two scenarios, we designed a mutant with deletion of the RBD (optoPlexin-delRBD, figure 21), speculating that lack of PRG recruitment would support a model of RBD providing additional binding sites, whereas efficient recruitment would support the second model. OptoPlexin-delRBD recruited PRG at levels comparable to WT . Further deletion of a short proline rich region in OptoPlexin-delRBD (optoPlexin-delRBD-PRR, figure 21) did not affect PRG recruitment (Figure 48b).

Recently, an additional binding site for GTP-Rac1 on Plexin-B1 has been identified, which if mutated disrupts Rac1 binding as well as RasGAP activity[71]. GTPase binding to this secondary site has been proposed to be regulated by the Plexin-B1 juxtamembrane helix, which facilitates a trimeric Plexin-B1-GTPase complex upon Sema4D binding. To test whether the juxtamembrane region of Plexin-B1 could regulate PRG recruitment through the GTPase binding site, we deleted the juxtamembrane helix in an optoPlexin mutant (optoPlexin-delN, figure 21). OptoPlexin-delN showed neither any defects nor any improvements in PRG recruitment when compared to WT (Figure 48b). It is possible that optoPlexin does not undergo the juxtamembrane helix dependent trimerization unlike endogenous Plexin-B1; or that even if present, Cry2 mediated clustering overshadows any effects such trimeric conformation may have on PRG recruitment. Regardless, our observations indicate that the juxtamembrane helix of Plexin-B1 was not critical for PRG recruitment. Furthermore, this indicates that the RBD predominantly mediates the effects of GTPase binding to Plexin-B1 on PRG recruitment.

Plexin-B1 is thought to recruit PRG through a constitutive interaction between the PBD in Plexin and PDZ domain in PRG[68]. To examine the importance of the PDZ-PBD interaction, previously we have shown that optoPlexin-delPBD failed to recruit PRG or activate RhoA (Figure 26c). Conversely, we introduced a mutation in the PDZ domain of PRG (V106E) to disrupt PBD-PDZ interaction (Figure 45). OptoPlexin failed to recruit PDZ(V106E) indicating that PDZ-PBD interaction is necessary for recruitment. To examine

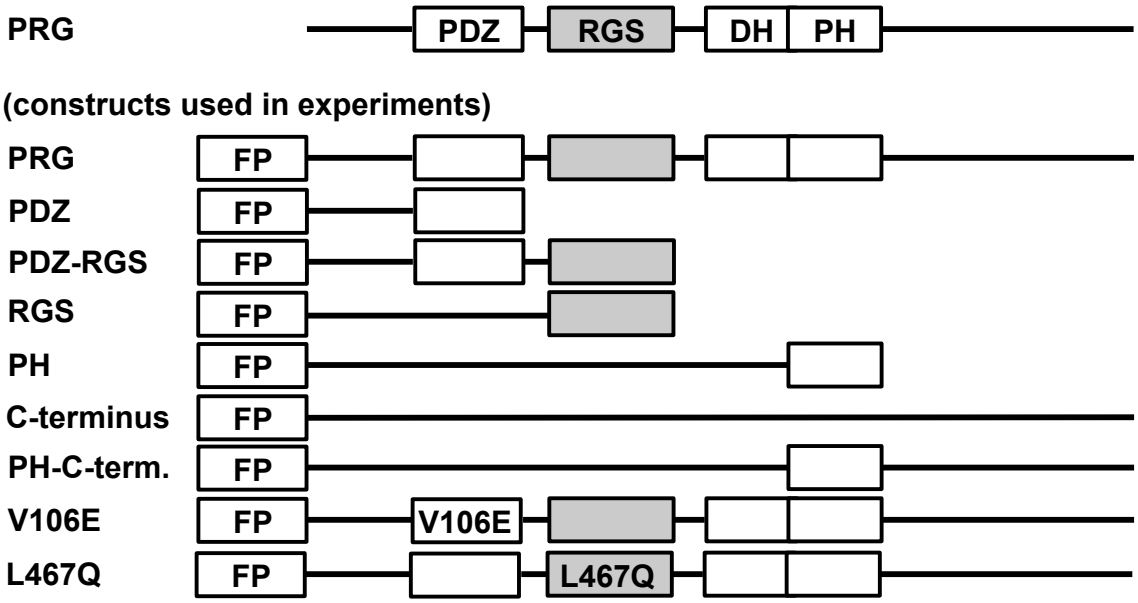

Figure 45. Functional domains of PDZ-RhoGEF. Domain organization of PDZ-RhoGEF and its mutants that were used in this study. FP, fluorescent protein.

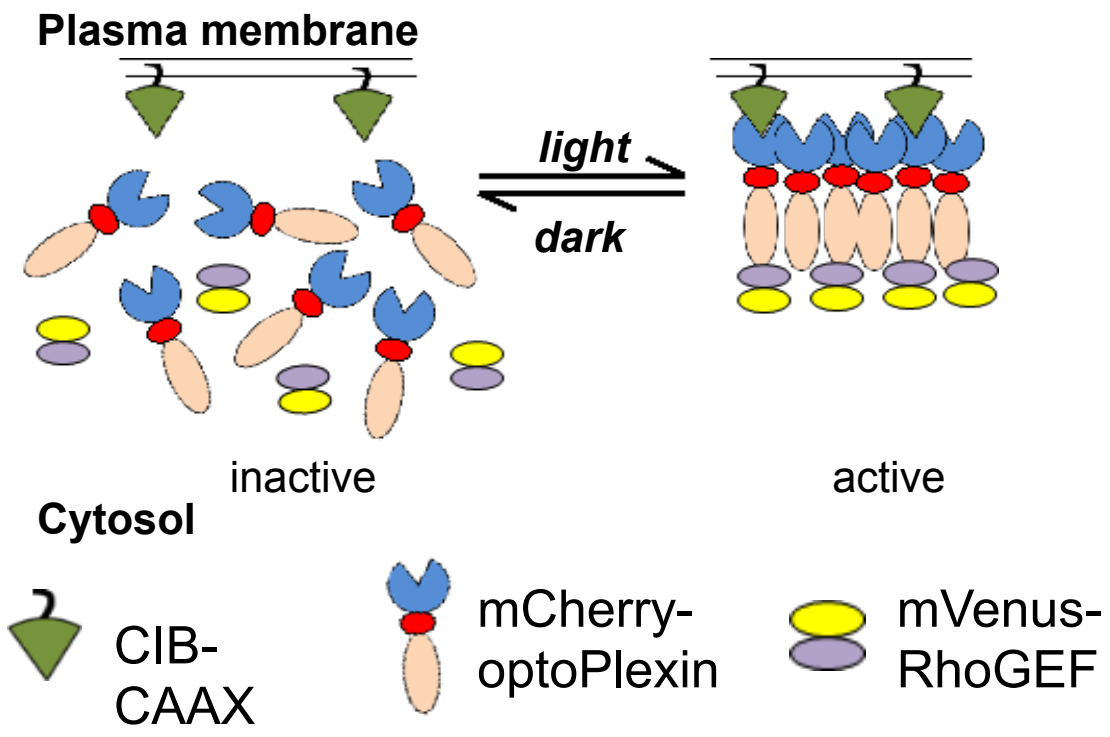

Figure 46. RhoGEF co-recruitment assay. Assay used to probe interaction between PRG and Plexin-B1

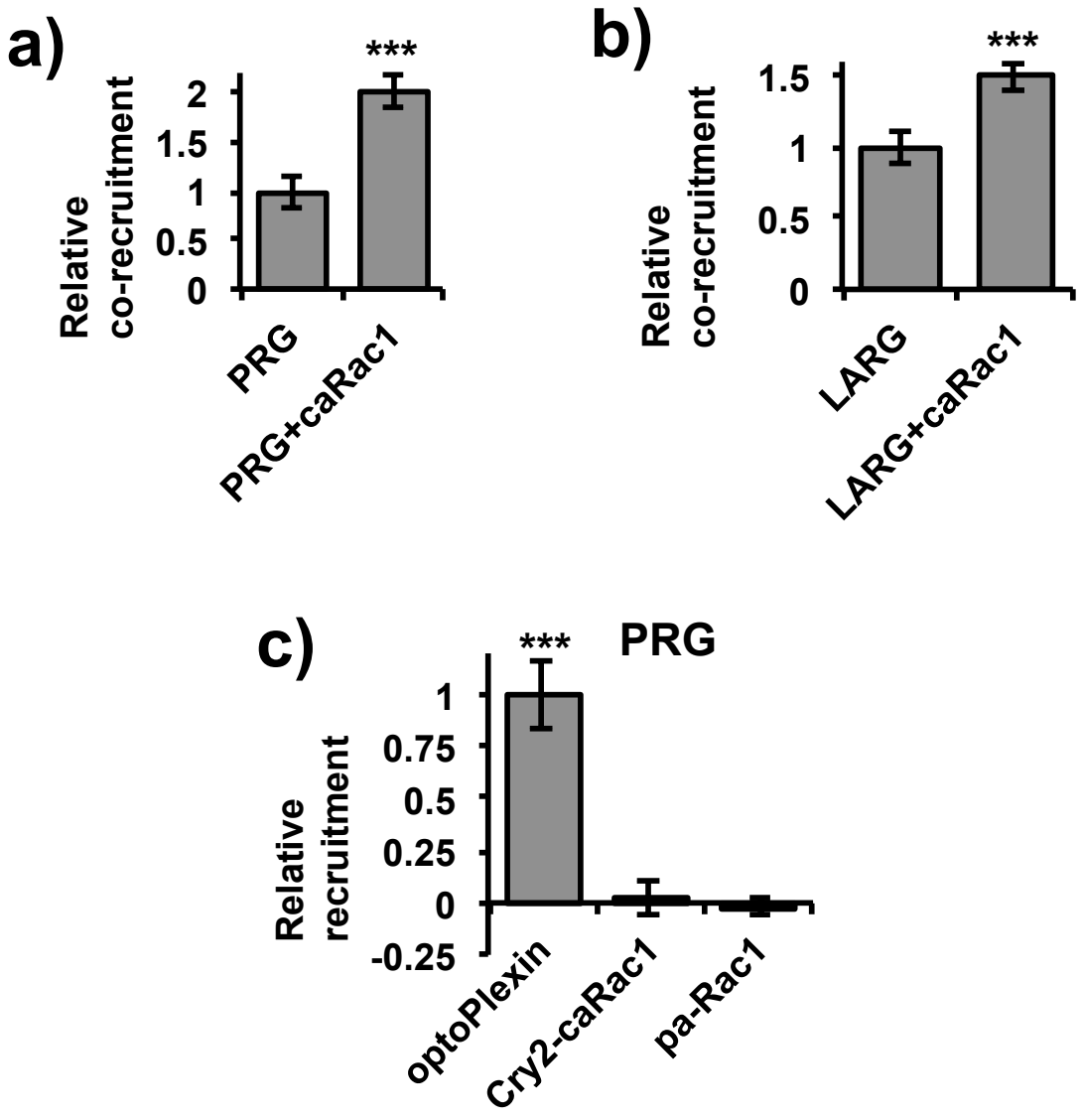

Figure 47. Rac1 association with Plexin-B1 promotes RhoGEF recruitment. Relative co-recruitment of (a) PRG and (b) LARG by optoPlexin with or without overexpression of caRac1. (c) Relative increase in membrane localization of mVenus-PRG upon illumination of optoPlexin, Cry2-mCherry-caRac1 or mCer3-Pa-Rac1. Note that for (c) pa-Rac1 is tethered to the membrane. The fluorescence signal of mVenus-PRG after one minute of blue light illumination was normalized to that before illumination. n>15. mean ± s.e.m. *** p<0.001 [there is no single asterisks on the figure.

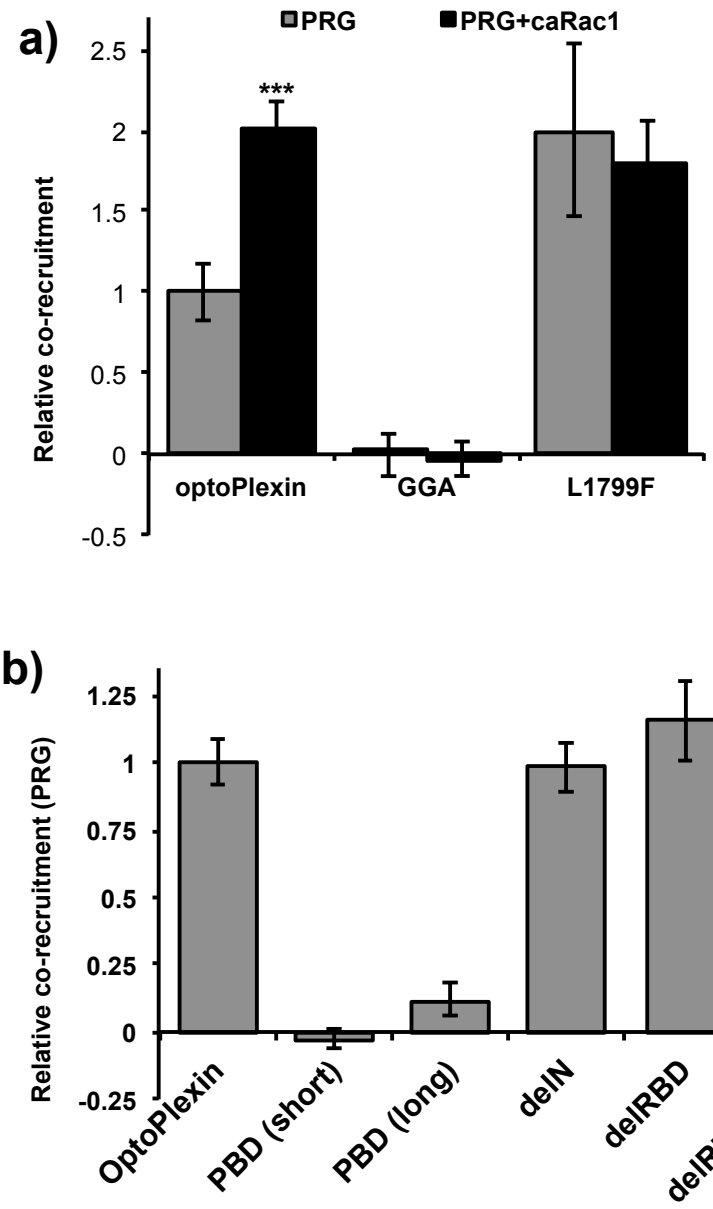

Figure 48. Plexin-B1-RBD is a regulatory switch for PDZ-RhoGEF recruitment. (a) Relative co-recruitment of PRG by optoPlexin, optoPlexin-GGA and optoPlexin-L1799F with or without overexpression of ca-Rac1. (b) Relative co-recruitment of PRG by optoPlexin mutants. n>15. mean ± s.e.m. *** $p<0.001$, * $p<0.05$.

whether the PBD alone is sufficient for PRG recruitment, we developed a construct with the C-terminal 10 residues of Plexin-B1 tethered to Cry2 (optoPlexin-PBD, figure 21). We reasoned that if Rac1 binding exposed a cryptic PBD, then optoPlexin-PBD ought to efficiently recruit PRG. We found that optoPlexin-PBD fail to recruit PRG (Figure 48b). Additional interactions between the PDZ domain of PRG and the RasGAP domain of B-plexins have been proposed to stabilize PDZ binding[178]. Nevertheless, tethering the 20 C-terminal residues of Plexin-B1, which included the additional interaction sites with PDZ domain (Figure 21), to Cry2 did not significantly rescue the recruitment of PRG (Figure 48b). It is likely that the PBD requires an intact RasGAP domain to stabilize the extended binding interface with PDZ and the above isolated PBDs may not be sufficient. Although crystal structures of B-family plexins did not indicate a cryptic PBD, the PBD could be cryptic in cells in the presence of other proteins. To investigate whether caRac1 binding affects the Plexin-B1-PDZ interaction, we utilized the PDZ domain of PRG (Figure 45) in the co-recruitment assay. Unexpectedly, co-expression of caRac1 did not promote recruitment of the PDZ domain (Figure 49a). Moreover, optoPlexin-GGA and optoPlexin-L1799F showed recruitment of PDZ domain not statistically different from the WT optoPlexin (Figure 49b). These data indicated that Rac1 promotion of PRG recruitment was not effected through increased PBD-PDZ binding.

Our data indicated that the PBD interaction, although necessary, was not sufficient for robust recruitment of PRG by Plexin-B1, suggesting that there might be additional interactions between Plexin-B1 and PRG. In both PRG and LARG

the N-terminal PDZ domain is followed by an RGS-like domain, catalytic DH-PH domain and an extended C-terminus. Particularly, the C-terminus and the RGS-like domain of PRG have been reported to mediate protein-protein interactions. The extended C-terminus of PRG and LARG mediates homo and hetero-oligomerization between PRG, LARG and p115-RhoGEF and may play a role in oncogenic transformation[179]. Furthermore, a proline-rich region in the C-terminus of PRG has been reported to bind with the SH3 domain of Phospholipase C–γ, whose SH2 domains bind to phosphorylated tyrosine residues in Plexin-B1[149]. We have previously shown that the tyrosine residues that mediate interaction with Phospholipase-Cγ are not critical for PRG recruitment by optoPlexin, RhoA activation, or optoPlexin mediated repulsion in migrating cells (Figure 26g, 28, 35). Furthermore, the proline-rich sequences in PRG are not conserved in LARG, further suggesting that these sequences are not critical for Rac1 mediated increase in PRG and LARG recruitment. The RGS-like domain is utilized by $G_{\alpha 12}$ and $G_{\alpha 13}$ components of G-protein coupled receptors to recruit PRG, LARG and p115-RhoGEF. However unlike those of p115-RhoGEF and LARG, the RGS-like domain of PRG lacks GAP activity for $G_{\alpha 12}$ and $G_{\alpha 13}$[180]. Unlike the PDZ domain, optoPlexin did not efficiently recruit the RGS-like domain of PRG (Figure 45) indicating that if present, any direct interactions with Plexin-B1 are significantly weaker than the Plexin-B1-PDZ binding or require PDZ domain interaction (Figure 50b,c). To investigate whether in the presence of the PDZ domain the RGS-like domain might mediate recruitment by Plexin-B1, we utilized the PDZ-RGS domains in recruitment assay (Figure 45). The PDZ-RGS domain was

efficiently recruited by optoPlexin, and co-expression of caRac1 increased the recruitment levels (Figure 49c). Moreover, optoPlexin-GGA failed to recruit PDZ-RGS domains whereas optoPlexin-L1799F showed very efficient recruitment levels, comparable to recruitment by optoPlexin in the presence of caRac1 (Figure 49d). Thus the PDZ-RGS domain recapitulated the Rac1 regulation of PRG recruitment indicating a role of RGS domain in Plexin-B1-PRG interaction.

The RGS-like domain of PRG interacts with GTP-loaded $G_{\alpha 13}$ through two distinct sites, which are conserved in LARG and p115-RhoGEF[174]. We speculated that these sites might also play a role in PRG recruitment by Plexin-B1. To investigate this possibility we introduced a mutation in the RGS-box subdomain of the RGS-like domain of PRG (L467Q) (Figure 45) to disrupt interaction with Ras-like domain of $G_{\alpha 12}$ and $G_{\alpha 13}$. To validate the mutation, we tethered a constitutive mutant of $G_{\alpha 12}$ to Cry2 (Cry2-$G_{\alpha 12}$) and utilized it for *in-cyto* recruitment of PRG and its sub-domains. Cry2-$G_{\alpha 12}$ efficiently recruited PRG, as well as the RGS-like domain, but not the PDZ domain of PRG (Figure 50a,b,c) demonstrating that Cry2-$G_{\alpha 12}$ interacted with PRG similar to GTP-loaded $G_{\alpha 12}$ and $G_{\alpha 13}$. In addition, Cry2-$G_{\alpha 12}$ did not show any defects in recruitment of PRG(V106E), suggesting that the PDZ domain does not significantly contribute to association of PRG with $G_{\alpha 12}$ (Figure 50d). As expected Cry2-$G_{\alpha 12}$ failed to recruit PRG(L467Q), thus validating the efficacy of the mutation. OptoPlexin failed to recruit PRG(L467Q). These data further supported an inhibitory role of the RGS-like domain in PDZ-PBD interaction (Figure 51).

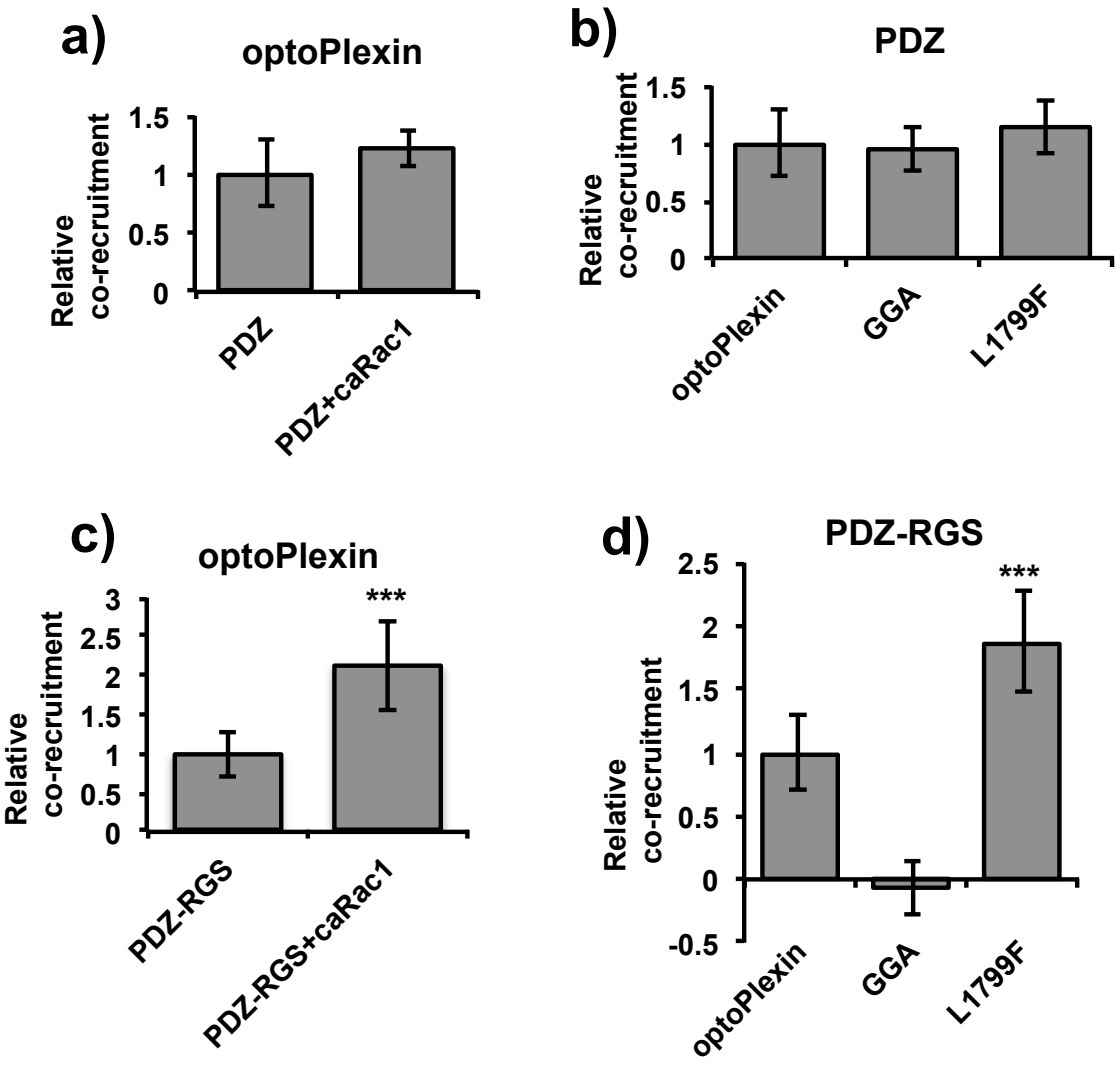

Figure 49. Rac1 regulation of PDZ-RhoGEF recruitment by Plexin-B1 is effected by the RGS domain. Relative co-recruitment of (a) PDZ domain and (c) PDZ-RGS domain by optoPlexin with or without overexpression of ca-Rac1. Relative co-recruitment of (b) PDZ domain and (d) PDZ-RGS domain by optoPlexin, optoPlexin-GGA and optoPlexin-L1799F. n>15. mean ± s.e.m. *** $p<0.001$, * $p<0.05$.

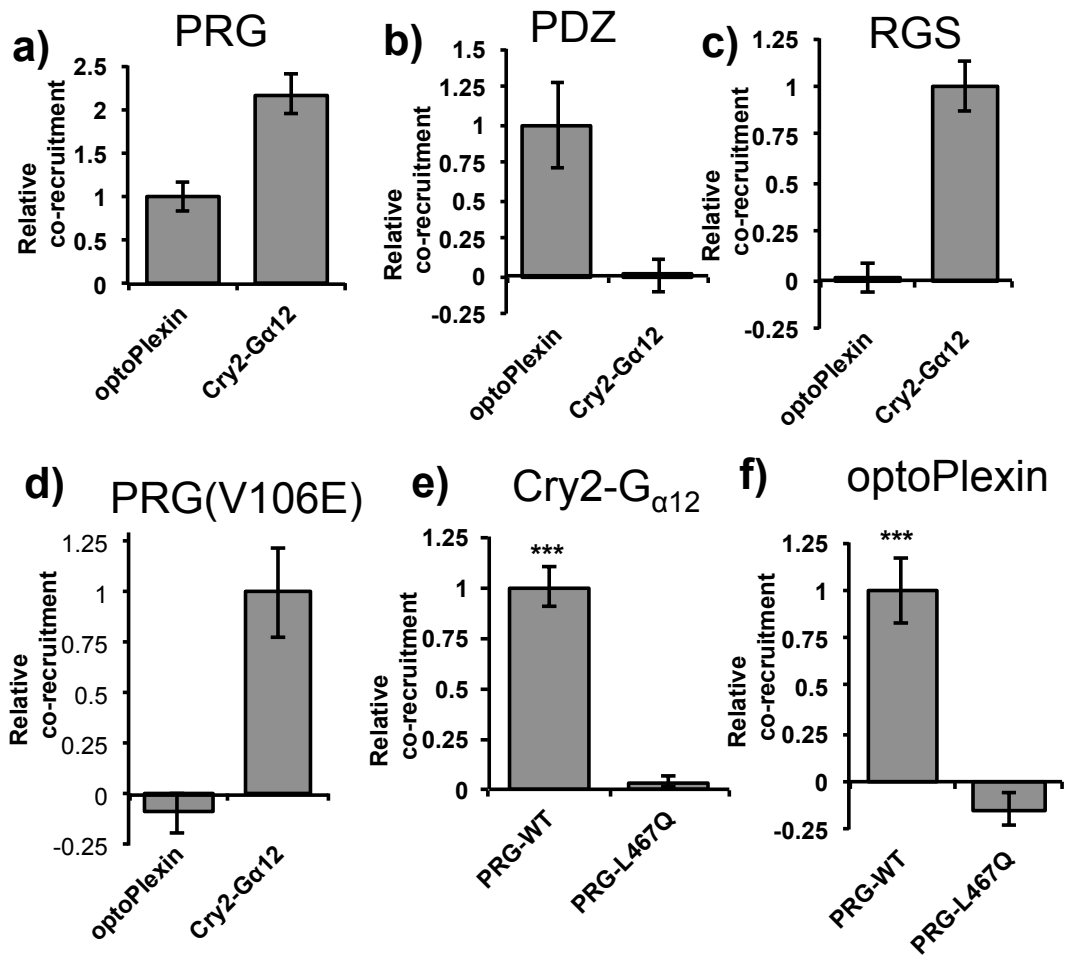

Figure 50. RGS domain mediates PDZ-RhoGEF association with both $G_{\alpha 12}$ and Plexin-B1. Relative co-recruitment of (a) PRG, (b) PDZ domain, (c) RGS domain, (d) PRG(V106E), (e) and (f) PRG(L467Q) by optoPlexin and Cry2-$G_{\alpha 12}$. n>15. mean ± s.e.m. *** p<0.001, * p<0.05.

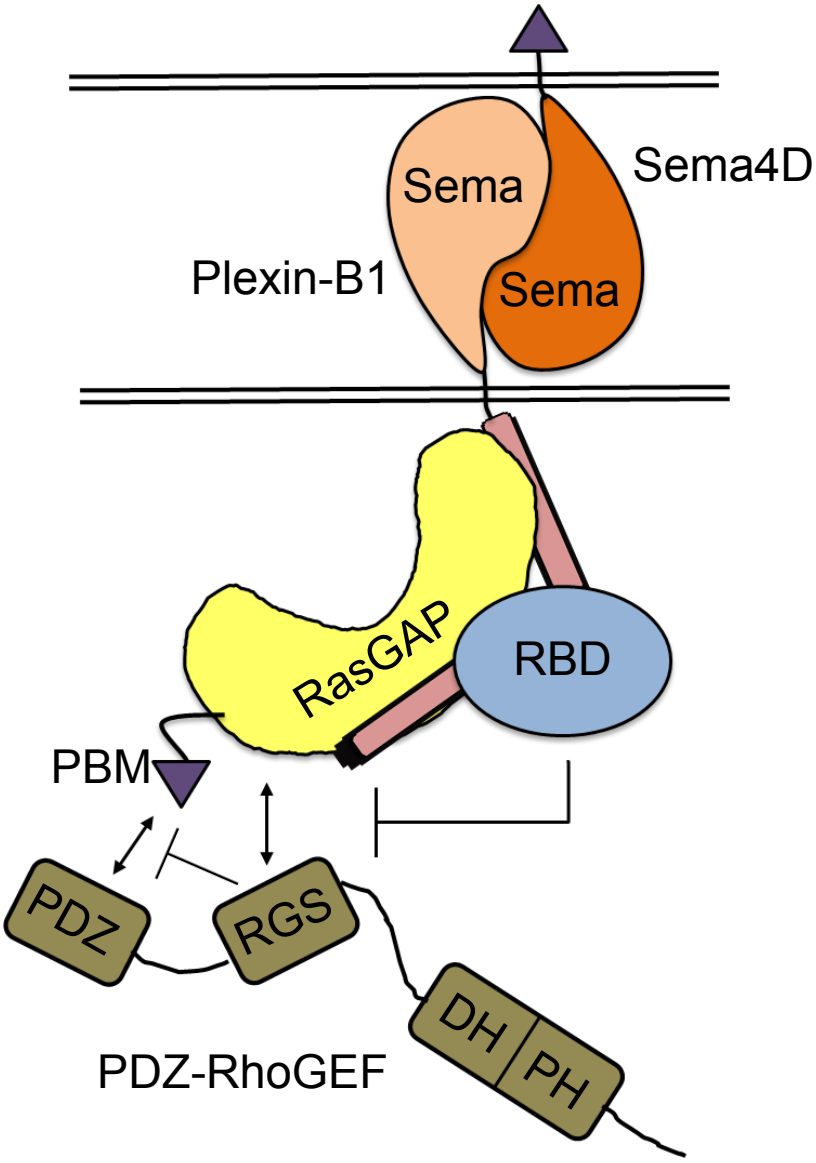

Figure 51. Proposed model for regulation of PRG recruitment through RBD of Plexin-B1. RGS may inhbit interaction between PDZ and PBM (same as PBD). RBD may inhibit interaction between the RGS domain and the RasGAP domain. This inhibition may be relieved upon Rac1 or Rnd1 binding to RBD.

Discussion and future directions: B family plexins utilize their C-terminal PBD to recruit PRG and LARG through what was thought to be a constitutive interaction with the PDZ domain of these RhoGEFs[68]. Our data suggests that PBD-PDZ interaction between Plexin-B1 and PRG is not constitutive, and is regulated by GTPase binding to Plexin-RBD. Lack of recruitment of PRG by optoPlexin-PBD indicated that the canonical PBD-PDZ interaction is not sufficient for efficient PRG recruitment, which is consistent with the low affinity (~ 30 μM) of bindng between PBD and PDZ domain[178]. Additional interactions between the RasGAP domain and the PDZ domain have been reported to significantly boost the affinity between Plexin-B1 and PDZ domain (to ~ 3 μM). This is reflected in our data wherein unlike optoPlexin, optoPlexin-PBD failed to efficiently recruit PRG. Regardless, these additional PDZ interactions do not explain why co-expression of caRac1 promoted recruitment of PRG and PDZ-RGS, but not of the PDZ domain alone. GTPase binding to Plexin-B1 is known to mediate its RasGAP activity[63]. Our data demonstrate a role of GTPase binding in RhoGEF recruitment. Furthermore, optoPlexin-GGA, which contains all the identified interaction sites between PDZ domain and PRG, recruited the PDZ domain efficiently, but not PRG or PDZ-RGS. Finally, mutating one of the known interaction sites between PRG-RGS-like domain and $G_{\alpha 12/13}$ abrogated PRG recruitment by optoPlexin. Taken together, these observations suggest a model where the RGS-like domain hinders PDZ-binding, through direct obstruction of the PBD-interaction or through allosteric inhibition (Figure 51). This obstruction is presumably relieved through some hitherto unknown interaction with Plexin-B1,

which is mediated by the Plexin-B1-RBD. Truncation of the RBD did not impact PRG or PDZ-RGS recruitment suggesting that it did not directly associate with the RGS domain. Since truncation of the juxtamembrane helix also did not impact PRG recruitment levels, we hypothesize that the RGS-like domain interacts with the RasGAP domain of Plexin-B1. Lack of efficient recruitment of the RGS-like domain with optoPlexin or any of its mutants suggests that the interaction is significantly weaker than that with PDZ domain. A pull-down assay might be appropriate to examine any interactions between purified Plexin-B1 (or its mutants) intracellular domain and the RGS-like domain of PRG. It is, of course, possible that $G_{\alpha 12}$ or $G_{\alpha 13}$ might co-operate with the Plexin-B1 signaling complex to respectively bind to the RGS-like and PDZ domain. Failure of optoPlexin in recruiting PRG(V106E) suggests that any association of the Plexin-B1 complex with the RGS domain is significantly weaker than the PDZ-PBD interaction, which is weaker than $G_{\alpha 12}$ or $G_{\alpha 13}$ association with RGS domain. This argues against a role of $G_{\alpha 12}$ or $G_{\alpha 13}$ GTPases in Plexin-B1 recruitment of PRG, since even in the absence of PDZ-PBD interaction, $G_{\alpha 12}$ or $G_{\alpha 13}$ associated with optoPlexin should have been able to recruit PRG(V106E).

Recently, Plexin-D1 has been reported to bind to GIPC1 (GAIP interacting protein, C-terminus 1) through the C-terminal PBD of Plexin-D1 and PDZ domain of GIPC1[181]. In the native state, GIPC1 exists in a dimerized state where the GH1 and GH2 domains that flank the PDZ domain inhibit interaction with Plexin-D1 C-terminal PBD. Our observations suggesting an inhibitory role of the RGS-like domain in mediating PDZ-PBD interaction appears, at least superficially, to

be similar in nature and might be another mode of conferring specificity to PDZ-PBD interactions. Investigating mechanisms that regulate interactions between other PDZ domain and PBD containing proteins might yield hints about Plexin-B1 and PRG regulation as well. GTPase binding does not significantly alter the conformation of the isolated Plexin-RBD[182]. Such binding may, however, relieve autoinhibition of the Plexin RasGAP domain by facilitating oligomerization wherein the RBD no longer blocks interaction between the RasGAP domain and GTP-loaded Ras or Rap proteins. GTPase binding may also induce conformational changes in the RasGAP domain to promote or stabilize its binding to small GTPases. Whether the same residues in the Plexin-B1 RasGAP domain might regulate interaction between small GTPases and PRG remains unexplored. While the plexins show remarkable homology in their intracellular domains, there are subtle differences that might explain their specificities for different Rho and Ras GTPases. In particular, all plexins have a conserved leucine residue (L1658 in Plexin-B1) in the RasGAP region that might directly interact with the GTP in GTP-loaded Ras or Rap proteins. In A family plexins, the L1658 residue is exposed to freely interact with GTP. However in B family plexins, a conserved tyrosine residue (Y1651 in Plexin-B1) appears to interact with L1658, and might regulate its interaction with GTP-Ras. Substituting the amino acid sequence in Plexin-B1 that spans through Y1651 with the corresponding sequence in Plexin-A1 and investigating PRG recruitment by the resultant protein might provide information regarding the role of these sites in PRG recruitment. If this indeed were the site of additional PRG interaction, it

would be interesting to examine whether GTP-Ras and PRG binding to Plexin-B1 are competitive or co-operative.

Materials and methods:

Cell culture and transfection. All the experiments in chapter II were performed on COS7 cells. COS-7 cells were obtained from American Type Culture Collection (ATCC) and were cultured in DMEM (Lonza, Basel, Switzerland) basal media, and were passaged every third day of culture. For optimal growth, the media were supplemented with 10% (v/v) FBS (Gibco, Billings, MO) and Penicillin/Streptomycin (Lonza), and the cells were maintained under standard cell culture conditions (37°C and 5% CO_2). The cell lines were regularly checked for mycoplasma contamination. FuGENE 6 reagent (Promega, Madison, WI) was used for transient transfections according to manufacturer's instructions.

DNA plasmids. psd44-G12QL (ca$G_{\alpha 12}$) was a gift from Agnese Mariotti (Addgene plasmid # 46825). OptoPlexin and optoPlexin mutants, PRG and LARG plasmids were generated as described in the materials and methods section of chapter II. Additional optoPlexin and PRG mutants were generated using overlapping polymerase chain reaction (PCR). Cry2-caRac1 and Cry2-ca$G_{\alpha 12}$ were designed in a manner similar to optoPlexin. Briefly, Cry2 was positioned at the N-terminus and caRac1 or ca$G_{\alpha 12}$ at the C-terminus. For the co-recruitment assay, Cry2 plasmids were tethered to mCherry and RhoGEF plasmids were tethered to mVenus. These constructs were initially subcloned into the pTriEx-4 vector (Novagen) using PCR and restriction digestion. Unless specified otherwise, the termini of tagging were positioned as in the orders they were written. The open reading frames of all DNA plasmids were verified by DNA sequencing.

Imaging setup. All time-lapse imaging were performed on a customized Nikon Ti-E inverted microscope. TIRF imaging was performed using a 60x oil TIRF objective (NA 1.49). The microscope was modified with a "stage-up" design which enables an insertion of two independent, motorized dichroic mirrors/filter cubes in the microscope infinity space. A dichroic mirror in the bottom cube was used to reflect excitation laser lines at 442, 514, 594 nm for imaging of mCerulean, mVenus, and mCherry respectively. The laser lines were launched from a fiber-coupled LMM5 system (Andor) equipped with an acousto-optic tunable filter (AOTF) for shutter and intensity control. Another dichroic mirror (495LP) in the top cube was used to bring in optogenetic illumination originated from a LED source at 440 nm (CoolLED). The 495LP mirror permitted immediate acquisition of mVenus or mCherry after optogenetic illumination. Alternatively, the top mirror can be rotated out to a blank position for Patterned illumination was generated using a commercial digital mirror device (Mosaic, Andor). The fluorescent emission was captured with an EMCCD camera (iXon Ultra, Andor). Metamorph software was used to control the imaging set up. Live cell imaging was performed at 37°C in a heated chamber (Bioptechs) with humidified 5% CO_2 supply. Vitamin and phenol red-free media (US Biological) supplemented with 2% FBS were used in imaging to reduce background and photobleaching.

Membrane recruitment assay. Co-recruitment of PRG and its variants by optoPlexin and it variants, and Cry2-$G_{\alpha 12}$ were assessed as described in Chapter II. Activation of paRac1 does not involve any membrane translocation. So, recruitment levels of PRG by Cry2-caRac1 and paRac1 were assessed by the

change in TIRF intensity of mVenus (tethered to PRG) after 100 seconds of blue light illumination relative to that before illumination.

Statistical analyses. Microsoft Excel and Matlab were used for statistical analyses. Sample sizes for different experiments were chosen based on the commonly used range in the field without conducting any statistical power analysis. Normal probability plot function of Matlab was utilized to confirm normal distribution of the data. Sample means and standard error of mean was calculated and shown on the graphs. P values were obtained from one-tailed Students t-test.

Chapter IV

General discussion and future directions

Spatial and temporal regulation is fundamental for coordination of signaling pathways that mediate physiological phenomena. Dysregulation of either can lead to development of pathologies. In this work, we investigated coordination of osteoblast migration by osteoclasts upon direct contact between the cells and elucidated spatiotemporal regulation of pathways that mediate resulting osteoblast response.

Further roles of CIL in bone remodeling. Bone remodeling is initiated by migration of osteoclasts to a site with damaged bone matrix and start resorption. How osteoclasts identify and migrate to these sites is a topic of extensive research, and is beyond the scope of this work. Osteoclasts are derived from hematopoietic lineage progenitors that differentiate towards macrophage-monocytic lineage upon exposure to macrophage-colony stimulating factor (MCSF), which is expressed by osteoblast lineage cells. While full-length MCSF precursor is membrane-tethered, the extracellular domain may be proteolytically cleaved to produce a soluble cytokine. These 'pre-osteoclasts' must come in contact with osteoblastic cells for RANKL stimulation, which is necessary for osteoclastogenesis. RANKL stimulates Sema4D expression in pre-osteoclasts, and this event may initiate the segregation of osteoblastic and osteoclastic cells, which persists through the rest of the bone remodeling cycle. Drosophila macrophages have been reported to undergo homotypic CIL[37,56], which facilitates its spread through the animal body. If osteoclast precursors also undergo similar homotypic CIL, either MCSFor RANKL stimulation may be expected to downregulate the factors that mediate such CIL, since homotypic CIL may render the fusion of the pre-osteoclasts very inefficient.

In addition to Plexin-B1 and Plexin-B2, osteoblastic cells also express their ligand, Sema4D[15]. The role of osteoblastic Sema4D in its motility and function is not understood. It is conceivable that homotypic CIL between osteoblasts may facilitate collective migration. In addition, Sema4D from osteoblasts undergoing collective motion may also act to keep the cells in a relatively undifferentiated state until the target site has been reached. Since Sema4D extracellular domain may be cleaved to obtain a soluble ligand[183], it may also act as a decoy ligand to compete against Sema4D expressed by other cells in the bone microenvironment. However the significance of Sema4D expressed by osteoblasts in migration and differentiation *in vivo* remains to be further investigated.

Spatial regulation of β-Pix in cell repolarization. In chapter II, we demonstrated spatial regulation of β-Pix in osteoblastic cells undergoing repolarization. β-Pix associates with Paxilin in adhesions through Git-1[184]. Our data suggest that β-Pix association with focal adhesions is negatively responsive to mechanical tension. To test whether β-Pix or Git1 responds to mechanical tension, we treated MC3T3-E1 cells expressing mCherry-Paxilin and mVenus-Git1 with Y-27632 ROCK inhibitor. Unlike β-Pix, Git1 showed a decrease in association with adhesions (Figure 52a). These data suggest that in response to RhoA-ROCK signaling, β-Pix dissociates from the Git1-Paxilin complex (Figure 52b), which in turn suggests that there might be a change in the state of either β-Pix or Git1 downstream of ROCK signaling. Indeed, if β-Pix redistribution during CIL is mediated by mechanical tension, our data would suggest the presence of a

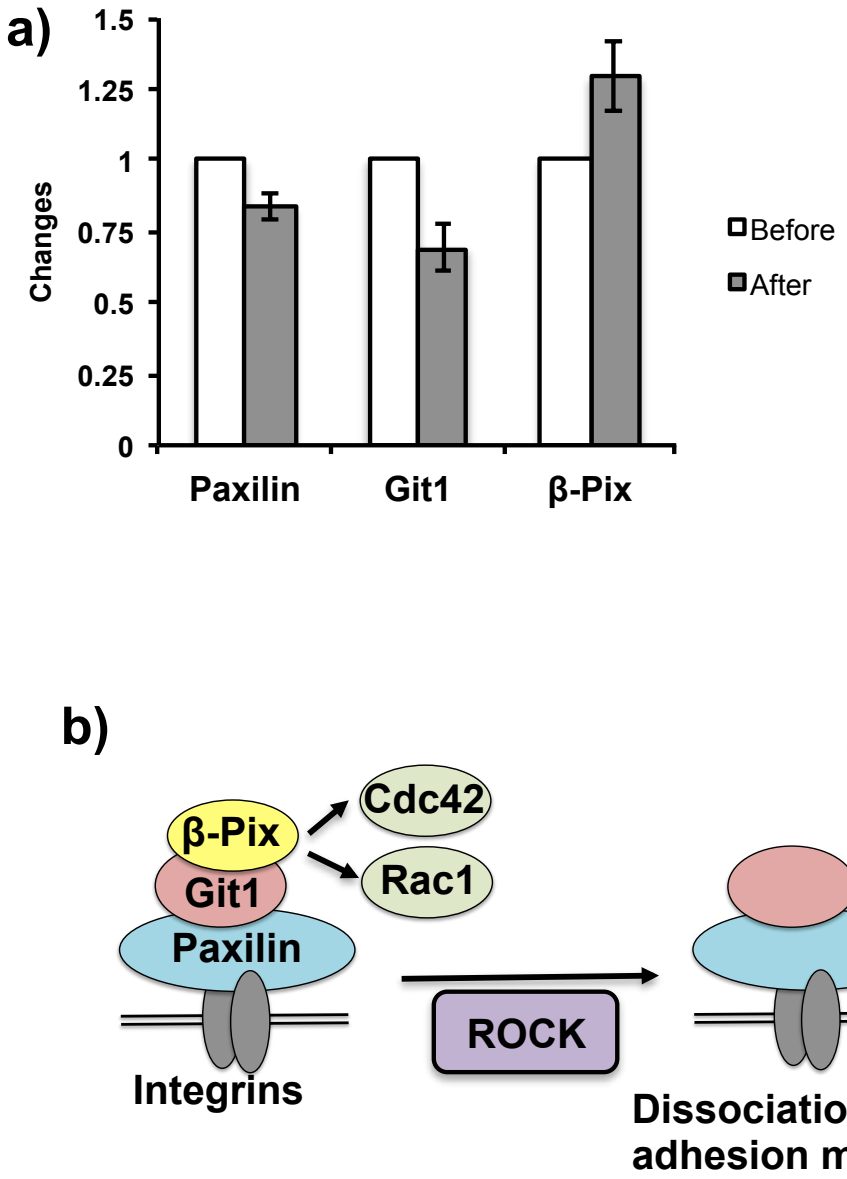

Figure 52. RhoA-ROCK mediates dissociation of β-Pix from Git1-Paxilin complex. (a) Changes in mCer3-Paxillin, mVenus-β-Pix and mCherry-Git1 in MC3T3-E1 cells on 10 μM Y-27632 ROCK inhibitor treatment, normalized to values prior to treatment. (b) Cartoon representation of the proposed model of β-Pix dissociation. n = 7 cells, mean ± s.e.m.

mechanosensitive element in either β-Pix or Git1, which directly responds to mechanical tension, or acts as a substrate to another enzyme that does. Further investigation into the signaling pathways that mediate β-Pix dissociation from Git1-Paxilin complex may provide interesting insight into how cells respond to mechanical tension.

Rac1 regulation of RhoGEF recruitment by Plexin-B1. Our data on the effect of GTP-loaded Rac1 on facilitating PRG recruitment by Plexin-B1 demonstrates a role of Plexin-B1 in integrating extracellular and intracellular signals to modulate cell response to its environment. Rac1 promotes actin polymerization and protrusions. By regulating PRG recruitment and activation by Plexin-B1, Rac1 provides a distinct spatial control of Plexin-B1, presumably localizing it to active protrusions, and minimizing any impact of Sema4D stimulation in non-protruding regions in a cell. Additionally, Rac1 and RhoA are generally thought to inhibit one another[55]. Thus, in Sema4D-Plexin-B1 signaling, Rac1 may act as a switch to rapidly convert a region of high Rac1 and low RhoA activity to one of high RhoA and low Rac1 activity. Such a change may facilitate rapid induction of CIL, enabling cells to efficiently respond to extracellular cues. Our data implicates the RGS domain of PRG in Rac1 regulation of Plexin-B1 signaling. This provides an interesting intersection of signaling cascades initiated by heterotrimeric G proteins and Plexins. Whether these two pathways compete for available RhoGEFs in a cell remains to be investigated. Although the exact mechanism by which PRG or LARG is activated by either pathways is not completely understood. Although mere plasma membrane recruitment of PRG may

be sufficient for activation[185], such recruitment clearly involves the RGS domain. Further investigation of both plexins and G-protein signaling may help elucidate the molecular mechanism of PRG and LARG activation.

In chapter II, I investigated the underlying signaling pathways that mediate spatial segregation of osteoblasts and osteoclasts *in vivo*. Using a co-culture system, I have demonstrated that osteoblasts undergo CIL upon contact with osteoclasts. Applying gene editing techniques, I have established a role of Plexin-B1 signaling in mediating said CIL, and by utilizing an optogenetic tool I have demonstrated that localized activation of Plexin-B1 signaling is capable of recapitulating the CIL-like behavior that osteoblasts exhibit upon contact with osteoclasts. The stark contrast between a collapse phenotype upon whole cell stimulation and cell repolarization upon localized stimulation underscores the necessity of investigating spatial regulation of signaling pathways to better understand their roles in cell behavior. Since Plexins show remarkable homology in their intracellular domains, the design for optoPlexin, pertinent to Plexin-B1, should be extendable to other plexins as well. In chapter III, I have explored the regulation of Plexin-B1 signaling by GTP-Rac1 association with Plexin-B1-RBD. Utilizing a co-recruitment assay of PRG with optoPlexin, I have demonstrated that GTP-Rac1 association with Plexin-B1 mediates PRG recruitment. Utilizing various mutations of optoPlexin and PRG, I have identified a role of the RGS domain of PDZ-RhoGEF in Plexin-B1-PRG association. Overall, these new findings increase our understanding of the nature of interactions between osteoclasts and osteoblasts,

the role of Plexin-B1 signaling and spatiotemporal regulation of other signaling molecules in CIL, and molecular mechanisms that mediate Plexin signaling.

List of movies:

Movie 1: Spatial segregation between an osteoclast and primary osteoblasts. Primary murine calvarial osteoblasts were co-cultured with murine osteoclasts and imaged using phase contrast at 5 minute intervals. Scale bar, 50 μm.

Movie 2: Osteoblast undergoing CIL on contact with osteoclast. Primary murine calvarial osteoblasts migrating towards murine osteoclasts were imaged using phase contrast at 5 minute intervals. Scale bar, 50 μm.

Movie 3: MC3T3-E1 cell undergoing CIL on contact with osteoclast. MC3T3-E1 osteoblastic cells migrating towards murine osteoclasts were imaged using phase contrast at 5 minute intervals. Scale bar, 50 μm.

Movie 4: MC3T3-E1 cell on contact with a bone marrow macrophage. MC3T3-E1 osteoblastic cells migrating towards murine BMMs were imaged using phase contrast at 5 minute intervals. Scale bar, 50 μm.

Movie 5: Cas9 MC3T3-E1 cell undergoing CIL on contact with osteoclast. Cas9 expressing MC3T3-E1 cells encountering murine osteoclasts were imaged using phase contrast at 2 minute intervals. Scale bar, 50 μm.

Movie 6: KO1 MC3T3-E1 cell CIL on contact with osteoclast. Plexin-B1 null KO1 MC3T3-E1 cells migrating towards murine osteoclasts were imaged using phase contrast at 2 minute intervals. Scale bar, 50 μm.

Movie 7: KO2 MC3T3-E1 cell CIL on contact with osteoclast. Plexin-B1 null KO2 MC3T3-E1 cells were co-cultured with murine osteoclasts and imaged using phase contrast at 2 minute intervals. Scale bar, 50 μm.

Movie 8: Clustering of Plexin-B1-mCherry around Sema4D-Fc silica beads. COS-7 cells were transfected with Plexin-B1-mCherry and Sema4D-Fc silica beads were added to the culture. Contact between the beads and the cells, and subsequent changes in mCherry fluorescence distribution were observed using using 60X objective at 1 minute intervals. Scale bar, 10 μm.

Movie 9: Translocation of optoPlexin to the plasma membrane upon blue light illuminaton. The fluorescence intensities of mCherry-optoPlexin or mCherry-optoPlexin(D393A) in COS-7 cells were imaged using TIRFM upon whole cell illumination at 440 nm and at 10 second intervals. The cells were coexpressing CIB-mEGFP-CAAX. Scale bar, 10 μm.

Movie 10: Corecruitment of PRG with optoPlexin upon whole cell illumination. Representative TIRF images showing simultaneous changes in membrane intensity of mCherry-optoPlexin and mVenus-PRG in COS-7 cells upon whole cell illumination with 440 nm light at 10 second intervals. The COS-7 cells were transiently expressing CIB-CAAX, mCherry-optoPlexin and mVenus-PRG. Timestamp shows minutes and seconds post illumination. Scale bar, 10 μm.

Movie 11: Induction of CIL upon local activation of optoPlexin. DIC and TIRF images showing local activation of mCherry-optoPlexin and subsequent induction of CIL in MC3T3-E1 cells. mEGFP-CIB-CAAX and mCherry-optoPlexin were transiently expressed in MC3T3-E1 cells and in one such migrating cell, mCherry-optoPlexin was stimulated at a protrusion using localized 440 nm light illumination at 10 second intervals. Timestamp shows minutes and seconds post illumination. Magenta circle, region of illumination (diameter, 5 μm). Scale bar, 10 μm.

Movie 12: Local optoPlexin stimulation induces change in direction in a migrating cell. DIC and TIRF images showing local activation of mCherry-optoPlexin and subsequent change in direction of migration in MC3T3-E1 cells. CIB-CAAX and mCherry-optoPlexin were transiently expressed in MC3T3-E1 cells and mCherry-optoPlexin was stimulated at a protrusion using localized 440 nm light illumination at 20 second intervals. Timestamp shows minutes and seconds post illumination. Magenta circle, region of illumination (diameter, 5 μm). Scale bar, 10 μm.

Movie 13: Local stimulation of optoPlexin-delPBD. DIC and TIRF images showing local accumulation of mCherry-optoPlexin-delPBD but no induction of CIL in a MC3T3-E1 cell. mEGFP-CIB-CAAX and mCherry-optoPlexin-delPBD were transiently expressed in MC3T3-E1 cells. OptoPlexin-delPBD was stimulated at a protrusion using localized 440 nm light illumination at 10 second intervals. Timestamp shows minutes and seconds post illumination. Magenta circle, region of illumination (diameter, 5 μm). Scale bar, 10 μm.

Movie 14: Induction of cell collapse upon whole cell activation of optoPlexin. DIC and TIRF images showing activation of mCherry-optoPlexin and subsequent morphological changes in MC3T3-E1 cells upon stimulation using 440 nm light illumination at 10 second intervals throughout the field of view. The MC3T3-E1 cells were transiently expressing mEGFP-CIB-CAAX and mCherry-optoPlexin. Timestamp shows minutes and seconds post illumination. Scale bar, 10 μm.

Movie 15: Co-recruitment of PRG with optoPlexin upon local illumination. TIRF images showing changes in membrane intensity of mCherry-optoPlexin and

mVenus-PRG upon localized illumination (as indicated by white arrowhead) with 440 nm light at 10 second intervals. MC3T3-E1 cells were transiently expressing CIB-CAAX, mCherry-optoPlexin and mVenus-PRG. Timestamp, minutes after illumination. Scale bar, 10 μm.

Movie 16: Polarized distribution of MyoRLC upon local optoPlexin activation. TIRF images showing localized activation of mVenus-optoPlexin and subsequent changes in mCherry-MyoRLC distribution. CIB-CAAX, mVenus-optoPlexin and mCherry-myoRLC were transiently expressed in MC3T3-E1 cells. mCherry-OptoPlexin was stimulated at a protrusion using localized 440 nm light illumination at 10 second intervals. Timestamp shows minutes and seconds post illumination. Magenta circle, region of illumination (diameter, 5 μm). Scale bar, 10 μm.

Movie 17: Local stimulation of optoPlexin-RA. DIC and TIRF images showing local accumulation of mCherry-optoPlexin-RA but no induction of CIL in a MC3T3-E1 cell. mEGFP-CIB-CAAX and mCherry-optoPlexin-delPBD were transiently expressed in MC3T3-E1 cells. OptoPlexin-RA was stimulated at a protrusion using localized 440 nm light illumination at 10 second intervals. Timestamp shows minutes and seconds post illumination. Magenta circle, region of illumination (diameter, 5 μm). Scale bar, 10 μm.

Movie 18: Local stimulation of optoPlexin-YF. DIC and TIRF images showing local activation of mCherry-optoPlexin-YF and subsequent induction of CIL in MC3T3-E1 cells. CIB-CAAX and mCherry-optoPlexin were transiently expressed in MC3T3-E1 cells and in one such migrating cell, mCherry-optoPlexin-YF was stimulated at a protrusion using localized 440 nm light illumination at 10 second

intervals. Timestamp shows minutes and seconds post illumination. Magenta circle, region of illumination (diameter, 5 μm). Scale bar, 10 μm.

Movie 19: Mobilization and redistribution of β-Pix upon local activation of optoPlexin. TIRF images showing redistribution of mVenus-β-Pix upon localized activation of mCherry-optoPlexin in a MC3T3-E1 cell. CIB-CAAX, mCherry-optoPlexin and mVenus-β-Pix were transiently expressed in MC3T3-E1 cells. mVenus-optoPlexin was stimulated at a protrusion using localized 440 nm light illumination at 10 second intervals. Timestamp shows minutes and seconds post illumination. Magenta circle, region of illumination (diameter, 5 μm). Scale bar, 10 μm.

Movie 20: Effects of local activation of optoPlexin on adhesions. TIRF images showing changes in mCherry-Paxillin distribution upon localized activation of mVenus-optoPlexin in a MC3T3-E1 cell. CIB-CAAX, mVenus-optoPlexin and mCherry-Paxillin were transiently expressed in MC3T3-E1 cells. mVenus-optoPlexin was stimulated at a protrusion using localized 440 nm light illumination at 10 second intervals. Timestamp shows minutes and seconds post illumination. Magenta circle, region of illumination (diameter, 5 μm). Scale bar, 10 μm.

References:

1. Florencio-Silva, R., Sasso, G. R. da S., Sasso-Cerri, E., Simões, M. J. & Cerri, P. S. Biology of Bone Tissue: Structure, Function, and Factors That Influence Bone Cells. *BioMed Res. Int.* **2015,** (2015).
2. Sims, N. A. & Gooi, J. H. Bone remodeling: Multiple cellular interactions required for coupling of bone formation and resorption. *Semin. Cell Dev. Biol.* **19,** 444–451 (2008).
3. Sims, N. A. & Martin, T. J. Coupling the activities of bone formation and resorption: a multitude of signals within the basic multicellular unit. *BoneKEy Rep.* **3,** 481 (2014).
4. Bonewald, L. F. The Amazing Osteocyte. *J. Bone Miner. Res.* **26,** 229–238 (2011).
5. Einhorn, T. A. & Gerstenfeld, L. C. Fracture healing: mechanisms and interventions. *Nat. Rev. Rheumatol.* **11,** 45–54 (2015).
6. Yasuda, H. *et al.* Osteoclast differentiation factor is a ligand for osteoprotegerin/osteoclastogenesis-inhibitory factor and is identical to TRANCE/RANKL. *Proc. Natl. Acad. Sci. U. S. A.* **95,** 3597–3602 (1998).
7. Drake, M. T., Clarke, B. L. & Khosla, S. Bisphosphonates: Mechanism of Action and Role in Clinical Practice. *Mayo Clin. Proc. Mayo Clin.* **83,** 1032–1045 (2008).
8. Sanchez-Fernandez, M. A., Gallois, A., Riedl, T., Jurdic, P. & Hoflack, B. Osteoclasts Control Osteoblast Chemotaxis via PDGF-BB/PDGF Receptor Beta Signaling. *PLoS ONE* **3,** e3537 (2008).

9. Tang, Y. *et al.* TGF-beta1-induced migration of bone mesenchymal stem cells couples bone resorption with formation. *Nat. Med.* **15,** 757–765 (2009).
10. Oreffo, R. O., Mundy, G. R., Seyedin, S. M. & Bonewald, L. F. Activation of the bone-derived latent TGF beta complex by isolated osteoclasts. *Biochem. Biophys. Res. Commun.* **158,** 817–823 (1989).
11. Walker, E. C. *et al.* Cardiotrophin-1 is an osteoclast-derived stimulus of bone formation required for normal bone remodeling. *J. Bone Miner. Res. Off. J. Am. Soc. Bone Miner. Res.* **23,** 2025–2032 (2008).
12. Pederson, L., Ruan, M., Westendorf, J. J., Khosla, S. & Oursler, M. J. Regulation of bone formation by osteoclasts involves Wnt/BMP signaling and the chemokine sphingosine-1-phosphate. *Proc. Natl. Acad. Sci. U. S. A.* **105,** 20764–20769 (2008).
13. Abdelgawad, M. E. *et al.* Does collagen trigger the recruitment of osteoblasts into vacated bone resorption lacunae during bone remodeling? *Bone* **67,** 181–188 (2014).
14. Tse, J. R. & Engler, A. J. Stiffness Gradients Mimicking In Vivo Tissue Variation Regulate Mesenchymal Stem Cell Fate. *PLOS ONE* **6,** e15978 (2011).
15. Negishi-Koga, T. *et al.* Suppression of bone formation by osteoclastic expression of semaphorin 4D. *Nat. Med.* **17,** 1473–1480 (2011).
16. Ishii, M., Fujimori, S., Kaneko, T. & Kikuta, J. Dynamic live imaging of bone: opening a new era with ‘bone histodynametry’. *J. Bone Miner. Metab.* (2013). doi:10.1007/s00774-013-0437-x

17. Ferrier, J., Xia, S. L., Lagan, E., Aubin, J. E. & Heersche, J. N. Displacement and translocation of osteoblast-like cells by osteoclasts. *J. Bone Miner. Res. Off. J. Am. Soc. Bone Miner. Res.* **9,** 1397–1405 (1994).
18. Perez-Amodio, S., Beertsen, W. & Everts, V. (Pre-)osteoclasts induce retraction of osteoblasts before their fusion to osteoclasts. *J. Bone Miner. Res. Off. J. Am. Soc. Bone Miner. Res.* **19,** 1722–1731 (2004).
19. Deman, J. J. & Bruyneel, E. A. Evidence for long-range electrostatic repulsion between HeLa cells. *Exp. Cell Res.* **89,** 206–216 (1974).
20. Deman, J. J., Vakaet, L. C. & Bruyneel, E. A. Cell size and mutual cell adhesion. II. Evidence for a relation between cell size, long-range electrostatic repulsion and intercellular adhesiveness during density-regulated growth in suspension. *J. Membr. Biol.* **26,** 205–215 (1976).
21. Pini, A. Chemorepulsion of axons in the developing mammalian central nervous system. *Science* **261,** 95–98 (1993).
22. Luo, Y., Raible, D. & Raper, J. A. Collapsin: a protein in brain that induces the collapse and paralysis of neuronal growth cones. *Cell* **75,** 217–227 (1993).
23. Drescher, U. *et al.* In vitro guidance of retinal ganglion cell axons by RAGS, a 25 kDa tectal protein related to ligands for Eph receptor tyrosine kinases. *Cell* **82,** 359–370 (1995).
24. Meima, L., Moran, P., Matthews, W. & Caras, I. W. Lerk2 (ephrin-B1) is a collapsing factor for a subset of cortical growth cones and acts by a mechanism different from AL-1 (ephrin-A5). *Mol. Cell. Neurosci.* **9,** 314–328 (1997).

25. Brose, K. *et al.* Slit proteins bind Robo receptors and have an evolutionarily conserved role in repulsive axon guidance. *Cell* **96,** 795–806 (1999).
26. Kidd, T., Bland, K. S. & Goodman, C. S. Slit is the midline repellent for the robo receptor in Drosophila. *Cell* **96,** 785–794 (1999).
27. Guthrie, S. Axon guidance: netrin receptors are revealed. *Curr. Biol. CB* **7,** R6-9 (1997).
28. Kolodkin, A. L. *et al.* Fasciclin IV: sequence, expression, and function during growth cone guidance in the grasshopper embryo. *Neuron* **9,** 831–845 (1992).
29. Tharp, W. G. *et al.* Neutrophil chemorepulsion in defined interleukin-8 gradients in vitro and in vivo. *J. Leukoc. Biol.* **79,** 539–554 (2006).
30. Messias, C. V. *et al.* Sphingosine-1-Phosphate Induces Dose-Dependent Chemotaxis or Fugetaxis of T-ALL Blasts through S1P1 Activation. *PloS One* **11,** e0148137 (2016).
31. Vianello, F. *et al.* Murine B16 melanomas expressing high levels of the chemokine stromal-derived factor-1/CXCL12 induce tumor-specific T cell chemorepulsion and escape from immune control. *J. Immunol. Baltim. Md 1950* **176,** 2902–2914 (2006).
32. Vianello, F., Olszak, I. T. & Poznansky, M. C. Fugetaxis: active movement of leukocytes away from a chemokinetic agent. *J. Mol. Med. Berl. Ger.* **83,** 752–763 (2005).
33. Wu, J. Y. *et al.* The neuronal repellent Slit inhibits leukocyte chemotaxis induced by chemotactic factors. *Nature* **410,** 948–952 (2001).

34. Poznansky, M. C. *et al.* Thymocyte emigration is mediated by active movement away from stroma-derived factors. *J. Clin. Invest.* **109,** 1101–1110 (2002).
35. Brainard, D. M. *et al.* Migration of antigen-specific T cells away from CXCR4-binding human immunodeficiency virus type 1 gp120. *J. Virol.* **78,** 5184–5193 (2004).
36. Abercrombie, M. & Heaysman, J. E. M. Observations on the social behavior of cells in tissue culture: I. Speed of movement of chick heart fibroblasts in relation to their mutual contacts. *Exp. Cell Res.* **5,** 111–131 (1953).
37. Stramer, B. & Mayor, R. Mechanisms and in vivo functions of contact inhibition of locomotion. *Nat. Rev. Mol. Cell Biol.* (2016). doi:10.1038/nrm.2016.118
38. Theveneau, E. & Mayor, R. Integrating chemotaxis and contact-inhibition during collective cell migration. *Small GTPases* **1,** 113–117 (2010).
39. Carmona-Fontaine, C. *et al.* Contact inhibition of locomotion in vivo controls neural crest directional migration. *Nature* **456,** 957–961 (2008).
40. Mayor, R. & Carmona-Fontaine, C. Keeping in touch with contact inhibition of locomotion. *Trends Cell Biol.* **20,** 319–328 (2010).
41. Abercrombie, M. Control mechanisms in cancer. *Eur. J. Cancer* **6,** 7–13 (1970).
42. Scarpa, E. *et al.* A novel method to study contact inhibition of locomotion using micropatterned substrates. *Biol. Open* **2,** 901–906 (2013).

43. Paddock, S. W. & Dunn, G. A. Analysing collisions between fibroblasts and fibrosarcoma cells: fibrosarcoma cells show an active invasionary response. *J. Cell Sci.* **81,** 163–187 (1986).

44. Astin, J. W. *et al.* Competition amongst Eph receptors regulates contact inhibition of locomotion and invasiveness in prostate cancer cells. *Nat. Cell Biol.* **12,** 1194–1204 (2010).

45. Lin, B., Yin, T., Wu, Y. I., Inoue, T. & Levchenko, A. Interplay between chemotaxis and contact inhibition of locomotion determines exploratory cell migration. *Nat. Commun.* **6,** 6619 (2015).

46. Becker, S. F. S., Mayor, R. & Kashef, J. Cadherin-11 mediates contact inhibition of locomotion during Xenopus neural crest cell migration. *PloS One* **8,** e85717 (2013).

47. Scarpa, E. *et al.* Cadherin Switch during EMT in Neural Crest Cells Leads to Contact Inhibition of Locomotion via Repolarization of Forces. *Dev. Cell* **34,** 421–434 (2015).

48. Anastasiadis, P. Z. & Reynolds, A. B. Regulation of Rho GTPases by p120-catenin. *Curr. Opin. Cell Biol.* **13,** 604–610 (2001).

49. Fritz, R. D. *et al.* SrGAP2-Dependent Integration of Membrane Geometry and Slit-Robo-Repulsive Cues Regulates Fibroblast Contact Inhibition of Locomotion. *Dev. Cell* **35,** 78–92 (2015).

50. Tanaka, M., Kuriyama, S. & Aiba, N. Nm23-H1 regulates contact inhibition of locomotion, which is affected by ephrin-B1. *J. Cell Sci.* **125,** 4343–4353 (2012).

51. Stramer, B. & Mayor, R. Mechanisms and in vivo functions of contact inhibition of locomotion. *Nat. Rev. Mol. Cell Biol.* (2016). doi:10.1038/nrm.2016.118

52. Okabe, T. *et al.* RICS, a novel GTPase-activating protein for Cdc42 and Rac1, is involved in the beta-catenin-N-cadherin and N-methyl-D-aspartate receptor signaling. *J. Biol. Chem.* **278,** 9920–9927 (2003).

53. Li, X. *et al.* Epithelia-derived wingless regulates dendrite directional growth of drosophila ddaE neuron through the Fz-Fmi-Dsh-Rac1 pathway. *Mol. Brain* **9,** 46 (2016).

54. Tep, C. *et al.* Brain-derived neurotrophic factor (BDNF) induces polarized signaling of small GTPase (Rac1) protein at the onset of Schwann cell myelination through partitioning-defective 3 (Par3) protein. *J. Biol. Chem.* **287,** 1600–1608 (2012).

55. Guilluy, C., Garcia-Mata, R. & Burridge, K. Rho protein crosstalk: another social network? *Trends Cell Biol.* **21,** 718–726 (2011).

56. Davis, J. R. *et al.* Inter-cellular forces orchestrate contact inhibition of locomotion. *Cell* **161,** 361–373 (2015).

57. Li, Z. *et al.* Regulation of PTEN by Rho small GTPases. *Nat. Cell Biol.* **7,** 399–404 (2005).

58. Villar-Cerviño, V. *et al.* Contact Repulsion Controls the Dispersion and Final Distribution of Cajal-Retzius Cells. *Neuron* **77,** 457–471 (2013).

59. Theveneau, E. *et al.* Chase-and-run between adjacent cell populations promotes directional collective migration. *Nat. Cell Biol.* **15,** 763–772 (2013).

60. Kruger, R. P., Aurandt, J. & Guan, K.-L. Semaphorins command cells to move. *Nat. Rev. Mol. Cell Biol.* **6,** 789–800 (2005).
61. Janssen, B. J. C. *et al.* Structural basis of semaphorin-plexin signalling. *Nature* **467,** 1118–1122 (2010).
62. Hota, P. K. & Buck, M. Plexin structures are coming: opportunities for multilevel investigations of semaphorin guidance receptors, their cell signaling mechanisms, and functions. *Cell. Mol. Life Sci. CMLS* (2012). doi:10.1007/s00018-012-1019-0
63. Oinuma, I., Ishikawa, Y., Katoh, H. & Negishi, M. The Semaphorin 4D receptor Plexin-B1 is a GTPase activating protein for R-Ras. *Science* **305,** 862–865 (2004).
64. Saito, Y., Oinuma, I., Fujimoto, S. & Negishi, M. Plexin-B1 is a GTPase activating protein for M-Ras, remodelling dendrite morphology. *EMBO Rep.* **10,** 614–621 (2009).
65. Wang, Y. *et al.* Plexins are GTPase-activating proteins for Rap and are activated by induced dimerization. *Sci. Signal.* **5,** ra6 (2012).
66. Swiercz, J. M., Kuner, R., Behrens, J. & Offermanns, S. Plexin-B1 directly interacts with PDZ-RhoGEF/LARG to regulate RhoA and growth cone morphology. *Neuron* **35,** 51–63 (2002).
67. Hirotani, M. *et al.* Interaction of plexin-B1 with PDZ domain-containing Rho guanine nucleotide exchange factors. *Biochem. Biophys. Res. Commun.* **297,** 32–37 (2002).

68. Driessens, M. H. E., Olivo, C., Nagata, K., Inagaki, M. & Collard, J. G. B plexins activate Rho through PDZ-RhoGEF. *FEBS Lett.* **529,** 168–172 (2002).
69. Oinuma, I., Katoh, H., Harada, A. & Negishi, M. Direct Interaction of Rnd1 with Plexin-B1 Regulates PDZ-RhoGEF-mediated Rho Activation by Plexin-B1 and Induces Cell Contraction in COS-7 Cells. *J. Biol. Chem.* **278,** 25671–25677 (2003).
70. Tong, Y. *et al.* Binding of Rac1, Rnd1, and RhoD to a Novel Rho GTPase Interaction Motif Destabilizes Dimerization of the Plexin-B1 Effector Domain. *J. Biol. Chem.* **282,** 37215–37224 (2007).
71. Bell, C. H., Aricescu, A. R., Jones, E. Y. & Siebold, C. A dual binding mode for RhoGTPases in plexin signalling. *PLoS Biol.* **9,** e1001134 (2011).
72. Herold, C., Elhabazi, A., Bismuth, G., Bensussan, A. & Boumsell, L. CD100 is associated with CD45 at the surface of human T lymphocytes. Role in T cell homotypic adhesion. *J. Immunol. Baltim. Md 1950* **157,** 5262–5268 (1996).
73. Inagaki, S. *et al.* Sema4c, a transmembrane semaphorin, interacts with a post-synaptic density protein, PSD-95. *J. Biol. Chem.* **276,** 9174–9181 (2001).
74. Schultze, W. *et al.* Semaphorin4F interacts with the synapse-associated protein SAP90/PSD-95. *J. Neurochem.* **78,** 482–489 (2001).
75. Sun, T. *et al.* A reverse signaling pathway downstream of Sema4A controls cell migration via Scrib. *J. Cell Biol.* **216,** 199–215 (2017).
76. Toyofuku, T. *et al.* Guidance of myocardial patterning in cardiac development by Sema6D reverse signalling. *Nat. Cell Biol.* **6,** 1204–1211 (2004).

77. Eckhardt, F. *et al.* A novel transmembrane semaphorin can bind c-src. *Mol. Cell. Neurosci.* **9,** 409–419 (1997).

78. Kikutani, H. & Kumanogoh, A. Semaphorins in interactions between T cells and antigen-presenting cells. *Nat. Rev. Immunol.* **3,** 159–167 (2003).

79. Cagnoni, G. & Tamagnone, L. Semaphorin receptors meet receptor tyrosine kinases on the way of tumor progression. *Oncogene* **33,** 4795–4802 (2014).

80. Takegahara, N. *et al.* Plexin-A1 and its interaction with DAP12 in immune responses and bone homeostasis. *Nat. Cell Biol.* **8,** 615–622 (2006).

81. Sasaki, Y. *et al.* Fyn and Cdk5 mediate semaphorin-3A signaling, which is involved in regulation of dendrite orientation in cerebral cortex. *Neuron* **35,** 907–920 (2002).

82. Toyofuku, T. *et al.* Dual roles of Sema6D in cardiac morphogenesis through region-specific association of its receptor, Plexin-A1, with off-track and vascular endothelial growth factor receptor type 2. *Genes Dev.* **18,** 435–447 (2004).

83. Takahashi, T. *et al.* Plexin-neuropilin-1 complexes form functional semaphorin-3A receptors. *Cell* **99,** 59–69 (1999).

84. Neufeld, G., Kessler, O. & Herzog, Y. The interaction of Neuropilin-1 and Neuropilin-2 with tyrosine-kinase receptors for VEGF. *Adv. Exp. Med. Biol.* **515,** 81–90 (2002).

85. Bechara, A. *et al.* FAK-MAPK-dependent adhesion disassembly downstream of L1 contributes to semaphorin3A-induced collapse. *EMBO J.* **27,** 1549–1562 (2008).

86. Swiercz, J. M., Kuner, R. & Offermanns, S. Plexin-B1/RhoGEF-mediated RhoA activation involves the receptor tyrosine kinase ErbB-2. *J. Cell Biol.* **165,** 869–880 (2004).
87. Conrotto, P. *et al.* Sema4D induces angiogenesis through Met recruitment by Plexin B1. *Blood* **105,** 4321–4329 (2005).
88. Swiercz, J. M., Worzfeld, T. & Offermanns, S. ErbB-2 and met reciprocally regulate cellular signaling via plexin-B1. *J. Biol. Chem.* **283,** 1893–1901 (2008).
89. Artigiani, S. *et al.* Plexin-B3 is a functional receptor for semaphorin 5A. *EMBO Rep.* **5,** 710–714 (2004).
90. Basile, J. R., Afkhami, T. & Gutkind, J. S. Semaphorin 4D/plexin-B1 induces endothelial cell migration through the activation of PYK2, Src, and the phosphatidylinositol 3-kinase-Akt pathway. *Mol. Cell. Biol.* **25,** 6889–6898 (2005).
91. Worzfeld, T. & Offermanns, S. Semaphorins and plexins as therapeutic targets. *Nat. Rev. Drug Discov.* **13,** 603–621 (2014).
92. Jin, Z. & Strittmatter, S. M. Rac1 mediates collapsin-1-induced growth cone collapse. *J. Neurosci. Off. J. Soc. Neurosci.* **17,** 6256–6263 (1997).
93. Schwamborn, J. C. *et al.* Semaphorin 3A Stimulates Neurite Extension and Regulates Gene Expression in PC12 Cells. *J. Biol. Chem.* **279,** 30923–30926 (2004).

94. Kaneko, S. *et al.* A selective Sema3A inhibitor enhances regenerative responses and functional recovery of the injured spinal cord. *Nat. Med.* **12,** 1380–1389 (2006).

95. Omoto, M. *et al.* The Semaphorin 3A Inhibitor SM-345431 Accelerates Peripheral Nerve Regeneration and Sensitivity in a Murine Corneal Transplantation Model. *PLoS ONE* **7,** (2012).

96. Lin, X. *et al.* Sema4D-plexin-B1 implicated in regulation of dendritic spine density through RhoA/ROCK pathway. *Neurosci. Lett.* **428,** 1–6 (2007).

97. Pecho-Vrieseling, E., Sigrist, M., Yoshida, Y., Jessell, T. M. & Arber, S. Specificity of sensory-motor connections encoded by Sema3e-Plxnd1 recognition. *Nature* **459,** 842–846 (2009).

98. Sakurai, A. *et al.* Semaphorin 3E initiates antiangiogenic signaling through plexin D1 by regulating Arf6 and R-Ras. *Mol. Cell. Biol.* **30,** 3086–3098 (2010).

99. Klagsbrun, M. & Shimizu, A. Semaphorin 3E, an exception to the rule. *J. Clin. Invest.* **120,** 2658–2660 (2010).

100. Chabbert-de Ponnat, I. *et al.* Soluble CD100 functions on human monocytes and immature dendritic cells require plexin C1 and plexin B1, respectively. *Int. Immunol.* **17,** 439–447 (2005).

101. Sultana, H. *et al.* Semaphorin 7A contributes to West Nile virus pathogenesis through TGF-β1/Smad6 signaling. *J. Immunol. Baltim. Md 1950* **189,** 3150–3158 (2012).

102. Capone, G., Pagoni, M., Delfino, A. P. & Kanduc, D. Evidence for a vast peptide overlap between West Nile virus and human proteomes. *J. Basic Microbiol.* **53,** 800–807 (2013).

103. Gardner, J. D., Tscharke, D. C., Reading, P. C. & Smith, G. L. Vaccinia virus semaphorin A39R is a 50-55 kDa secreted glycoprotein that affects the outcome of infection in a murine intradermal model. *J. Gen. Virol.* **82,** 2083–2093 (2001).

104. Liu, H. *et al.* Structural basis of semaphorin-plexin recognition and viral mimicry from Sema7A and A39R complexes with PlexinC1. *Cell* **142,** 749–761 (2010).

105. Izmailova, E. *et al.* HIV-1 Tat reprograms immature dendritic cells to express chemoattractants for activated T cells and macrophages. *Nat. Med.* **9,** 191–197 (2003).

106. Yamada, D., Watanabe, S., Kawahara, K. & Maeda, T. Plexin A1 signaling confers malignant phenotypes in lung cancer cells. *Biochem. Biophys. Res. Commun.* **480,** 75–80 (2016).

107. Kigel, B., Rabinowicz, N., Varshavsky, A., Kessler, O. & Neufeld, G. Plexin-A4 promotes tumor progression and tumor angiogenesis by enhancement of VEGF and bFGF signaling. *Blood* **118,** 4285–4296 (2011).

108. Jacob, L. *et al.* Inhibition of PlexA1-mediated brain tumor growth and tumor-associated angiogenesis using a transmembrane domain targeting peptide. *Oncotarget* **7,** 57851–57865 (2016).

109. Staton, C. A. *et al.* Expression of class 3 semaphorins and their receptors in human breast neoplasia. *Histopathology* **59,** 274–282 (2011).

110. Yang, Y.-H., Zhou, H., Binmadi, N. O., Proia, P. & Basile, J. R. Plexin-B1 Activates NF-κB and IL-8 to Promote a Pro-Angiogenic Response in Endothelial Cells. *PLoS ONE* **6,** e25826 (2011).

111. Zhou, H., Binmadi, N. O., Yang, Y.-H., Proia, P. & Basile, J. R. Semaphorin 4D cooperates with VEGF to promote angiogenesis and tumor progression. *Angiogenesis* **15,** 391–407 (2012).

112. Worzfeld, T. *et al.* ErbB-2 signals through Plexin-B1 to promote breast cancer metastasis. *J. Clin. Invest.* **122,** 1296–1305 (2012).

113. Hu, G. & Yu, W. Modulators of Plexin B2 activity. (2016).

114. Casazza, A. *et al.* Sema3E-Plexin D1 signaling drives human cancer cell invasiveness and metastatic spreading in mice. *J. Clin. Invest.* **120,** 2684–2698 (2010).

115. Casazza, A. *et al.* Tumour growth inhibition and anti-metastatic activity of a mutated furin-resistant Semaphorin 3E isoform. *EMBO Mol. Med.* **4,** 234–250 (2012).

116. Luchino, J. *et al.* Semaphorin 3E suppresses tumor cell death triggered by the plexin D1 dependence receptor in metastatic breast cancers. *Cancer Cell* **24,** 673–685 (2013).

117. Negishi-Koga, T. & Takayanagi, H. Bone cell communication factors and Semaphorins. *BoneKEy Rep.* **1,** (2012).

118. Hayashi, M. *et al.* Osteoprotection by semaphorin 3A. *Nature* **485,** 69–74 (2012).

119. Dacquin, R. *et al.* Control of bone resorption by semaphorin 4D is dependent on ovarian function. *PloS One* **6,** e26627 (2011).

120. Offermanns, S., Swiercz, J. & Worzfeld, T. Monoclonal antibodies for the treatment of osteoporosis, multiple sclerosis and neoplastic diseases. (2016).

121. Li, X. *et al.* Fast noninvasive activation and inhibition of neural and network activity by vertebrate rhodopsin and green algae channelrhodopsin. *Proc. Natl. Acad. Sci. U. S. A.* **102,** 17816–17821 (2005).

122. Boyden, E. S., Zhang, F., Bamberg, E., Nagel, G. & Deisseroth, K. Millisecond-timescale, genetically targeted optical control of neural activity. *Nat. Neurosci.* **8,** 1263–1268 (2005).

123. Zoltowski, B. D., Vaccaro, B. & Crane, B. R. Mechanism-based tuning of a LOV domain photoreceptor. *Nat. Chem. Biol.* **5,** 827–834 (2009).

124. Strickland, D. *et al.* Rationally improving LOV domain-based photoswitches. *Nat. Methods* **7,** 623–626 (2010).

125. Wu, Y. I. *et al.* A genetically encoded photoactivatable Rac controls the motility of living cells. *Nature* **461,** 104–108 (2009).

126. Wang, X., He, L., Wu, Y. I., Hahn, K. M. & Montell, D. J. Light-mediated activation reveals a key role for Rac in collective guidance of cell movement in vivo. *Nat. Cell Biol.* **12,** 591–597 (2010).

127. Guntas, G. *et al.* Engineering an improved light-induced dimer (iLID) for controlling the localization and activity of signaling proteins. *Proc. Natl. Acad. Sci. U. S. A.* **112,** 112–117 (2015).

128. Wang, H. *et al.* LOVTRAP: an optogenetic system for photoinduced protein dissociation. *Nat. Methods* **13,** 755–758 (2016).

129. Zoltowski, B. D. & Crane, B. R. Light activation of the LOV protein vivid generates a rapidly exchanging dimer. *Biochemistry (Mosc.)* **47,** 7012–7019 (2008).

130. Kawano, F., Suzuki, H., Furuya, A. & Sato, M. Engineered pairs of distinct photoswitches for optogenetic control of cellular proteins. *Nat. Commun.* **6,** ncomms7256 (2015).

131. Levskaya, A., Weiner, O. D., Lim, W. A. & Voigt, C. A. Spatiotemporal Control of Cell Signalling Using A Light-Switchable Protein Interaction. *Nature* **461,** 997–1001 (2009).

132. Kennedy, M. J. *et al.* Rapid blue-light-mediated induction of protein interactions in living cells. *Nat. Methods* **7,** 973–975 (2010).

133. Bugaj, L. J., Choksi, A. T., Mesuda, C. K., Kane, R. S. & Schaffer, D. V. Optogenetic protein clustering and signaling activation in mammalian cells. *Nat. Methods* **10,** 249–252 (2013).

134. Che, D. L., Duan, L., Zhang, K. & Cui, B. The Dual Characteristics of Light-Induced Cryptochrome 2, Homo-oligomerization and Heterodimerization, for Optogenetic Manipulation in Mammalian Cells. *ACS Synth. Biol.* **4,** 1124–1135 (2015).

135. Taslimi, A. *et al.* An optimized optogenetic clustering tool for probing protein interaction and function. *Nat. Commun.* **5,** 4925 (2014).

136. Abercrombie, M. & Heaysman, J. E. Observations on the social behavior of cells in tissue culture. II. Monolayering of fibroblasts. *Exp. Cell Res.* **6,** 293–306 (1954).

137. Stramer, B. *et al.* Clasp-mediated microtubule bundling regulates persistent motility and contact repulsion in Drosophila macrophages in vivo. *J. Cell Biol.* **189,** 681–689 (2010).

138. Füller, T., Korff, T., Kilian, A., Dandekar, G. & Augustin, H. G. Forward EphB4 signaling in endothelial cells controls cellular repulsion and segregation from ephrinB2 positive cells. *J. Cell Sci.* **116,** 2461–2470 (2003).

139. Urbich, C. *et al.* MicroRNA-27a/b controls endothelial cell repulsion and angiogenesis by targeting semaphorin 6A. *Blood* **119,** 1607–1616 (2012).

140. Nogi, T. *et al.* Structural basis for semaphorin signalling through the plexin receptor. *Nature* **467,** 1123–1127 (2010).

141. Driessens, M. H. *et al.* Plexin-B semaphorin receptors interact directly with active Rac and regulate the actin cytoskeleton by activating Rho. *Curr. Biol. CB* **11,** 339–344 (2001).

142. Oinuma, I., Katoh, H. & Negishi, M. Molecular dissection of the semaphorin 4D receptor plexin-B1-stimulated R-Ras GTPase-activating protein activity and neurite remodeling in hippocampal neurons. *J. Neurosci. Off. J. Soc. Neurosci.* **24,** 11473–11480 (2004).

143. Aurandt, J., Vikis, H. G., Gutkind, J. S., Ahn, N. & Guan, K.-L. The semaphorin receptor plexin-B1 signals through a direct interaction with the Rho-specific nucleotide exchange factor, LARG. *Proc. Natl. Acad. Sci. U. S. A.* **99,** 12085–12090 (2002).

144. Lucas, P. A. Chemotactic response of osteoblast-like cells to transforming growth factor beta. *Bone* **10,** 459–463 (1989).

145. Lind, M. *et al.* Chemotaxis of human osteoblasts. Effects of osteotropic growth factors. *APMIS Acta Pathol. Microbiol. Immunol. Scand.* **103,** 140–146 (1995).

146. Liu, H. *et al.* Photoexcited CRY2 interacts with CIB1 to regulate transcription and floral initiation in Arabidopsis. *Science* **322,** 1535–1539 (2008).

147. Kottke, T., Batschauer, A., Ahmad, M. & Heberle, J. Blue-light-induced changes in Arabidopsis cryptochrome 1 probed by FTIR difference spectroscopy. *Biochemistry (Mosc.)* **45,** 2472–2479 (2006).

148. Hense, A., Herman, E., Oldemeyer, S. & Kottke, T. Proton transfer to flavin stabilizes the signaling state of the blue light receptor plant cryptochrome. *J. Biol. Chem.* **290,** 1743–1751 (2015).

149. Swiercz, J. M., Worzfeld, T. & Offermanns, S. Semaphorin 4D signaling requires the recruitment of phospholipase C gamma into the plexin-B1 receptor complex. *Mol. Cell. Biol.* **29,** 6321–6334 (2009).

150. Schaefer, G., Shao, L., Totpal, K. & Akita, R. W. Erlotinib Directly Inhibits HER2 Kinase Activation and Downstream Signaling Events in Intact Cells

Lacking Epidermal Growth Factor Receptor Expression. *Cancer Res.* **67,** 1228–1238 (2007).

151. Vicente-Manzanares, M., Ma, X., Adelstein, R. S. & Horwitz, A. R. Non-muscle myosin II takes centre stage in cell adhesion and migration. *Nat. Rev. Mol. Cell Biol.* **10,** 778–790 (2009).

152. Di Paolo, G. & De Camilli, P. Phosphoinositides in cell regulation and membrane dynamics. *Nature* **443,** 651–657 (2006).

153. Welf, E. S., Ahmed, S., Johnson, H. E., Melvin, A. T. & Haugh, J. M. Migrating fibroblasts reorient directionality by a metastable, PI3K-dependent mechanism. *J. Cell Biol.* **197,** 105–114 (2012).

154. Kedziora, K. M. *et al.* Rapid Remodeling of Invadosomes by Gi-coupled Receptors: DISSECTING THE ROLE OF Rho GTPases. *J. Biol. Chem.* **291,** 4323–4333 (2016).

155. Kutys, M. L. & Yamada, K. M. An extracellular-matrix-specific GEF-GAP interaction regulates Rho GTPase crosstalk for 3D collagen migration. *Nat. Cell Biol.* **16,** 909–917 (2014).

156. ten Klooster, J. P., Jaffer, Z. M., Chernoff, J. & Hordijk, P. L. Targeting and activation of Rac1 are mediated by the exchange factor beta-Pix. *J. Cell Biol.* **172,** 759–769 (2006).

157. Kuo, J.-C., Han, X., Hsiao, C.-T., Yates, J. R. & Waterman, C. M. Analysis of the myosin-II-responsive focal adhesion proteome reveals a role for β-Pix in negative regulation of focal adhesion maturation. *Nat. Cell Biol.* **13,** 383–393 (2011).

158. Airan, R. D., Thompson, K. R., Fenno, L. E., Bernstein, H. & Deisseroth, K. Temporally precise in vivo control of intracellular signalling. *Nature* **458,** 1025–1029 (2009).

159. Toettcher, J. E., Weiner, O. D. & Lim, W. A. Using Optogenetics to Interrogate the Dynamic Control of Signal Transmission by the Ras/Erk Module. *Cell* **155,** 1422–1434 (2013).

160. Chang, K.-Y. *et al.* Light-inducible receptor tyrosine kinases that regulate neurotrophin signalling. *Nat. Commun.* **5,** 4057 (2014).

161. Xu, Y. *et al.* Optogenetic control of chemokine receptor signal and T-cell migration. *Proc. Natl. Acad. Sci.* **111,** 6371–6376 (2014).

162. Shin, E.-Y. *et al.* Phosphorylation of p85 beta PIX, a Rac/Cdc42-specific guanine nucleotide exchange factor, via the Ras/ERK/PAK2 pathway is required for basic fibroblast growth factor-induced neurite outgrowth. *J. Biol. Chem.* **277,** 44417–44430 (2002).

163. Oinuma, I., Ito, Y., Katoh, H. & Negishi, M. Semaphorin 4D/Plexin-B1 stimulates PTEN activity through R-Ras GTPase-activating protein activity, inducing growth cone collapse in hippocampal neurons. *J. Biol. Chem.* **285,** 28200–28209 (2010).

164. Kato, K. *et al.* The inositol 5-phosphatase SHIP2 is an effector of RhoA and is involved in cell polarity and migration. *Mol. Biol. Cell* **23,** 2593–2604 (2012).

165. Basile, J. R., Gavard, J. & Gutkind, J. S. Plexin-B1 utilizes RhoA and Rho kinase to promote the integrin-dependent activation of Akt and ERK and endothelial cell motility. *J. Biol. Chem.* **282,** 34888–34895 (2007).

166. Woods, M. L. *et al.* Directional Collective Cell Migration Emerges as a Property of Cell Interactions. *PLoS ONE* **9,** (2014).

167. Heaysman, J. E. & Pegrum, S. M. Early contacts between fibroblasts. An ultrastructural study. *Exp. Cell Res.* **78,** 71–78 (1973).

168. Gloushankova, N. A. *et al.* Dynamics of contacts between lamellae of fibroblasts: Essential role of the actin cytoskeleton. *Proc. Natl. Acad. Sci. U. S. A.* **95,** 4362–4367 (1998).

169. Choudhary, S., Blackwell, K., Voznesensky, O., Deb Roy, A. & Pilbeam, C. Prostaglandin E2 acts via bone marrow macrophages to block PTH-stimulated osteoblast differentiation in vitro. *Bone* **56,** 31–41 (2013).

170. Sanjana, N. E., Shalem, O. & Zhang, F. Improved vectors and genome-wide libraries for CRISPR screening. *Nat. Methods* **11,** 783–784 (2014).

171. Hodgson, L., Pertz, O. & Hahn, K. M. Design and optimization of genetically encoded fluorescent biosensors: GTPase biosensors. *Methods Cell Biol.* **85,** 63–81 (2008).

172. Fukuhara, S., Chikumi, H. & Gutkind, J. S. RGS-containing RhoGEFs: the missing link between transforming G proteins and Rho? *Oncogene* **20,** 1661–1668 (2001).

173. Bielnicki, J. A. *et al.* Insights into the molecular activation mechanism of the RhoA-specific guanine nucleotide exchange factor, PDZRhoGEF. *J. Biol. Chem.* **286,** 35163–35175 (2011).

174. Chen, Z. *et al.* Activation of p115-RhoGEF requires direct association of Gα13 and the Dbl homology domain. *J. Biol. Chem.* **287,** 25490–25500 (2012).

175. Tong, Y. *et al.* Binding of Rac1, Rnd1, and RhoD to a Novel Rho GTPase Interaction Motif Destabilizes Dimerization of the Plexin-B1 Effector Domain. *J. Biol. Chem.* **282,** 37215–37224 (2007).

176. Wong, O. G.-W. *et al.* Plexin-B1 mutations in prostate cancer. *Proc. Natl. Acad. Sci. U. S. A.* **104,** 19040–19045 (2007).

177. Williamson, M. & Masters, J. Cancer associated plexin B1 mutations. (2011).

178. Pascoe, H. G. *et al.* Secondary PDZ domain-binding site on class B plexins enhances the affinity for PDZ–RhoGEF. *Proc. Natl. Acad. Sci.* **112,** 14852–14857 (2015).

179. Chikumi, H. *et al.* Homo- and hetero-oligomerization of PDZ-RhoGEF, LARG and p115RhoGEF by their C-terminal region regulates their in vivo Rho GEF activity and transforming potential. *Oncogene* **23,** 233–240 (2004).

180. Tanabe, S., Kreutz, B., Suzuki, N. & Kozasa, T. Regulation of RGS-RhoGEFs by Galpha12 and Galpha13 proteins. *Methods Enzymol.* **390,** 285–294 (2004).

181. Shang, G. *et al.* Structure analyses reveal a regulated oligomerization mechanism of the PlexinD1/GIPC/myosin VI complex. *eLife* **6,** (2017).

182. Hota, P. K. & Buck, M. Thermodynamic characterization of two homologous protein complexes: associations of the semaphorin receptor plexin-B1 RhoGTPase binding domain with Rnd1 and active Rac1. *Protein Sci. Publ. Protein Soc.* **18,** 1060–1071 (2009).

183. Ito, T. *et al.* Estrogen-Dependent Proteolytic Cleavage of Semaphorin 4D and Plexin-B1 Enhances Semaphorin 4D-Induced Apoptosis during Postnatal Vaginal Remodeling in Pubescent Mice. *PLoS ONE* **9,** e97909 (2014).

184. Hoefen, R. J. & Berk, B. C. The multifunctional GIT family of proteins. *J. Cell Sci.* **119,** 1469–1475 (2006).

185. Carter, A. M., Gutowski, S. & Sternweis, P. C. Regulated localization is sufficient for hormonal control of regulator of G protein signaling homology Rho guanine nucleotide exchange factors (RH-RhoGEFs). *J. Biol. Chem.* **289,** 19737–19746 (2014).